IOWA STATE UNIVERSITY
Digital Repository

2010

Rapid optimization of interior permanent magnet (IPM) machines using the response surface method and dimensionless parameters

Ron D. Bremner
Iowa State University

Follow this and additional works at: http://lib.dr.iastate.edu/etd

Part of the Mechanical Engineering Commons

Rapid optimization of interior permanent magnet (IPM) machines using the response surface method and dimensionless parameters

by

Ronald Dean Bremner

A dissertation submitted to the graduate faculty

in partial fulfillment of the requirements for the degree of

DOCTOR OF PHILOSOPHY

Major: Mechanical Engineering

Program of Study Committee:
Ron M. Nelson, Major Professor
Venkataramana Ajjarapu
Dionysios Aliprantis
Gregory Maxwell
Ken Bryden

Iowa State University

Ames, Iowa

2010

TABLE OF CONTENTS

LIST OF FIGURES

LIST OF TABLES

ACKNOWLEDGEMENTS

I would like to thank my wife Diane, for your love and patience while I spent so much time on the computer. While the research has been enjoyable, we can now look forward to time together.

I would like to thank Katie, Brian and Dusty, my kids, and Lauren, my 'newest kid'. Thanks for putting up with your dad's studies over the past few years. Education and knowledge are important, but you are more important than anything.

I would like to thank Dad and Mom for your love and encouragement. What an incredible privilege, growing up in a home like ours.

I would like to thank Dr. Ron Nelson, my Major Professor, for guiding me in this research, and for encouraging me to continue pursuing a PhD, after you advised me on my Master's education. I would also like to thank the other members of my Program of Study Committee, Dr. Venkataramana Ajjarapu, Dr. Dionysios Aliprantis, Dr. Ken Bryden, and Dr. Gregory M. Maxwell. You wisely asked me to limit the scope of this research. Having experienced the amount of effort required to do this 'limited' research, I am extremely thankful for that guidance.

I would like to thank Reno Rodeghiero, one of the best bosses a guy could ever have. You were more of a coach than a boss. Your desire to help people 'become all they can be' is incredibly rare, and I am thankful for your encouragement.

ABSTRACT

The primary objective for this work is to create a method to rapidly optimize interior permanent magnet (IPM) machines. For this research, a method was created called dimensionless optimization (DO). Eight dimensionless parameters determine nineteen dimensions of the machine based on design rules, stresses in the rotor and back EMF. Given a maximum torque specification and a local design space, a hypercube design of 64 machines is created using an 8 factor I-optimal design. Analysis is performed using a commercial program which incorporates electromagnetic FEA, and provides the current and phase angle requirements, and efficiency of the machines at the defined test points. Response surfaces are created for efficiency and current at each test point. The method determines the variance of the response surfaces, the optimum predicted design in the local design space, and the location of design spaces which may yield better designs. The method was validated by comparing 20 kW and 50 kW machines designed by an electric machines manufacturer, to machines designed using dimensionless optimization. The efficiencies of both machines were improved using dimensionless optimization.

CHAPTER I.   INTRODUCTION

This chapter introduces the motivation and objectives of the current research, covers the fundamental subjects utilized in the research, describes the organization of the dissertation, and includes a literature review.

A.   Motivation

A rapid method of machine design is desirable.

Increasing the efficiencies of vehicles is a crucial need today, due to the increasing environmental and economic costs of energy. Hybrid vehicles are highly efficient, and help meet this need. All major automotive manufacturers have hybrid cars and/or pickup trucks in production. There are also hybrid buses, postal vehicles, delivery and garbage trucks, and construction vehicles in production, with even larger hybrid vehicles which have been announced. Automobiles which are battery powered (pure electric) have also been announced for production.

Nearly all of these vehicles are designed around motors and generators (electric machines) that use interior permanent magnet (IPM) topology. These machines can be extremely efficient and compact. However, much of the knowledge of efficient IPM machine design is proprietary to the developers of these machines or vehicles.

The companies owning this technology benefit from keeping this information proprietary, as the design of these electric machines is complex, and publicly available knowledge is scarce. Yet there is a larger benefit to society if methods of designing efficient IPM machines are shared.

Machine design is complex and time consuming.

Electric machines incorporate magnetic materials which saturate (the electric steels), are non-linear in nature (the magnets and the electrical steels), and have complex interactions (the magnetic fields of the magnets and electrical current; power losses in the stator steel vs. power losses in the copper windings, etc). Because of the complexity and non-linearities in electric machines, the design of IPM machines requires software which incorporates electromagnetic FEA and other sophisticated features.

Starting with good initial values for parameters significantly speeds up optimizations. However, there are no general guidelines or widespread knowledge for the values of these dimensions. In surface permanent magnet (PM) machines, for example, it is believed that the rotor length should be nearly the same as the rotor diameter. This is not always true in IPM machines, in fact the optimal value to start with, if it exists, is not known.

The dimensions of the electric machine interact with each other in ways that are not understood, and this lack of knowledge about these interactions slows down the design process. Some dimensions tend to become fixed (e.g. the rotor and stator diameters), and it is impossible to alter those dimensions significantly without changing many other dimensions. A method which allows dimensions to be independent of each other would allow more rapid optimization; and would also lead to an increased understanding of the interactions in electric machines.

Mathematical models are approximations

Mathematical models, including response surface models, are approximations to the performance of real systems. At the initiation of this research, it was not known whether

response surface models could be used effectively to predict the response of IPM machines. If accurate models of regions of the design space could be created, optimization solutions could be created more rapidly.

B.   Objectives

The goals of this research are to:

- Provide a method to rapidly design efficient IPM machines

- Provide a method which allows independent changes in machine dimensions

- Provide a method which allows better comparison between machines of differing power or speed requirements

- Determine if response surface methods are feasible for creating these models

The method developed is not dependent on a specific program language, or on a specific electric machine analysis tool. The intent is to provide a *method,* not a *tool.*

C.   Organization of Dissertation

This dissertation is organized as follows:

Method, describing the steps of implementing the design method

Results, showing the method's application to specific machine requirements, and its ability to allow changes to parameters independently of other parameters

Discussion, describing how the method was created, discussing the results and benefits, and describing anomalies found in executing the method

Conclusions, summarizing the contributions of this dissertation, and the limitations of this method

Future work, describing areas where more research is needed

D.   Literature Review

The literature review is divided into the following sections:

- Optimization methods, describing some of the methods used to optimize electric machines in general, and IPM machines specifically

- Methods for optimizing current or phase angle

- Use of the response surface method, and I-optimal designs

- Dimensionless optimization (DO), showing the use of dimensionless parameters with electric machines

1. Optimization methods used for electric machine design

Optimization methods for electric machines are the focus of a large body of research. Kim et al. in [1] applied response surface methodology and full factorial design (FFD) to the shape of the rotor of IPM machines, to minimize torque ripple. This paper included the V-type configuration focused on in this research, as well as IPM machines where the magnet is normal to the d-axis. This would correspond to the machines of this research, with a magnet depth ratio (R_{MDp}) of 0.0.

Three parameters were varied; the included magnet angle, the magnet thickness, and the distance from the shaft. A 2^3 FFD was initially set up that varied the included angle of the magnets from 100-120°, the magnet thickness from 3.5-4.5 mm, and the distance of the magnet to the shaft from 1.0-3.5 mm. This was followed with a 15 point central composite design (CCD).

Muetze in [2] studied global optimization of PM machines, and convex structures within the optimization. It noted that the design process of DC brushless motors is

becoming increasingly complex. Modeling and problem formulation; and selection of the optimization method must be integrated. Design optimization is often achieved using "trial and error" techniques and subjective judgment. This is slow, costly, and contains elements of uncertainty.

Methods were divided between stochastic methods and deterministic methods. For deterministic methods, convex optimization is widely applied, as these methods can be coded efficiently. Stochastic, evolutionary algorithms are often applied because they treat large-scale problems as a black box. Often a single cost function is used, which is a weighted combination of the "component objective function."

Where convex characteristics can be identified, solution methods for convex problems can be exploited. For the example problem from the paper, an equivalent circuit of the machine was created, based on geometric dimensions. The B-H characteristics of the iron and magnets were assumed to be linear, simplifying the problem. Optimizations were performed for maximum flux density, maximization of magnetic energy vs. magnet cost, and maximization of torque.

The author recognized that mapping techniques and derivation of equations from finite element analysis might be useful.

Preis et al. in [3] studied the use of genetic algorithms (GA) in the design of electromagnetic devices (not specifically electric machines). These are considered especially useful for strongly nonlinear optimization problems, of which electric machine design qualifies.

Finite element modeling (FEM) is an analytic tool while optimal design is a synthetic problem. If FEM is to be used for a number of designs, a strategy must be found to keep the number of trials low.

Three evolutionary methods were compared. The problem was to optimize the pole shape of a magnet. 2D and 3D FEM was used for each of these problems. Non-linearity of the pole was neglected. The use of GA was compared with the Gauss-Seidel method. For the 2D problem the evolutionary scheme yielded slightly better results.

Gottvald et al. in [4] proposed the question "what optimization methods are adequate for solving specific types of optimization problems?" Convexity, differentiability, and the accuracy of the function are not considered guaranteed. It presented a method called Global Evolution Strategy (GES), which combined evolutionary algorithms, simulated annealing, and Monte Carlo iteration.

The authors recognized that the non-linearity of electromagnetic problems requires the use of global optimization methods.

Arpino et al. in [5] studied the design of a DC torque motor using 2D and 3D FEM, and accounted for the magnetization curves of the iron and magnets. It mentioned that there are two fundamental functional bodies in the design optimization problem, the analysis tool and the search algorithm.

The motor was used to control the angular position of a carburetor throttle. A stochastic optimizer was applied to identify the optimal shape exhibiting the lowest cost, within constraints.

Nine parameters, shown in Figure 1 were varied:

- the external diameter (DEE)

- the thickness of the stator yoke (SPST)

- the air gap width (TRAF)

- the angular dimension of the magnets (ALFR)

- the iron core width (HF)

- the difference between the axial length of the rotor and stator (HDRO)

- the axial length of the stator (HSTA)

- the angular dimension of the winding (ANVV)

- the radial dimension of the iron core (DLF)
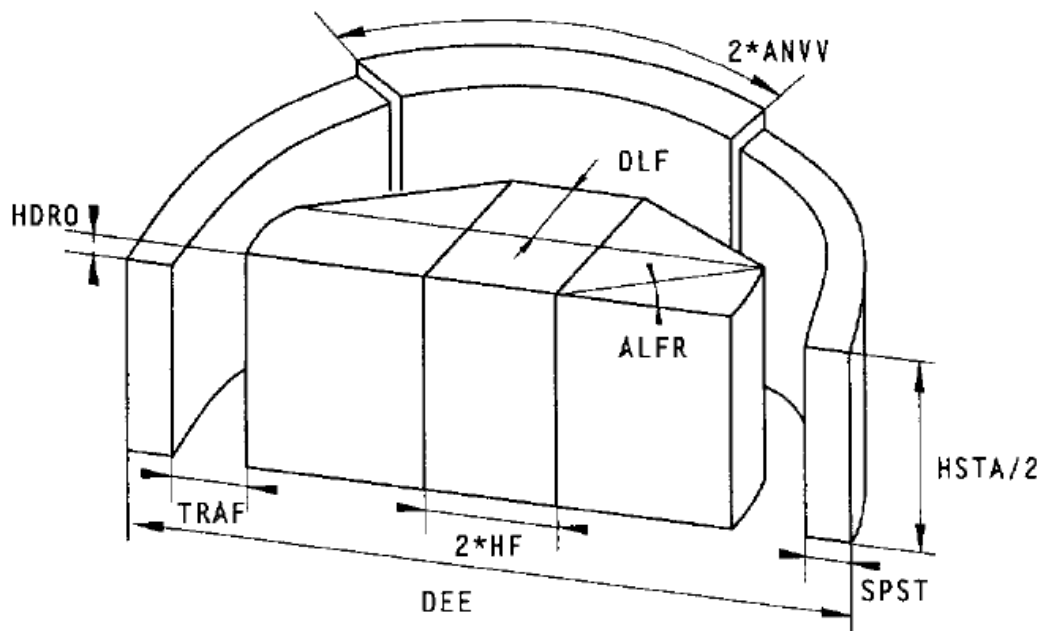
Figure 1, Solid model (one fourth) of the motor optimized

Bilateral bounds were introduced. The objective function was the total cost of copper and magnets. The algorithm used repetition of generation, mutation and annealing, until convergence. When 3D FEA was used, a 2D FEA was run first. If the torque had the potential to be acceptable, a 3D FEA was then run. Total runtime was 225 hours on a

Sun Sparc-Station 2. The savings in cost was approximately 16%. The solution was not guaranteed to be global.

Uler et al. in [6] applied GA to the design of a pole face in a motor, and incorporated 2D electromagnetic FEA. GA were considered to be a unique method of optimization because they: 1) work on a population of points in the search space 'simultaneously', rather than on one point at a time, 2) work with a coded string representing the parameters, 3) use the objective function, but not its derivatives or other information, and 4) use rules for transition that are probabilistic.

This paper states it was the first use of GA in electromagnetic devices (1994). As used in [6], as in most other contexts, GA included reproduction, crossover and mutation. The parents are comprised of finite length chromosomes (string members). Binary and gray codings are commonly used. The fitness value was calculated based on the objective function, along with an average fitness value for the population. Convergence was determined by the average fitness value.

Constant permeability for the electrical steel was assumed. The goal was to achieve a sinusoidal magnetic flux density. In Figure 2, points P1 through P4 were allowed to move in the y direction between y = 22.5 and y = 28.0 mm, but not in the x direction. The initial population had 30 members. The y directions were encoded as four 16 bit string segments, to form a 64 bit chromosome. The crossover probability was 0.95, the mutation probability 0.005. The error criteria was 0.5% for the average fitness. The search converged in 24 iterations (720 function evaluations).
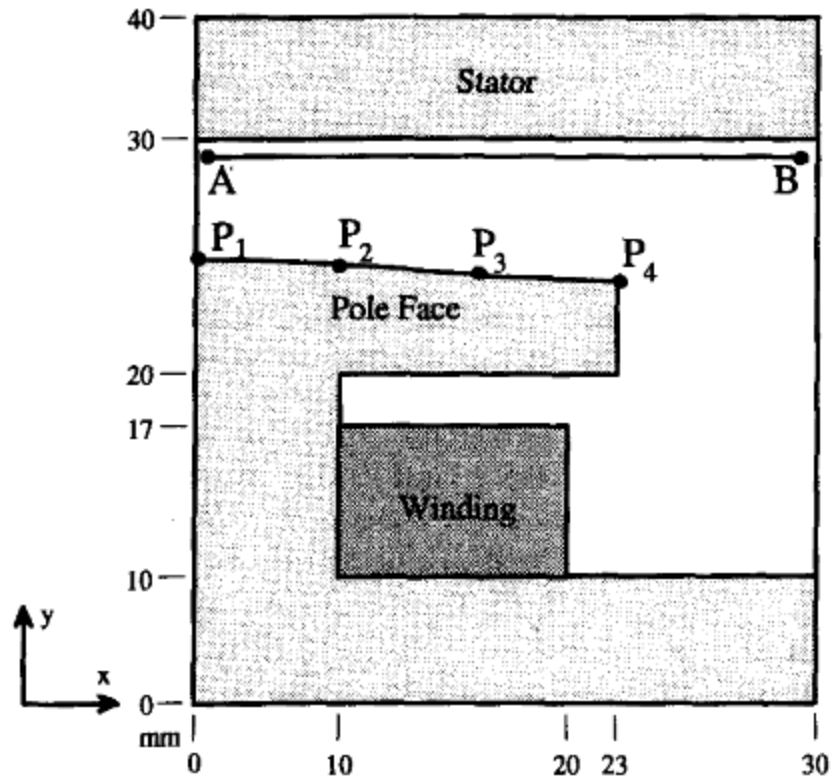
Figure 2, Geometry of the pole to be optimized

Mohammed et al. in [7], written two years later, by the same authors as [6],
approached the same problem, but added a direct search method. It was recognized that a
GA can be effective in the "explore and exploit" portion of an optimization algorithm, as
it does not "lock in" to local minima. These are helpful characteristics with non-convex
objective functions, which can be encountered in magneto-static problems. Therefore, a
GA was used to locate the "zone" of the global optimum. The gradient technique took
over inside this zone, as it was assumed that the objective function is differentiable inside
this zone. Use of the gradient technique helped the problem converge rapidly. The
problem was similar to the problem in [6], but six points were used, and the points moved
radially.

Oh et al. in [8] applied an algorithm to minimize the ripple torque of the DC motor. The variables were the height of rotor teeth (Htr), the width of the rotor teeth Wtr), and the width of the magnet edge (Wm). This algorithm included both GA and the direct search method, as well as FEA. The authors recognized that stochastic methods require a higher number of objective function calculations than deterministic methods.

Genetic algorithms are known to have sub-optimal convergence characteristics. The direct search method is deterministic, but does not require the derivative. This is advantageous when the objective function is not expressed explicitly. The efficiency of the search depends on the initial point, which must be chosen carefully. The solution may point to a local optimum, which may not be global if the problem is not unimodal.

The coupled approach of this paper used GA until the current point was in the global convex hull. The direct search method then converged more rapidly and accurately than GA. The algorithm switched from GA to direct search when

$$| Fitness_{avg} - Fitness_{best} | < \varepsilon \tag{1.1}$$

where

$$\varepsilon = 0.05\, Fitness_{best} \tag{1.2}$$

Using only GA, solving the problem required an average of 1294 calls to the cost function, while using the mixed approach required an average of 639.4 calls to the cost function. The direct search yielded an exact answer. The problem converged 10 steps after the direct search method was begun.

Figure 3, Cross section of DC motor

Tusar et al. in [9] surveyed methods used for optimizing universal (not IPM) electric motors. The traditional approach of machine design is for experts to begin with candidate designs, and then improve them through multiple iterations. This improvement is dependent on the experience of the designer, and is done manually.

Figure 4, Universal motor laminations

The presence of reliable simulation tools allowed the design process to be automated. This study looked at the ability of six stochastic methods to perform this automation. Both the rotor and stator geometries are varied with these approaches. Three evolutionary methods, two particle based methods, and an ant stigmergy algorithm were evaluated.

The objective function was to minimize power losses. This paper included non-linearity and saturation in the calculations.

Equations were written for power loss in terms of current, flux density, frequency (related to speed), etc. Iron and copper losses were modeled. Eddy current and hysteresis equations assumed that properties obtained at 50 Hz could be used to calculate losses at higher frequencies. Brush, ventilation and friction losses were not modeled, as they were assumed to be equal regardless of rotor and stator geometry.

Dimensions varied

Ten dimensions were varied. These are the rotor yoke thickness (ryt), rotor external radius (rer), rotor pole width (rpw), stator width (sw), stator yoke horizontal thickness (svh), stator yoke vertical thickness (syv), stator middle part length (sml), stator internal edge radius (sie), stator teeth radius (str), and stator slot radius (ssr).

Some dimensions were fixed, including the rotor air gap.

Methods for that paper

The authors employed ANSYS electromagnetic FEA for analysis. Three evolutionary algorithms were used, with an initial population of random individuals. The first method was a 'standard' application of GA. The second was called Steady-State Evolutionary Algorithm, and continuously replaced the worst pair in the population with the new offspring.

The third evolutionary method is called differential evolution and calculated new candidate's genetic material from a parent and two other individuals. For that method, each parent was selected sequentially, and a single offspring was generated. The candidate replaced the parent if it was better than the parent.

Particle swarm optimization (PSO) and a similar approach called Electromagnetism-like algorithm (EM) were also used. EM uses information from every particle, rather than only the global best and the particle's previous best. In EM, particles exert attractive or repulsive forces on other particles.

A multilevel ant stigmergy algorithm was also used. The 'ants' follow predetermined paths through the design space. All paths start at the same point (A), and end at another specific point (B). Points along the paths are weighed, and 'pheremones' (values) are left at points, depending on the objective functions. The parameters for all methods were discretized using 0.1mm steps. There are approximately 1.92×10^{20} points. The stopping criterion was 1400 function evaluations. Each evaluation took about 2 minutes, the evaluation time for each method being about two days. GA and PSO used populations of 20. MASA operated at seven levels, with 200 evaluations at each level to obtain the 1400 evaluations. To determine how well each algorithm performed, the optimizations were run 20 times. The initial engineering solution (before optimization) had a loss of 178 W. After optimization, this decreased to 135 W on average.

Manufacturability of solutions

The solutions were evaluated, to determine if they were feasible from a manufacturing standpoint. The design with minimum losses was not manufacturable.

Cupertino et al. in [10] examined two methods for optimizing an induction machine using Simultaneous Perturbation Stochastic Analysis (SPSA) and a Compact Genetic Algorithm (CGA).

The optimization was done within the closed loop control system. In the experiments, with five parameters to be optimized, the SPSA was three times less demanding, but the CGA produced better answers. The SPSA was sensitive to the initial choices.

SPSA is based on a highly efficient approximation to the gradient, and required only two loss measurements to estimate the gradient, regardless of the number of dimensions.

CGAs are similar to conventional GAs, but use a probability vector which evolved during the search, using processes similar to GAs. CGAs require less memory than GAs. The primary contribution of the authors was the application of "light" and effective algorithms.

[10] briefly described the implementation of SPSAs and CGAs. They referred to [11], which described SPSA in greater detail, and [12] which explained CGA more thoroughly. [10] included pseudocode of the CGA.

2. Methods for optimizing current or phase angle

Many papers describe methods of optimization of the geometry of electric machines. In the optimization of permanent magnet synchronous machines, to find the peak efficiency of a machine, it is necessary to determine the optimal current and phase angle. The papers which describe optimization of machine design rarely describe how the current and phase angle were determined.

Bandler et al. in [13] describes optimization methods for computer aided design. A number of search methods, including Fibonacci and golden section search were discussed. These are direct elimination methods, and require that the functions be unimodal. The golden section search eliminates 38.2% of the search region each iteration, and is based on the number:

$$\frac{1+\sqrt{5}}{2} = 1.6180... \tag{1.3}$$

and its multiplicative inverse:

$$\frac{2}{1+\sqrt{5}} = \frac{1+\sqrt{5}}{2} - 1 = 0.6180 \tag{1.4}$$

The Fibonacci search method does not eliminate a fixed percentage of the search region of each iteration, but rather uses the Fibonacci sequence (1, 1, 2, 3, 5, 8, 13, 21…) to decrease the search region.

As each region is eliminated, the width of the remaining region follows the Fibonacci sequence in reverse. As an example, if the region was initially divided into 21 equal segments, after the first elimination, 13/21 of the region would be left, after the second the limitation, 8/21 of the region would be left, etc.

The Golden Section search method results in an interval of uncertainty that is 17% larger than the Fibonacci method, for the same number of steps. However, for the Fibonacci method, the number of function evaluations must be known in advance. If higher resolution is desired, a larger initial Fibonacci number would be used, such as 34, 55, etc.

Interpolation methods were also mentioned. Some of these involve fitting a low order polynomial through a number of points until a minimum is obtained to the desired accuracy.

Cao et al. in [14] describes the use of the gradient search technique and the golden section technique to find the optimum current vector, for a real time automotive control system, with a PM synchronous motor. Iron and copper losses were included. Iron loss was shown to be a concave function of i_d (for a given torque), as shown in Figure 5.
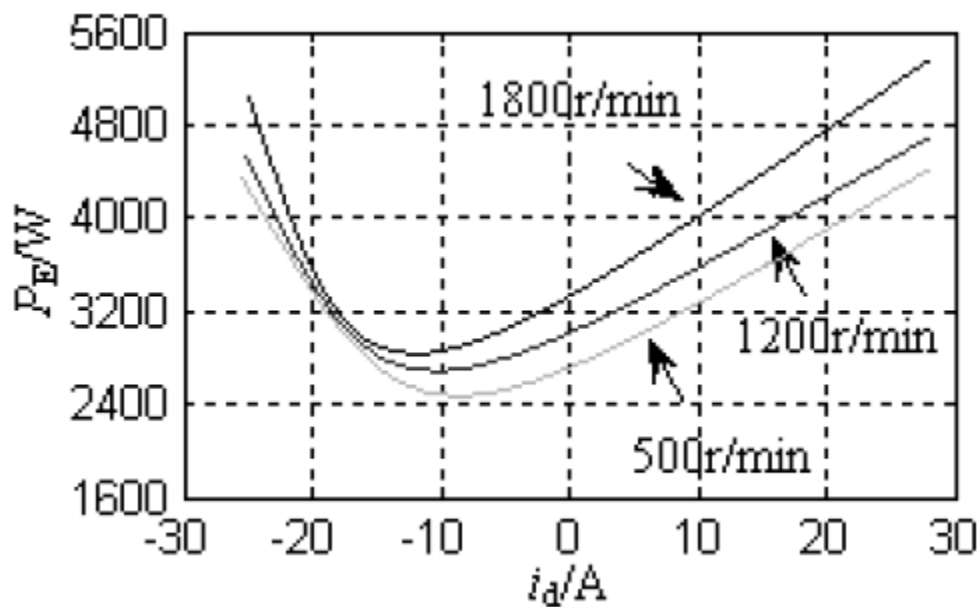
Figure 5, Electrical losses vs i_d for a given motor at constant torque output, from [14]

The optimum i_d at various operating conditions of torque and speed were stored in lookup tables. For this method, an initial value of i_d was taken from this table. Values about 30% above and below i_d are used as data points. The losses for these three data points are calculated. The gradients are used to indicate whether an additional point is required, or whether the algorithm should precede to the next step (golden section). The

golden section method was used until ε (the step size) was less than 0.5% of the rated current.

3. Use of Response Surface Method and I-Optimal Designs

Mays et al. in [15] described the use of CCDs to provide estimations of second order regression models. CCDs involve factorial design, axial points, and replicated runs in the design center. The paper noted that standard CCDs are sometimes not optimal. D-optimal and I-optimal designs were also presented, with two, three and four variables.

For second-order models, the fractional three-level (or 3^k) factorial design is often used. CCDs (Box and Wilson) are an alternative, which reduces the size of the design when k is large.

D-optimality attempts to minimize the generalized variance of the model coefficients. I-optimality, (integrated variance optimality) attempts to minimize the variance of prediction averaged over the design region.

For CCDs, design levels are often coded -1, 0 and +1. The design center is coded (0, 0,… 0), and the axial points coded $(\pm\alpha,0,0,...0)$, $(0,\pm\alpha,0,...0)$, etc. CCDs were created using both I-optimal and D-optimal designs.

The SAS Institute in [16] states that I-optimality:

- "Minimizes the average variance of prediction over the region of the data."

- "Is more appropriate than D- Optimality if your goal is to predict the response rather than the coefficients, such as in response surface design problems. Using the I-Optimality criterion is more appropriate because

you can predict the response anywhere inside the region of data and

therefore find the factor settings that produce the most desirable response

value. It is more appropriate when your objective is to determine

optimum operating conditions, and also is appropriate to determine

regions in the design space where the response falls within an acceptable

range; or to develop feedback-control models. Precise estimation of the

response therefore takes precedence over precise estimation of the

parameters."

4. Optimization using dimensionless parameters

Electrical engineers use dimensionless variables in electric machine analysis. These

include the 'per unit' numbers used in machine design. Even more common is the use of

dimensionless parameters as output parameters; efficiency being the most common, as

well as saliency ratio. Other common uses are slots per pole, skew, and the magnet

thickness / air gap ratio. Another common ratio in IPM or switched reluctance (SR)

machines would be the ratio of the direct to the quadrature inductance.

Extensive use of geometric ratios in electric machine optimization is not widely

practiced. Of the dimensions used this way, the most common dimensionless parameter is

the split ratio, mentioned by name in some electric machine design and optimization

papers. Of the papers that make use of dimensionless parameters, few use them

extensively.

Zhu et al. in [17] studied the influence of various design parameters on the torque of

flux-switching PM machines, and used the split ratio, as well as normalizing the stator

and rotor tooth widths, rotor tooth height, magnet thickness, bridge thickness and back-iron thickness. This paper recognized the split ratio as being one of the most important design parameters. They were seeking to find general trends in optimal design, and stated that the optimal split ratio was between 0.55-0.6 for their specific machine requirements. The ratios used were normalized.

Faiz et al. in [18] discussed design optimization of SR motors, and utilized four dimensionless parameters, all of them ratios. These included the tooth width /tooth pitch ratio (t/ λ), for which the optimum was shown to be between 0.33 and 0.40; the split ratio, for which the optimum was estimated to be between 0.57 and 0.63; the ratio between the back iron width and ½ the stator tooth width, for which the optimum was found to be between 1.1 and 1.3; and the tooth pitch/air gap length ratio (λ/g). For this paper, the stator OD was fixed.

This paper included studies of ratios compared to each other, as well as their effects on various figures of merit (see Fig. 3-8 in their paper). This paper referred to earlier papers on SR machines, which it stated made significant errors. This paper emphasized the importance of the ratios t/λ and λ/g, recognizing their significance to SR machines.

Yu et al. in [19] focused on the split ratio in the design of PM brushless DC motors, using NdFeB and SmCo magnets. FEA and analytical calculations were used. This motor was designed for short duty operation, approximately 300 seconds, and this paper looked at the split ratio's effect on the thermal behavior of the motor. They showed a unimodal curve for power vs. the split ratio, with the maximum from 0.47-0.55.

As the split ratio changed, the slot area also changed. Copper loss was fairly unimodal with the split ratio, but iron loss was not. The iron loss was significantly lower

at a split ratio of 51.5%. The eddy current loss in the magnets was also calculated. The optimal split ratio for the specific sized machine with NdFeB magnets was 52.5%, while for the SmCo magnets it was 55%. They noted that the split ratio impacts the length of the thermal path, assuming the heat will be transferred radially through the stator lamination to the case.

Pang et al. in [20] compared 100W flux switching permanent magnet (FSPM) and IPM machines, specifically their torque capability and flux-weakening. It included evaluating the effect of the split ratio. They referred to the 'V' shaped magnet configuration, and noted that buried magnets are protected from demagnetization in IPM machines. The effect of saturation was included. Due to the concentrated windings on their machine, they were not able to use the reluctance torque. For the most part, this paper used analytical equations, which were then verified through FEA. A single stator outer diameter, stack length and air gap length were used. Standard engineering units (mm) were used.

Chaaban in [21] derived a formula for the optimum split ratio. It also evaluated the impact of the split ratio on the magnet volume and machine cost.

Wu et al. in [22] optimized the split ratio for fractional slot IPM machines with concentrated windings. This paper used a 'V' shaped configuration of the magnets, similar to the configuration of this studied in this research. This paper used the flux focusing effect of the V configuration to increase the air gap flux density. The specific machine had 10-poles and 12-slots. The optimal split ratio for a specified air gap flux density, the optimal flux density for a given split ratio, and a global optimum flux density and split ratio were derived. Uniform air gap flux density distribution was assumed, and

iron losses were ignored. Copper losses in the slots were included. Curves showed the relationship between torque density, split ratio, and the ratio of flux in the air gap to flux in the magnet. Formulas were also given to determine the optimal air gap flux density for a given split ratio.

Pang et al. in [23] study brushless DC motors with surface permanent magnets. The split ratio was considered to be extremely crucial. The paper found an optimal split ratio analytically. A plot of the optimal split ratio vs. flux density in the gap for a machine with a fixed stator diameter was shown. Iron losses were neglected in order to make the analysis more tractable.

Soong et al. in [24] described the design of an axial laminated IPM motor, and mentioned the rotor insulation ratio (the ratio of insulation thickness/[lamination + insulation thickness]). They typically used a ratio of 0.5, but Boldea recommended 0.33-0.40, and Little suggested a value of about 1/3. They (as well as many others) also refer to the saliency ratio (L_d/L_q), and the constant-power speed range (CPSR).

Bianchi et al. in [25] described the design of a high-speed PM motor, and utilized the diameter ratio, (split ratio in other papers). Curves of torque vs. diameter ratio were shown, for various magnetic materials. The interaction of the diameter ratio with frequency was also studied, as well as the interaction of the diameter ratio with the flux density. The study also included slotted and slotless stators. The copper fill factor (the ratio between the copper and available surface), a commonly used dimensionless factor, was also defined.

Bianchi et al. in [26] optimized the design of a surface permanent magnet (SPM) machine. It used the dimensionless variable L/D of the stator; the ratio between

inner/outer stator diameters (related to the split ratio); and the tooth length ratio (the radial length of the tooth/the radial length of the back iron). This last variable is for a composite (non-laminated) component. Figures in the paper show losses vs. these ratios.

Feng et al. in [27] analyzed the torque of a double-stator permanent magnet synchronous motor, using the split ratio. In this case, there were two stators, an inner and outer stator, and the split ratios had a different meaning than the typical one. For that paper, no other ratios were used.

Paul et al. in [28] studied the design of induction AC traction motors, and used the ratio of the rotor slot width at the root/slot pitch at the root, and determined that the optimum ratios were between 0.4995 and 0.5004. For that paper, no other ratios were used.

Liu et al. in [29] analyzed the performance of PM stepping motors with a trapezoidal stator tooth (a claw poled PM machine), and utilized the ratio of the upper and lower bases of the trapezoidal teeth; and the ratio of the heights of individual teeth/the separation between the yokes. What this paper referred to as 'the upper and lower bases' are often called the claw tooth tip and base. The optimal ratio for the tip/base ratio was between 1/3 and 1/5 for the specifications. To lower the detent torque, the tooth height / yoke separation ratio was optimal at between 11/15 and 13/15. For that paper, no other ratios were used.

Bremner [30] described a method used to render 10 of the dimensions of an IPM machine dimensionless. GA was used for this research. A method was created which makes comparisons between machines having different power levels simpler. This paper was followed a few months later by [31], using a similar approach. [31] referenced [32].

Jahns et al. in [33] studied the optimal design of a 50 kW IPM machine. It included the use of the slot height/slot width ratio; the tooth width/slot pitch ratio; and a stator diameter to length aspect ratio between 2/3 and 3/2. This study is of interest as it falls inside of the scope (25 kW to 200 kW) of this research, and used some of the same variables.

Rajagopal et al. in [34] studied the optimal tooth-geometry for hybrid motors. This included the use of tooth width/tooth pitch ratios; slot depth/tooth pitch ratios; as well as tooth slot shapes. The optimum slot depth/tooth pitch ratio was observed to be 0.5, which agreed with previous studies by others.

Boughrara et al. in [35] studied PM synchronous machine design. It used only one dimensionless parameter, the magnet arc / pole pitch ratio. The effect of this ratio on the peak value of cogging torque was analyzed.

CHAPTER II.   METHOD

The primary goal of this research is to create a rapid method for optimizing IPM machines. This required selecting and applying an analysis tool and search algorithms, and setting up the problem so that it can be efficiently solved. The focus of this research is on how the problem was set up, and how the search algorithms were applied. Details which may be common to the use of various analysis tools are included.

This chapter describes the method developed to speed up machine design and optimization. The primary ways electric machine design was sped up were by using dimensionless parameters to simplify the dimensional scheme; automating many of the repetitive steps of machine design; selecting experimental designs which are compact, and are designed for prediction; adopting or creating methods to speed up convergence; and using the response surface method to find the optimum design.

This chapter describes the following:

- Overview of the design method

- Defining the dimensionless parameters used

- Entering specifications

- Defining the searchable design space

- Setting the local design space

- Defining the designs

- Using a graphical user interface to select design spaces

- Determining physical dimensions

- Analyzing the designs

- Modifying the golden section search method to determine the phase angle

- Modifying the Newton-Raphson method to determine current levels

- Defining the objective function

- Defining the response surfaces

- Finding the optimum

- Validating the method

A.   Overview of the design method

The following are the basic steps of the design method:

1. Specifications are entered for an electric machine (motor or generator), including power, speed, torque, voltage, etc.

2. A global design space is created based on dimensionless parameters.

3. A portion of the global design space is selected, and an algorithm creates 64[1] dimensionless designs, based on an I-optimal design.

4. The algorithm translates the dimensionless designs into the physical dimensions of the stator and rotor.

5. The designs are analyzed with structural FEA, and the bridge and post widths are modified so that the rotor has a structurally sound design.

6. Each machine design is analyzed once with electromagnetic FEA, to verify that it will mesh correctly.[2]

---

[1] The I-optimal design employed had 64 data points. I-optimal designs with fewer points are possible.
[2] If the analysis program can be guaranteed to mesh without operator intervention, this step is not required

7. The algorithm analyzes the 64 machine designs at each specified design point, using electric machine analysis software which incorporates electromagnetic FEA[3]. If necessary, the number of turns is reduced.

8. During the analysis, the current and phase angle are adjusted to maximize the machine or system efficiency. If necessary, the number of turns is reduced.

9. Separate response surfaces are created for each speed and torque level combination.

10. The response surfaces and the objective function are used to determine the optimum design.

11. If the optimum design is in the interior of the design hypercube, or on a constraint boundary, the optimization is complete.

12. If the optimum point is on an edge or surface of the hypercube, the algorithm recommends settings for a new portion of the design space. In this case, a new set of designs can be created, and the process repeated from step 3.

B.   Defining the dimensionless parameters

The method uses eight dimensionless parameters as variables:

- Stator aspect ratio (stator diameter/length), R_{SDL}

- Stator diameter ratio/rotor diameter ratio (commonly called the split ratio), R_{Spl}

- Slot depth ratio, R_{SDp}

- Top and bottom slot width ratios (2 ratios), R_{SW2} , R_{SW3}

- Magnet thickness ratio, R_{MTh}

- Magnet depth ratio, R_{MDp}

---

[3] For the validation algorithms, an electric machines analysis program called SPEED, a product of the University of Glasgow, Scotland, was used

- Web width ratio, R_{Web}

Stator aspect ratio

For this research, the stator aspect ratio is defined as:

$$R_{SDL} = \frac{D_{sta}}{L_{sta}}$$

(2.1)

where the stator diameter (D_{sta}) and stator length (L_{sta}) are shown in Figure 6.
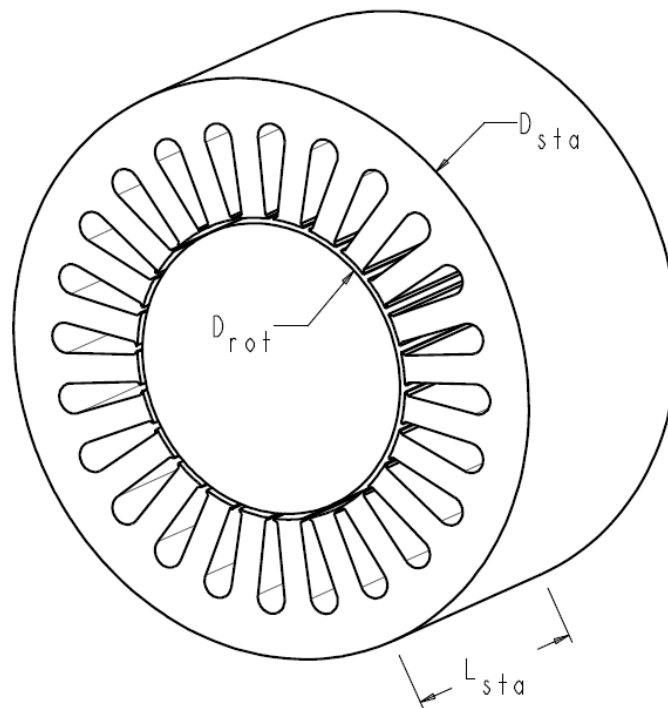
Figure 6, Stator aspect ratio (R_{SDL}) and split ratio (R_{SPL})

For electric machine design, performance points must be specified. One of these will determine the maximum torque of the electric machine, unless it is specified separately. A torque density[4] is also specified, and therefore the volume of the stator envelope can be determined.

---

[4] Torque density is defined as the maximum torque divided by the volume of the stator envelope

The stator aspect ratio, in combination with the stator's envelope volume ($L_{sta} \, \pi \, D^2/4$) determines the diameter and length of the stator.

The split ratio

The split ratio is defined as:

$$R_{SPL} = \frac{D_{rot}}{D_{sta}} \tag{2.2}$$

where the stator diameter (D_{sta}), and rotor diameter (D_{rot}) are shown in Figure 6

For some electric machines, the stators and rotors have differing lengths. For the validation examples, the stator and rotor lengths were the same. If there is a need for them to be different, the algorithms could be written to accept these.

Slot depth ratio, R_{SDp}

The stator slots contain the copper coils, which conduct electrical current. The slot depth ratio is defined as:

$$R_{SDp} = \frac{H_3}{H_{3\max}} \tag{2.3}$$

$$H_{3\max} = r_{SOR} - r_{SIR} \tag{2.4}$$

where the slot depth (H_3), is the slot depth at which the slot would become tangent with the outer surface of the stator (H_{3max}), the stator outside radius (r_{SOR}) and the stator inside radius (r_{SIR}) are shown in Figure 7. An R_{SDp} of 0.65 is shown in the figure.
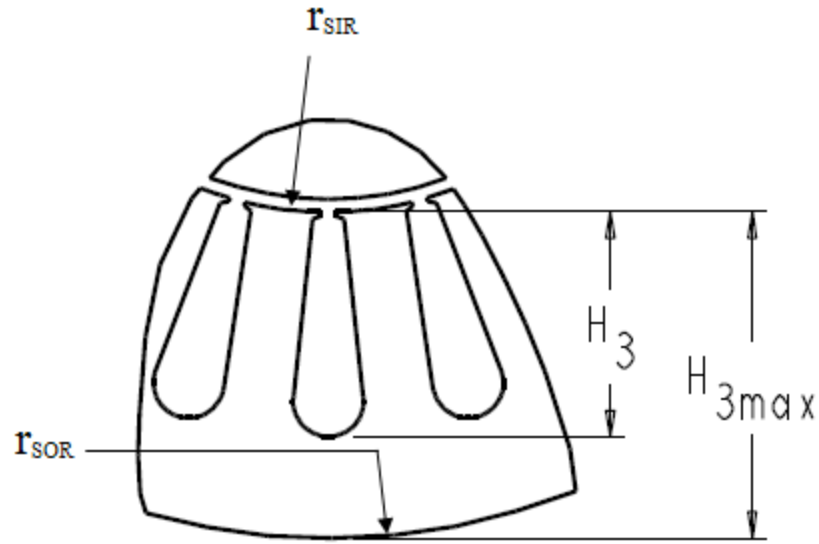
Figure 7, Slot depth ratio (R_{SDp})

In the validation software, a slot with a round end was used. Other shapes could be optimized in a similar manner; however a slot shape with a rounded end is typical of electric machines used in hybrid vehicles.

Slot width ratios R_{SW2}, R_{SW3}

The ratio for width at the upper shoulder for the slot is:

$$R_{SW2} = \frac{A_{W2}}{A_{W\,max}} \tag{2.5}$$

where A_{W2} is the angle from the center of the slot to the upper corner of the slot, and A_{Wmax} is the angle from the center of the slot to the center of the adjacent tooth, as shown in Figure 8. A value of 1.0 would result in wide slots, with adjacent slots touching each other. A value of 0.0 would result in the slots having no width at this point. An R_{SW2} of 0.33 is shown in the figure.
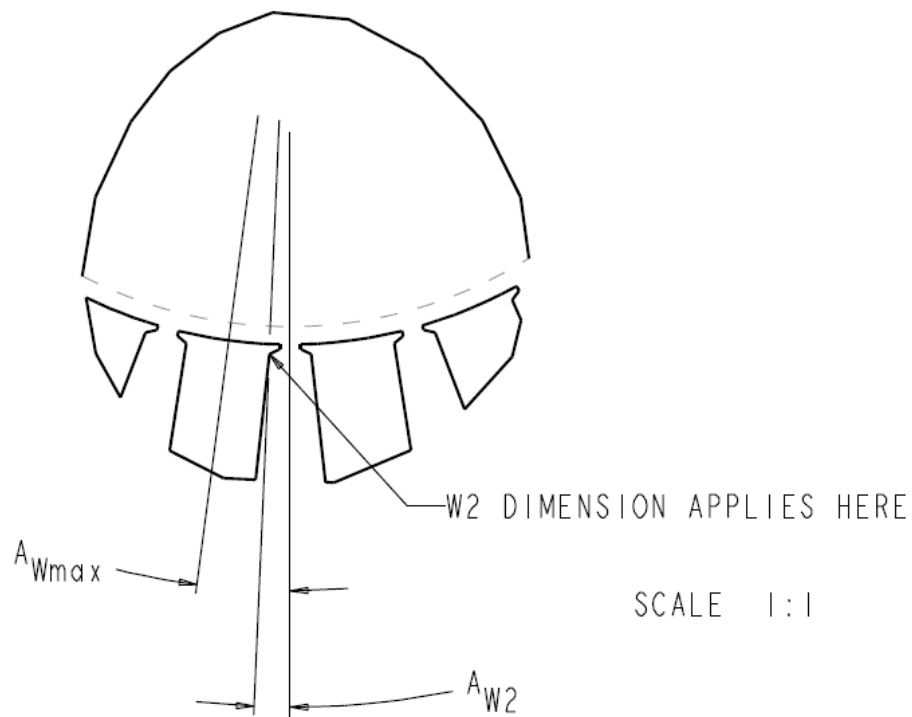
Figure 8, Upper slot width ratio (R$_{SW2}$)

The slot width ratio at the lower end of the slot is defined as:

$$R_{SW3} = \frac{A_{W3}}{A_{W\,max}}$$

(2.6)

where A_{W3} is the angle from the center of the slot to the tangent point of the bottom of

the slot, as shown in Figure 9. A value of 1.0 would result in wide slots, with adjacent

slots touching each other, and cutting through the teeth at the lower radius. A value of

0.0 would result in the slots forming a 'V' at the bottom, with no radius. An R$_{SW3}$ of 0.5

is shown in the figure.
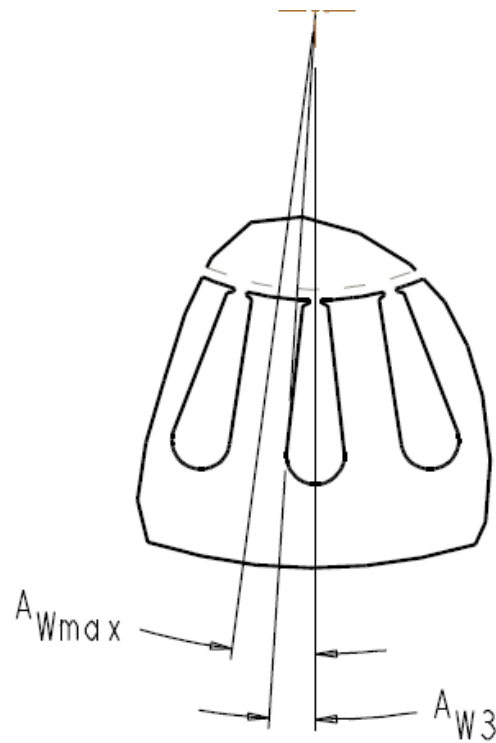
Figure 9, Lower slot width ratio (R_{SW3})

Magnet depth ratio, R_{MDp}

The magnet depth ratio is calculated as:

$$R_{MDp} = \frac{A_{md}}{A_{mmd}}$$ (2.7)

where A_{mmd} is the maximum magnet depth angle, the angle between lines P and Q, which is a line from the center of the rotor between two adjacent poles, and A_{md} is the angle between line P and the outer face of a magnet as shown in Figure 10. Line Q is a line which lies directly between the poles. Line P is a line perpendicular to a pole. An R_{MDp} of 0.2 is shown in the figure.
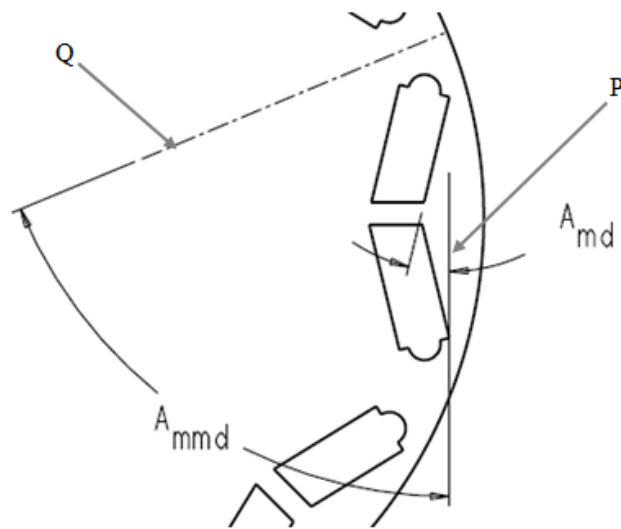
Figure 10, Magnet depth ratio (R$_{MDp}$)

In Figure 11 (right), a portion of the rotor is grayed out. The portion which is not grayed out represents one pole of the rotor. The shallowest magnet depth occurs when the angle A_{md} is 0.0, as shown in the left view. The deepest magnet depth which this method allows is if the magnet lies parallel to line Q, and the corresponding ratio is 1.0, as shown in the right view.
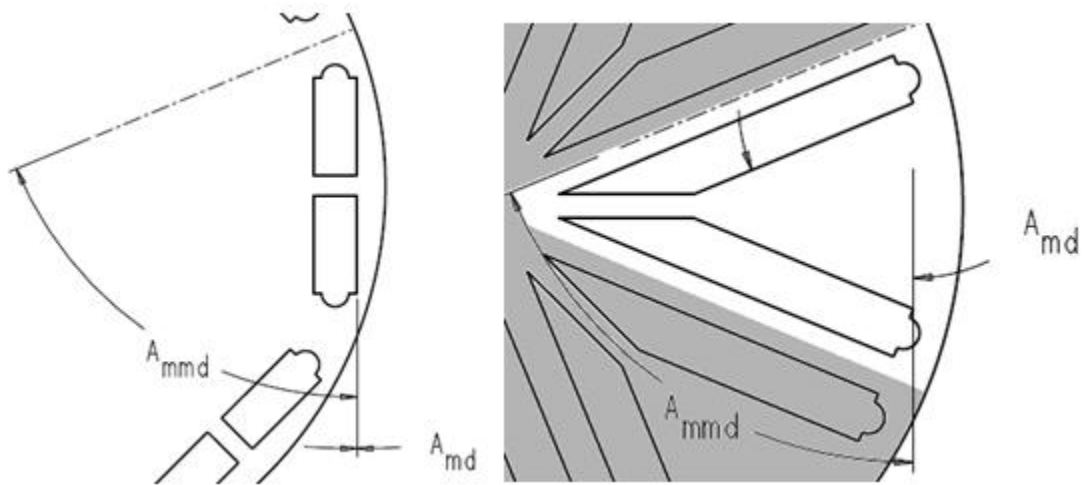
Figure 11, Magnet depth ratios of 0.0 (left), and 1.0 (right)

Web width ratio, R_{Web}

The web width ratio is defined as

$$R_{Web} = \frac{A_{web}}{A_{pol}} \qquad (2.8)$$

where A_{web} is the angle formed between the magnets of opposite poles, and A_{pol} is the angle formed between the centerlines of the two poles, as shown in Figure 12. An R_{Web} of 0.17 is shown in the figure.
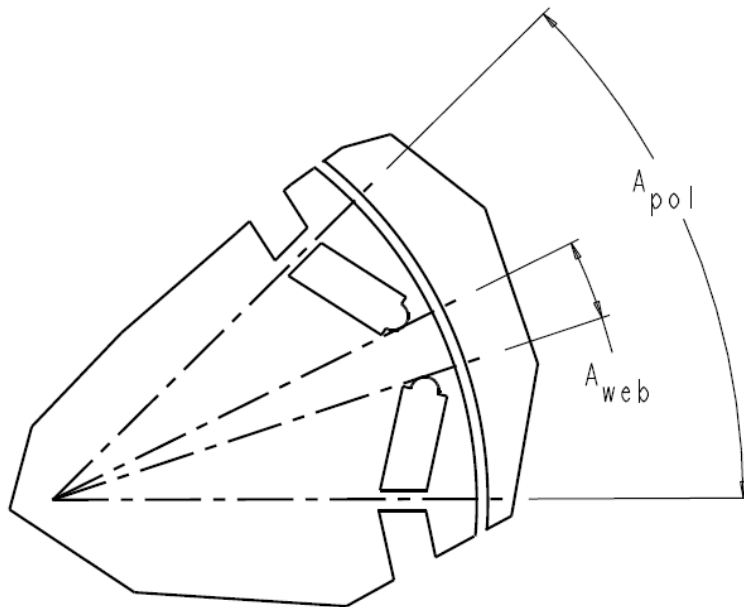
Figure 12, Web width ratio (R_{Web})

The formula for A_{pol} is

$$A_{pol} = 360 / P \qquad (2.9)$$

where A_{pol} is the angle between pole centers (degrees), and is shown in Figure 12. P is the number of poles, and is not shown.

If this ratio is 0.0, the magnet slots touch each other, and there would be no web between them. If this ratio were 1.0, there would be no magnet slots. Because of the thickness of the magnets, at some value less than 1.0, the magnets would have zero length.

Magnet thickness ratio, R_{MTh}

The magnet thickness ratio is calculated as:

$$R_{MTh} = \frac{T_{mag}}{T_{gap}} \qquad (2.10)$$

where T_{mag} is the magnet thickness and T_{gap} is the air gap thickness, the distance between the rotor and the stator, as shown in Figure 13. Typical values range from 6-10.
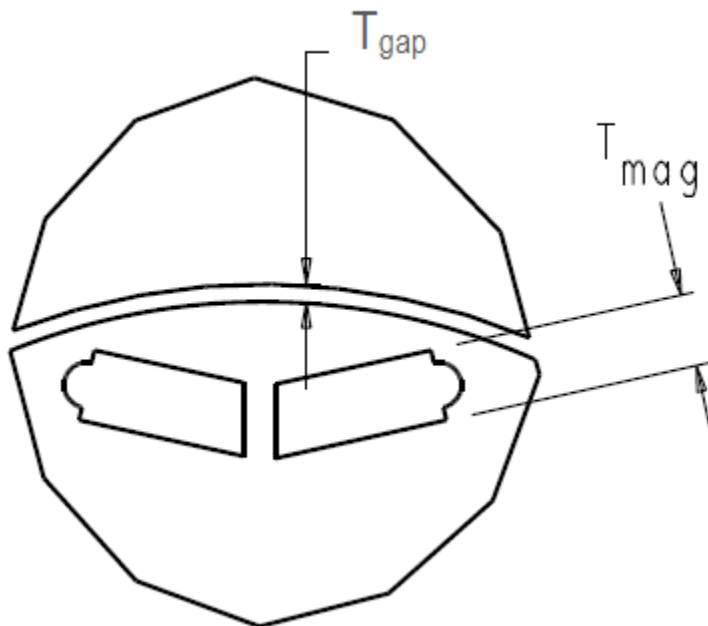
Figure 13, Magnet thickness ratio (R_{MTh})

C.   Entering specifications

Electric machine design requires a large number of specifications. For the user, the

first step of the method is to define the specifications. Specifications can be classified in

six areas: performance, material, machine, geometry, environment and controller. The

specifications (with the default variables used for validation) required include:

Table 1, Electric machine specifications

Performance Specifications		Material specifications	
Speed and Power		Lamination material and thickness	M19-29 ga. [0.35mm]
Overspeed condition	140% of max operating speed	Magnet material	L35UHT NdFeB
Torque density	50 Nm/liter[5]	Maximum material stress allowed	250 kPa
Machine specifications		Geometry Specifications	
3 phases		Stator specifications	
Number of poles	8	Slot shape	round bottom[6]
Slots per pole	6	Maximum diameter	NA
Throw	5	Rotor specifications	
Skew	None	Magnet slot shape	V, with center spoke
Parallel paths in the winding	4	Magnet slot lip	1.0 mm
DC link voltage	700 V	Corner radius	0.4mm
Maximum back-EMF	900 V	Minimum bridge thickness[7]	1%
Power level[8]	50 kW		

---

[5] Liters of stator volume envelope
[6] 'HW' option in SPEED
[7] As a percentage of the rotor radius
[8] This program has been used to optimize electric machine were two speeds were specified at differing power levels.

Environment		Controller definition[9]	
Winding temperature for analysis	140 °C	Drive type	sine
Magnet temperature for analysis	140 °C	Max. phase angle [10]	55 °
Minimum magnet temperature for back EMF	-10 °C	Forward voltage drop in transistors, V_q	
		Resistance in transistors, R_q, ohms	
		Switching time, t_q	
		Voltage drop in diodes, V_d	
		DC link capacitance, µF	
		Maximum switching frequency, Hz	

Other parameters could be specified, including constraints such as maximum total or

magnet weight, maximum inertia, current, etc. These parameters were not specified in

the validation algorithm, though they were recorded.

D.   Defining the searchable design space

The searchable design space is a portion of the design space where optimal values of

electric machines are found. The parameters were restricted by the algorithms to the

values shown in Table 2. This eliminated some regions of the design space which yield

highly inefficient designs, or designs which cannot produce rated power.

---

[9] Controllers input variables depend on the type of controller, all are not listed here.
[10] specified by inverter engineers to make controllability of the inverter better

Table 2, Parameter bounds of searchable design space

Parameter	Design space limitation	Design range	Parameter	Design space limitation	Design Range
R_{Spl}	0.40-0.70	0.10	R_{SDL}	0.5 – 4.0 (logarithmic)	$x_u = x_l \times \sqrt{2}$
R_{SDp}	0.40-0.80	0.10	R_{Web}	0.05-0.35	0.10
R_{SW2}	0.25-0.65	0.10	R_{MDp}	0.05-0.55	0.10
R_{SW3}	0.35-0.65	0.10	R_{MTh}	6.0-10.0	2.0

x_u above is the upper bound of the design hypercube's range, and x_l is the lower bound of

the design hypercube's range.
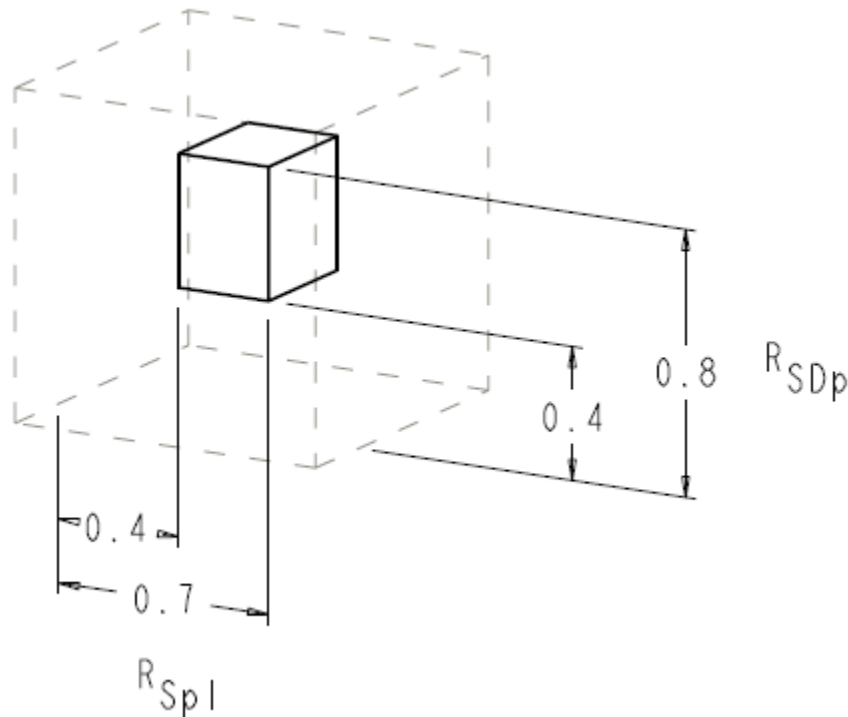
Figure 14, Restricting the design space, to eliminate infeasible or inefficient designs

Figure 14 graphically shows the searchable design space for three of the parameters.

The larger cube, shown with dashed lines, is the global design space for R_{Spl}, R_{SDp} and

R_{SW2} (which is not labeled, but is represented as the depth into the paper). The global design space for these parameters ranges from 0.0-1.0. The searchable design space is the smaller cuboid inside of the global design space. The figure represents restrictions of three parameters, all other parameters are restricted in a similar manner.

A mistake-proofing part of the method was to implement restrictions like these into the algorithms, so that these boundaries could not be over-ridden without modifying the software. This eliminated errors of selecting parameters outside of the bounds of the searchable design space.

E.   Defining the local design space

For this research, the local design space is the region in which all designs within a range of parameter values can reside. As an example, if the local design space can be described as R_{Spl} (0.55-0.65), R_{SDp} (0.70-0.80), R_{SW2} (0.35-0.45), R_{SW3} (0.55-0.65), R_{SDL} (2.00 – 2.83), R_{Web} (0.15-0.25), R_{MDp}(0.15-0.25), R_{MTh} (8.0-10.0) then the local design space consists of the infinite set of designs which have values that fall within those ranges.

For this research, a design hypercube is a set of 64 designs, created using the I-optimal design shown in Table 4. Each local design space has a unique design hypercube. Each design hypercube has one central point, which is unique to that hypercube. All other machine designs are on the boundaries of the hypercube, and may be shared with other design hypercubes.

Seven of the parameters have fixed interval sizes, listed as the 'Design Range' in Table 2. The stator aspect ratio, R_{SDL} (stator diameter/length) varies in a manner that is

logarithmic, with ranges which are: (0.5-0.707), (0.707-1.0), (1.0-1.414), (1.414-2.0),

(2.0-2.828) and (2.828-4.0). R_{MTh} (magnet thickness ratio) has a fixed interval size, but

the ranges are 2.0, compared to the other fixed ranges which are 0.1.

The extents of the design space were limited by the dimensions shown in Table 2.

The method searches one design hypercube at a time. An initial design space was

selected based on previous research with larger machines. The ranges for each parameter

of this design space are shown in Table 3.

Table 3, Initial design space for optimization

Parameter	Design space	Design range	Parameter	Design space	Design Range
R_{Spl}	0.40-0. 50	0.10	R_{SDL}	1.414 – 2.0	$x_u = x_l \times \sqrt{2}$
R_{SDp}	0.70-0.80	0.10	R_{Web}	0.15-0.25	0.10
R_{SW2}	0.35-0.45	0.10	R_{MDp}	0.15-0.25	0.10
R_{SW3}	0.55-0.65	0.10	R_{MTh}	8.0-10.0	2.0

where x_u is the upper bound of the design space, and x_l is the lower bound of the

design space. The numbers shown in the column labeled 'Design range' were used for

the validation analyses. Future research will refine these numbers, to increase the

accuracy of the response surface models, and to decrease the time required for

convergence.
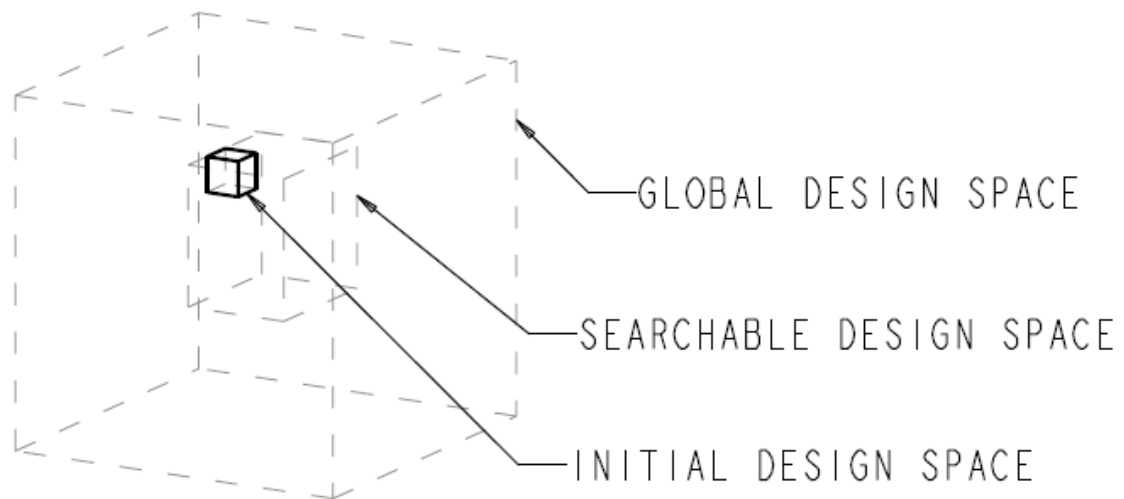
Figure 15, Initial design space

Figure 15 shows the location of the initial design space given in Table 3. While the local design space represents only a fraction of the designs which are geometrically possible, experience with this method allows narrowing down the design space to regions which are likely to contain optimal designs.

F. Using a graphical user interface to select design spaces

For mistake-proofing, a graphical user interface (GUI) was created, which as a default selected the design space with the lowest bound for all parameters. The initial design was created by incrementing or decrementing any parameter, in any sequence. The GUI forced the bounds of the design spaces to fall on the boundaries shown in Table 6 and Table 7.

If a design hypercube had previously been evaluated, the algorithm notified the user, and did not re-analyze those designs. As a learning tool, the range of the design space was sometimes extended (creating multiple design spaces) before launching the

program.[11] If the range was to be extended, the GUI could copy the values from a previous hypercube, and allowed modification by incrementing or decrementing any set of parameters.

In cases where the initial design space did not contain an optimal design, the GUI was used to add additional design spaces.

G. Defining the designs

The design hypercube is created by mapping the range values of the design space to an eight factor I-optimal design.

The points of the design hypercube were coded using output from a statistical program called JMP, by SAS [36]. This design has 64 points, with one center point (run number one) and no replications. The coded design for the 8 factor I-optimal design of experiments used for validation is shown in Table 4.

Table 4, Coded I-optimal 8 factor design

Run no.	x_1	x_2	x_3	x_4	x_5	x_6	x_7	x_8
1	0	0	0	0	0	0	0	0
2	-1	-1	-1	-1	-1	-1	1	1
3	-1	-1	-1	-1	1	1	-1	-1
4	-1	-1	-1	1	1	-1	0	0
5	-1	-1	0	-1	1	1	1	1
6	-1	-1	0	1	-1	1	0	0
7	-1	-1	1	-1	0	-1	-1	-1
8	-1	-1	1	1	0	0	1	-1
9	-1	0	-1	-1	-1	0	0	-1

---

[11] Extending the design space added more data points, so that more than one hypercube could be evaluated at one time.

Run no.	x_1	x_2	x_3	x_4	x_5	x_6	x_7	x_8
10	-1	0	-1	0	0	1	1	1
11	-1	0	0	0	-1	-1	1	-1
12	-1	0	0	0	0	0	-1	0
13	-1	0	1	1	-1	-1	0	1
14	-1	0	1	1	1	1	-1	1
15	-1	1	-1	-1	-1	-1	-1	1
16	-1	1	-1	0	0	0	0	-1
17	-1	1	-1	1	1	0	1	1
18	-1	1	1	-1	-1	0	1	1
19	-1	1	1	-1	1	-1	0	0
20	-1	1	1	-1	1	1	1	-1
21	-1	1	1	1	-1	1	0	-1
22	-1	1	1	1	1	-1	-1	-1
23	0	-1	-1	-1	1	-1	1	-1
24	0	-1	-1	0	1	0	-1	1
25	0	-1	-1	1	-1	-1	-1	-1
26	0	-1	-1	1	-1	0	1	1
27	0	-1	0	0	1	0	0	-1
28	0	-1	1	-1	-1	1	1	-1
29	0	-1	1	0	-1	1	-1	1
30	0	-1	1	0	1	-1	1	1
31	0	0	-1	-1	0	1	0	1
32	0	0	-1	1	1	1	1	-1
33	0	0	0	-1	0	0	0	0
34	0	0	0	-1	1	-1	-1	1
35	0	0	0	0	0	0	1	0
36	0	0	1	0	0	0	0	0
37	0	1	-1	0	-1	-1	1	0
38	0	1	-1	1	1	1	-1	0
39	0	1	0	-1	-1	1	-1	0

Run no.	x_1	x_2	x_3	x_4	x_5	x_6	x_7	x_8
40	0	1	0	0	1	0	0	1
41	0	1	1	1	0	-1	1	0
42	1	-1	-1	-1	-1	0	-1	0
43	1	-1	-1	0	-1	1	1	-1
44	1	-1	-1	0	0	-1	0	0
45	1	-1	0	1	0	1	-1	-1
46	1	-1	0	1	1	1	0	1
47	1	-1	1	-1	1	0	1	0
48	1	-1	1	1	-1	-1	1	-1
49	1	-1	1	1	1	-1	-1	0
50	1	0	-1	1	-1	1	-1	1
51	1	0	-1	1	1	-1	1	1
52	1	0	0	-1	-1	-1	0	1
53	1	0	1	0	1	1	0	-1
54	1	0	1	1	-1	0	-1	0
55	1	1	-1	-1	1	-1	-1	-1
56	1	1	-1	-1	1	-1	1	1
57	1	1	-1	0	1	1	1	0
58	1	1	-1	1	-1	0	0	-1
59	1	1	0	-1	0	1	1	-1
60	1	1	0	1	0	-1	-1	1
61	1	1	1	-1	-1	-1	-1	-1
62	1	1	1	-1	1	1	-1	1
63	1	1	1	1	-1	1	1	1
64	1	1	1	1	1	-1	1	-1

Mapping of points

Using the I-optimal design from Table 4, and the initial design space limits from

Table 3, the algorithm created the designs to be analyzed. The designs were mapped

using Table 5. As can be seen in the table, points coded with -1 were not necessarily mapped to the smallest value, nor were points coded with +1 necessarily mapped to the largest value. Coding the points in this manner allowed adding subsequent design spaces to be created using some points from previous design spaces.

Table 5, Mapping of points from I-optimal design to dimensionless parameters

Parameter	I-Optimal Table Value		
	-1	0	1
$x_1 - R_{Spl}$ (0.4-0.5)	0.5	0.45	0.4
$x_2 - R_{SDp}$ (0.7-0.8)	0.7	0.75	0.8
$x_3 - R_{SW2}$ (0.35-0.45)	0.45	0.4	0.35
$x_4 - R_{SW3}$ (0.55-0.65)	0.65	0.6	0.55
$x_5 - R_{SDL}$ (1.414 – 2.0)	2.0	1.6818	1.414
$x_6 - R_{Web}$ (0.15-0.25)	0.25	0.2	0.15
$x_7 - R_{MDp}$ (0.15-0.25)	0.25	0.2	0.15
$x_8 - R_{Mth}$ (8.0-10.0)	10.0	9.0	8.0

Table 6 was used as the basis for Table 5. x_1 corresponded to R_{Spl}, and x_2

corresponded to R_{SDp}. The coded values were determined for R_{Spl} and for R_{SDp}. For

these, the range of the global design space extended from 0.10-0.90, and the width of a

range was 0.10. Therefore, the lowest range was from 0.10-0.20 for that factor. The

lowest range was always mapped in an ascending order, as shown in Table 6. For the next

range (0.20-0.30), the values were mapped in descending order.

Table 6, Factor, code and index values for R_{Spl} and R_{SDp}

Ascending Ranges	Index value	I-optimal coded value	x Factor value	Descending Ranges
0.10-0.20	1	-1	0.10	

Ascending Ranges	Index value	I-optimal coded value	x Factor value	Descending Ranges
	2	0	0.15	
	3	1	0.20	0.20-0.30
	4	0	0.25	
0.30-0.40	5	-1	0.30	
	6	0	0.35	
	7	1	0.40	0.40-0.50
	8	0	0.45	
0.50-0.60	9	-1	0.50	
	10	0	0.55	
	11	1	0.60	0.60-0.70
	12	0	0.65	
0.70-0.80	13	-1	0.70	
	14	0	0.75	
	15	1	0.80	

The shaded rows in Table 6 indicate the range of R_{Spl} for the initial design space, and therefore, the mapping. A (-1) in column x_1 of Table 4 would be replaced with 0.50, a (0) in column x_1 would be replaced with 0.45, and a (1) in column x_1 would be replaced with 0.40. Similarly, for R_{SDp}, a (-1) in column x_2 would be replaced with 0.70, a (0) would be replaced with 0.75 and a (1) would be replaced with 0.80.

The index value (column 2) is used to determine whether the mapping will be in ascending or descending order. If the lowest index value for the design parameter is 1, 5, 9, etc. the points are mapped in ascending order. If the lowest index value for the design parameter is 3, 7, 11, etc. the points are mapped in descending order.

Table 7 shows how the coded values are determined for R_{SW2}, R_{SW3s}, R_{Web} and R_{MDp}. For these, the range of the global design space extends from 0.05-0.95, the width of a range being 0.10. Therefore, the lowest range is from 0.05-0.15 for those factors, and is mapped in an ascending order, as shown in Table 7. For the next range (0.15-0.25), the values are mapped in descending order.

Table 7, Factor, code and index values for R_{W2s}, R_{W3s} R_{Web} and R_{MDp}

Ascending Ranges	Index value	I-optimal coded value	x Factor value	Descending Ranges
0.05-0.15	1	-1	0.05	
	2	0	0.10	
	3	1	0.15	0.15-0.25
	4	0	0.20	
0.25-0.35	5	-1	0.25	
	6	0	0.30	
	7	1	0.35	0.35-0.45
	8	0	0.40	
0.45-0.55	9	-1	0.45	
	10	0	0.50	
	11	1	0.55	0.55-0.65
	12	0	0.60	
	13	-1	0.65	

The mapping of R_{SW2}, R_{SW3}, R_{Web} and R_{MDp} is determined using Table 7. The shaded rows in Table 7 indicate the range of R_{SW2} for the initial local design space, and therefore the mapping. A (-1) in column x_3 of Table 4 would be replaced with 0.45, a (0) in column x_3 would be replaced with 0.40, and a (1) would be replaced with 0.35.

The reversal in order reduces the number of designs which must be analyzed, if the design space is to be extended. Because of the reversal in order, when two adjacent hypercubes (hypercubes which shared all common values, except for one factor) are mapped, either the value coded as (1) is common to both hypercubes, or the value coded as (-1) is common to both hypercubes. For adjacent hypercubes, this eliminates analysis of approximately one third of the designs in the adjacent design hypercube.

H.   Determining physical dimensions

The eight parameters, along with the specifications, determine most of the geometry. This section explains how geometry is determined by these parameters, as well as by the speed of the electrical machine, and by manufacturing practice. Dependencies for dimensions are shown in Table 8. The calculations for most dimensions are based on the definitions of dimensionless parameters given previously.

Table 8, Dependencies of dimensions

Dimension	Determined by:
Stator volume	Rated torque, torque density
Stator outer diameter (OD) and length	Stator volume, R_{SDL}
Rotor diameter	Stator diameter, R_{Spl}
Air gap	Rotor diameter, see (2.11)
Stator inner diameter (ID)	Rotor diameter, air gap
Slot depth	Stator OD, ID, R_{SDp}
Slot width ratios (top and bottom)	Stator ID, OD, poles, R_{SW2}, R_{SW3}, slot depth
Slot opening width	Stator ID, R_{SW2}
Tooth tip thickness (2)	Slot opening width, slot overhang angle (a specification)

Dimension	Determined by:
Tooth fillet radius	Specification (0.35mm)
Magnet thickness	Air gap, R_{MTh}
Magnet angle	Poles, R_{MDp}
Magnet length	R_{Web} , Magnet angle, post width
Magnet slot radius	Magnet thickness, lip (specification, 0.5)
Bridge width	Structural FEA
Post width	Structural FEA

Air gap and slot opening width

The air gap is determined by the following equations:

$$Gap = 1.0; \quad D_r > 355mm \tag{2.11}$$

$$Gap = 0.6777 * \ln(D_r) - 2.9771; \quad 203 < D_r < 355mm \tag{2.12}$$

$$Gap = 0.1832 * \log(D_r); \quad D_r < 203 \tag{2.13}$$

where D_r is the diameter of the rotor. The above are based on manufacturing

considerations, and input from an industry consultant.
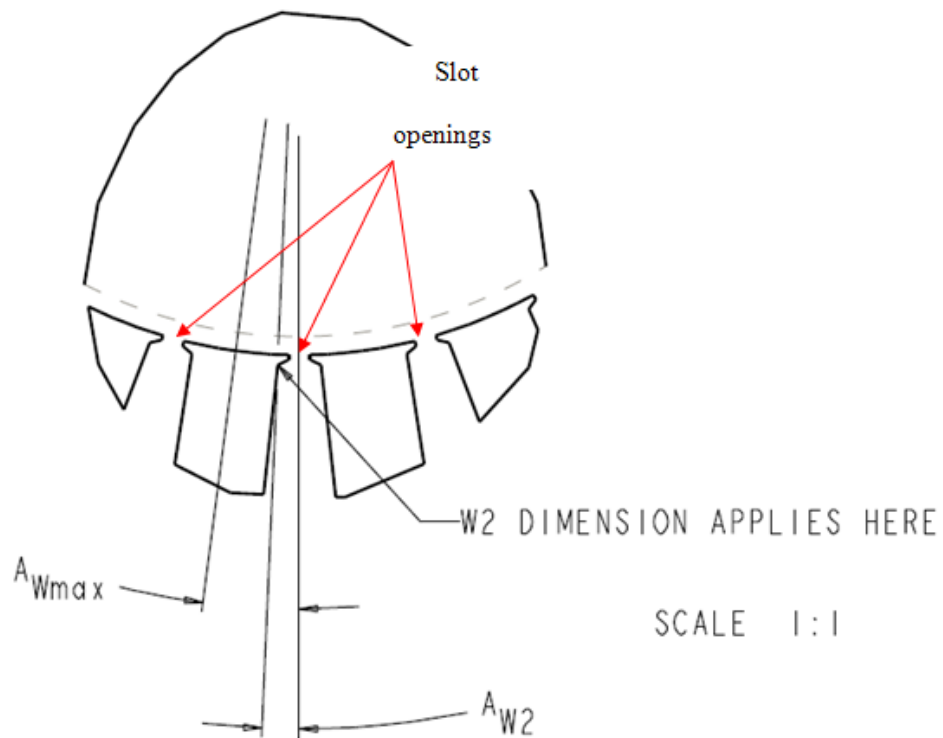
Figure 16, Upper slot width ratio (R_{SW2})

The slot opening width is not one of the parameters used to describe the response surface. The slot opening width is calculated as ½ the distance between the shoulders where the W2 dimension applies, as shown in Figure 16, and is twice the dimension A_{W1} shown in Figure 17. R_{SW2} is 0.33 in Figure 16.

Tooth tip thickness
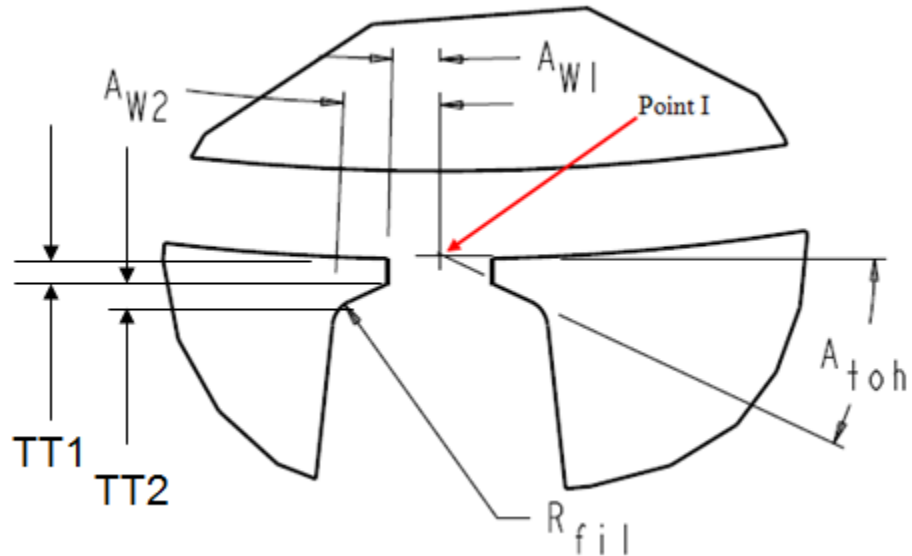
Figure 17, Tooth tip overhang angle and thicknesses

The tooth tip thicknesses (TT1 and TT2) are shown in Figure 17, and are determined by the overhang angle, and a requirement for this method that the bottom of the tooth tips intersect as shown above. Extensions of the lines which form the bottom of the tooth tip intersect on the bore of the stator at Point I. The geometry is defined so that TT1 and TT2 are equal.

Bridge and post width

The bridge and post width are determined by structural FEA. The bridge and post width determine the final rotor geometry of the part. Stresses are analyzed using structural 2D FEA. The geometry is created, and the body forces in the rotor are set to

$$F_r = \rho \omega^2 r \qquad (2.14)$$

Where F_r is the body force in the radial direction (N/m³), ρ is the density of electrical steel (7650 kg/m³), ω is the overspeed condition in the specifications (rad/sec), and r is the distance of each point from the center of the rotor (m).

The 2D model was created in MATLAB, and some details specific to MATLAB are in the appendix. As seen in Figure 18 only one half of a pole was modeled, which sped up the structural FEA. Because of symmetry, the inner surfaces of the rotor (shown in red) are constrained to remain on their original planes. As the rotor stretches, those surfaces remain coplanar with the original material.
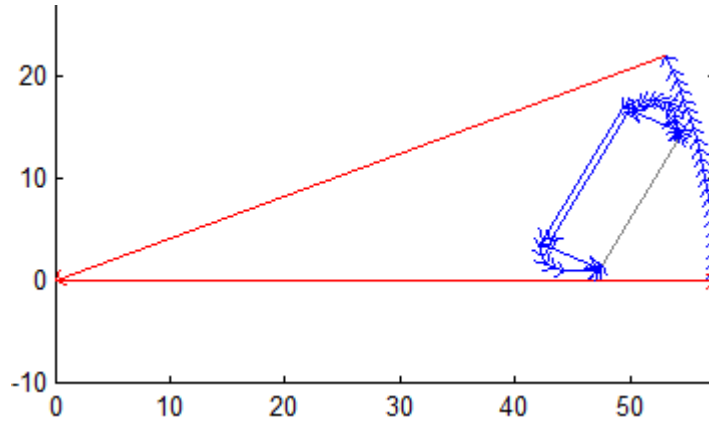
Figure 18, Boundary conditions of structural FEA model

For electrical steel, Young's modulus is equal to 200E9 Pa, Poisson's ratio, nu, is 0.29. The centrifugal forces are based on the radial acceleration:

$$a = \omega^2 r \qquad (2.15)$$

At 11,200 RPM (the peak speed used for the validation example):

$$a_{11200} = \left(\frac{2 * \pi * 11,200}{60} \right)^2 r = 1.376E6r\left(m / s^2 \right) \qquad (2.16)$$

where a_{11200} is the radial acceleration at 11,200 rpm. The body force is then:

$$k_r = \frac{F}{A} = \rho\alpha = (7650kg \ / \ m^3)(1.38E6)r = 1.05E10 \ r \ (N \ / \ m^2)$$
$$= 1.05E4 \, r \left(N \ / \ mm^2 = Pa\right)$$

(2.17)

$$k_{r11200} = 1.052 \, E \, 1 \, r_{mm} \left(N \ / \ mm^2\right)$$
$$= 1.052 \, E - 2 \, r_m \left(kPa\right)$$

(2.18)

where k_{r11200} is the force at 11200 rpm (N/mm²), A is the area (m²), r_{mm} is the radius

(mm), and r_m is the radius (m). The units of N/mm² were used, as the dimensions are

modeled in terms of mm. Forces for other speeds or units can be scaled from the above.

The initial bridge thickness was initialized to 1% of the rotor radius. If this was less

than the minimum bridge thickness allowed in the specifications, the minimum bridge

thickness was used. The minimum bridge thickness is specified based on punching

considerations, and is material and manufacturer specific. The width of the post is a

multiple of the width of the bridge, and this ratio is included as a specification.
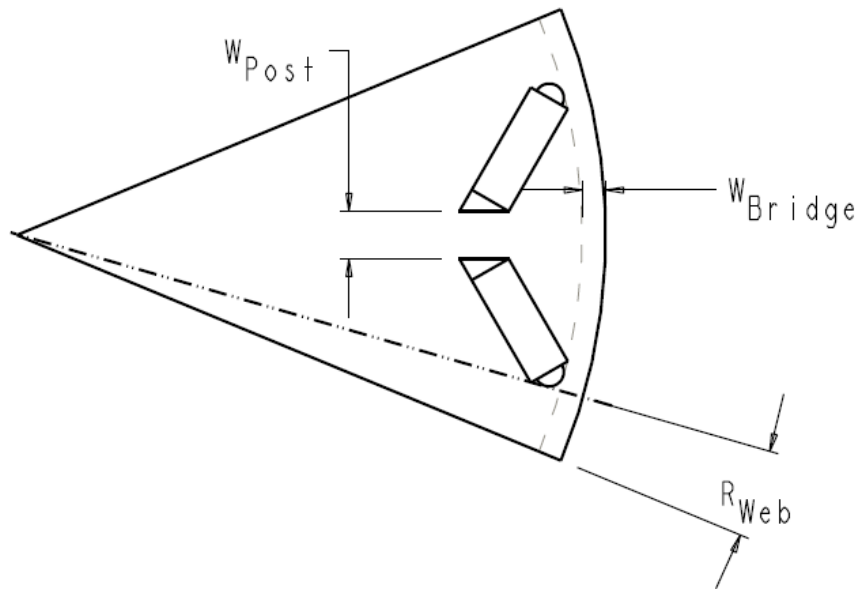
Figure 19, Dimensions for bridge and post thickness calculation, at $R_{Post} = 0.5$

The dimensions which are modified for the bridge and post calculation are shown in Figure 19. The corner of the magnet, or the arc at the end of the magnet slot (dimensioned as R_{End} in Figure 20), lie along the line dimensioned R_{Web}. The equation for the width of the post is

$$W_{Post} = R_{Post} W_{Leakage} \tag{2.19}$$

where R_{Post} is the post ratio, $W_{Leakage}$ is the leakage width (mm), and W_{Post} is the post width (mm) shown in Figure 19.

For the validation algorithms, R_{Post} was set to 0.5, so that

$$W_{Post} = 0.5 W_{Leakage} \tag{2.20}$$

$$W_{Bridge} = 0.5(1 - R_{Post})W_{Leakage} = 0.25 W_{Leakage} \tag{2.21}$$

where W_{Bridge} is the bridge width (mm).

Magnet slot post radius and end radius

Prior to structural FEA, a radius is put into the corner of the magnet slot near the post, indicated by R_{MSl} (see Figure 20). The radius is made tangent to the point where the magnet would touch the radius, if the magnet were not chamfered.

A radius is also put into the other end of the slot, near the bridge (dimensioned as R_{End}). The radius of this slot is determined by the width of the magnet, and the 'Lip' dimension, which is part of the specifications, based on manufacturing considerations.
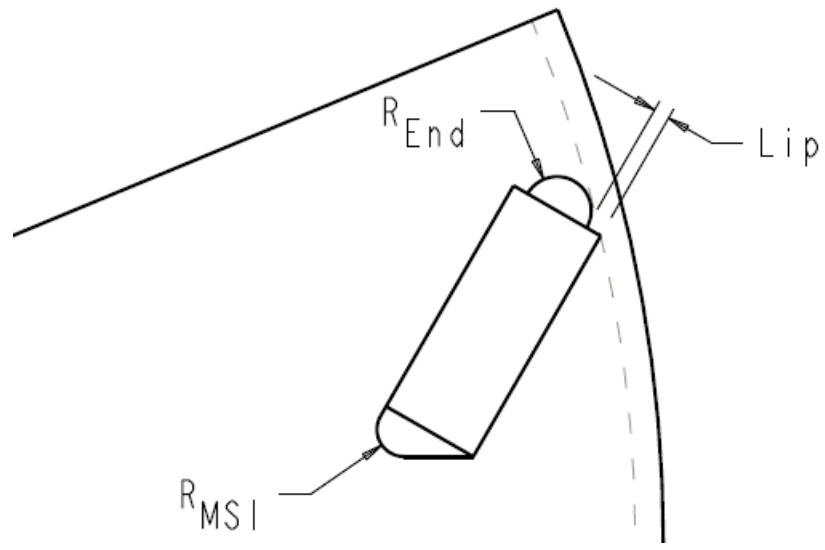
Figure 20, Detail of magnet slot radius

Structural FEA is run, and adjustments to the bridge and post are made, until the

stresses are below the yield strength of the material. A plot of convergence is shown in

Figure 21.
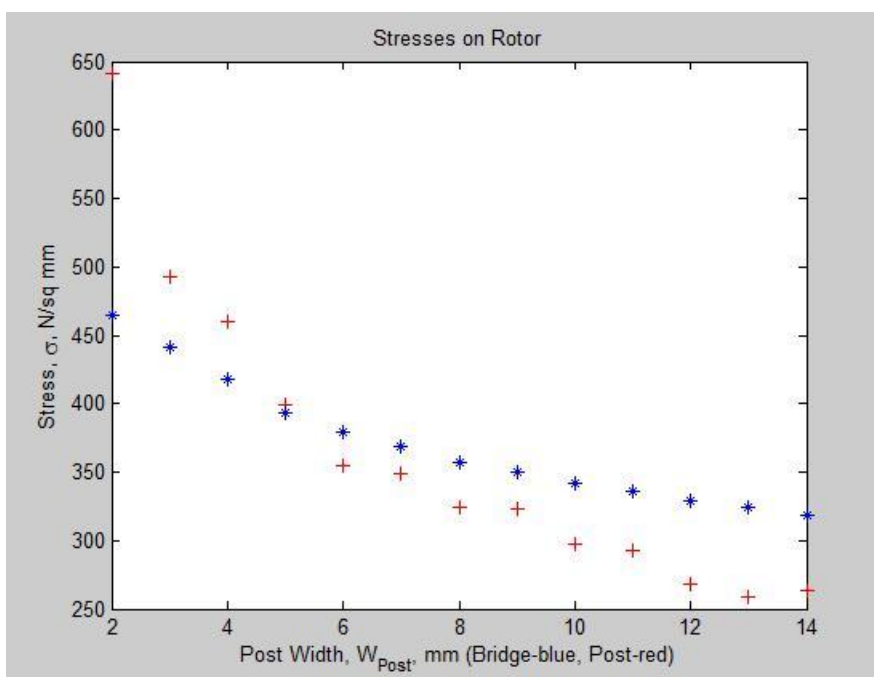
Figure 21, Convergence of bridge and post stresses with increase in post width

Qualifying the mesh, and determining the number of turns per coil

For the validation algorithms, the number of turns per coil was initialized at 7. For the turns per coil calculations, the speed of the machine is set to the maximum overspeed condition and the magnet temperature is set to the minimum magnet temperature specified (for NdFeB magnets, which have a negative temperature coefficient). The machine is analyzed with electromagnetic FEA at this speed, to determine the maximum back EMF. The number of turns is maximized below the amount which would produce the peak voltage allowed in the specification.

Finite element meshing for the structural and electromagnetic FEA is done without operator intervention. Because electromagnetic meshing sometimes failed, which required operator intervention, each of the designs was run once[12] with the operator present in case meshing failed. This was called 'qualifying the FEA mesh'. The actions below are specific to the commercial program used, but similar actions may be required by other analysis programs.

Initially, the maximum meshing angle was set to 120 degrees, and the FEA model was meshed. After this, the following could occur:

- Meshing of the model could succeed, and the algorithm qualifies each model once, successively.

- If the model fails to mesh, the commercial software returns an error message, which must be acknowledged by the operator pressing the enter key. When the operator

---

[12] Approx 4.5 seconds per design, using SPEED PC-BDC® and Windows® PC with AMD® 6000 dual core processor (available in 2008).

presses the key, the optimization algorithm increments the maximum mesh angle by 5 degrees (to 125 degrees), and attempts to mesh again.

- If this fails, the maximum mesh angle is increased to 130 degrees, and meshes again.

- If this fails, the algorithm reduces the maximum mesh angle to 115 degrees, and attempts to mesh again.

- If this fails, the algorithm reduces the maximum mesh angle to 110 degrees, and attempts to mesh again.

- When a maximum mesh angle is entered which is acceptable, this is stored automatically, and the program continues to qualify the other machine designs.

I. Analyzing machine performance

After all designs in the design hypercubes are qualified, the algorithm sets the magnet and winding temperatures to the temperatures in the specification file, and begins final analysis. The algorithm returns to the first design, and analyzes the performance of each design in order, without operator intervention. The machines are set to the low speed condition (2000 or 5000 rpm for most validation cases) and analyzed, then set to the high speed condition (6500 or 8000 rpm for most validation cases) and analyzed at rated power. Efficiencies, power levels,[13] phase angles, currents, resistive and iron losses are recorded at both speeds, along with magnet, steel and copper masses.

1. Determining the phase angle using a modified golden section search

When the machines are being analyzed, it is necessary to determine the correct current and phase angle to optimize the efficiency of the machine. A modified golden

---

[13] Power levels were stored to verify that the specification requirements had been met for each design.

section search is done to optimize the phase angle setting. The method was modified by eliminating analysis of the first and fourth points of the golden section. The efficiencies of those points is recorded as 0%, guaranteeing they will be thrown out. Following this, a standard golden section search is performed.

The range of phase angles was set from 15-55 degrees for motors. These limits are adjustable. The upper limit was determined by the designers of the inverter to be the stability limit of the controller for the specific machine being designed.

The phase angle is set to 38.1966% of the range, corresponding to the 2nd point of 4, shown as (b) in Figure 22, of a golden ratio. The current required at that point to achieve rated power is determined and the efficiency recorded. The phase angle is then set to 61.8034% of the range, corresponding to the 3rd point of a golden section, with current and efficiency recorded again.

A standard golden section search is applied as follows: if the second point (b) has higher losses than the third point (c), the 1st point (a, which has not been analyzed) is thrown away. A new point is analyzed, which is 38.1966% of the new range from point d, on the orange phantom line.
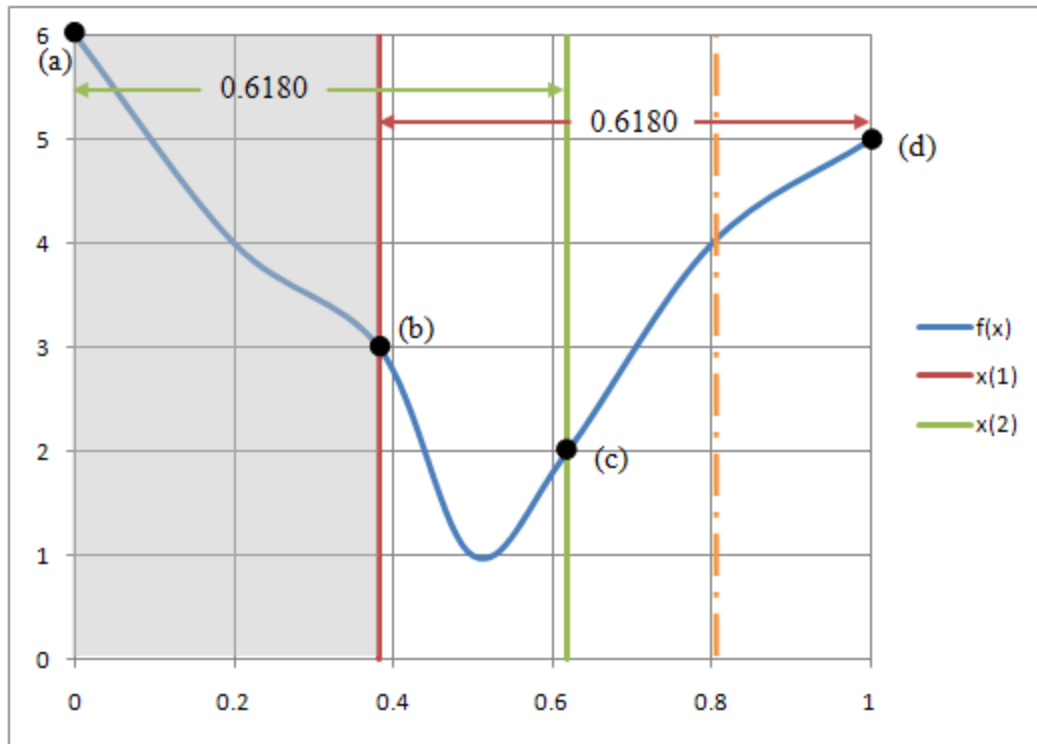
Figure 22, Illustration of golden section method, applying the golden section search to a curve

If the third point is less efficient (higher) than the second point, the inverse occurs.

The 4th point (never having been analyzed) is thrown away, and a new point is created.

This process continues for seven iterations, unless the efficiency converges prior to that.

Convergence is defined as less than 0.01% change in the last 3 data points, or seven

iterations. For a 40 degree range, 7 iterations result in a maximum 1.38 electrical degree

difference between data points (0.34 mechanical degrees for an 8 pole machine).

Modifying the golden section search for insufficient power

If a machine configuration cannot develop the required power at the phase angle

setting, the algorithm determines the current required to develop maximum power. For

this case, the golden section search algorithm eliminates regions which produce the

lowest power. This causes the algorithm to converge to the highest power achievable, up to the rated power. Phase angles which are able to achieve rated power are kept in favor of points which cannot achieve rated power. This creates a more accurate response surface than keeping efficiencies of currents which do not achieve rated power.

2. Determining the required current using a modified Newton's method

For each phase angle analysis, the correct current to achieve rated power is determined as follows:

For the first design of a new hypercube (the center point), the initial current for the first two phase angles[14] corresponding to (b) and (c) in Figure 22 is set at

$$I_1 = P_R / V_{DCLink} \tag{2.22}$$

where I_1 is the current (Amps rms), P_R is the rated power (Watts), V_{DCLink} is the DC link voltage (Volts). The initial current for the first two phase angles at the high speed is set to

$$I_2 = \frac{I_1}{CPSR} \tag{2.23}$$

where I_2 is the current at high speed (Amps, rms), $CPSR$ is the constant power speed range, which was $8{,}000/2{,}000 = 4.0$ for some of the validation examples.

For all successive designs of the hypercube, the initial guess for the first two phase angles is taken as the electrical current values from the previous design, for the corresponding phase angles. In other words, the initial current setting for the first point

---

[14] At the low speed, 2000 rpm

of the golden section search will be the value from the previous machine's analysis of the same point.

The algorithm uses the current and phase angle, and determines the efficiency, the actual current used, and the power developed at those settings. If the motor is not capable of attaining the current within a specified percentage (2% for most validation analyses), this indicates that the waveform is distorted. When this occurs, the number of turns is reduced.

Determining subsequent current settings

When the initial setting does not result in rated power, the subsequent current setting is based on a straight line approximation from (0, 0) through the first point, and intersecting with rated power, using the equations

$$m_1 = \frac{P_1}{I_1} \tag{2.24}$$

$$I_2' = m_1 P_R \tag{2.25}$$

$$\Delta I_2' = I_2' - I_1 \tag{2.26}$$

$$\Delta I_2 = k_d \, \Delta I_2'$$
$$\begin{bmatrix} if \ \Delta I_2 > 0, \ k_d = 1.3 \\ if \ \Delta I_2 < 0, \ k_d = 0.75 \end{bmatrix} \tag{2.27}$$

$$I_2 = I_1 + \Delta I_2 \tag{2.28}$$

where m_1 is the slope of line at the first point (W/Amp), P_1 is the power at the first point (W), I_1 is the current at the first point (A), I'_2 is a straight line approximation for current at the rated power (A), P_R is the rated power (W), and k_d is a correction factor.

The analysis is run with this second current setting (I_2). The solution is considered converged if the error is 0.5% or less. If convergence is not achieved on the second trial, an approximation of the current is made, using Newton's method without a correction factor.

$$m_k = \frac{P_k - P_{k-1}}{I_k - I_{k-1}} \tag{2.29}$$

$$b_k = P_k - m_k I_k \tag{2.30}$$

$$I_{k+1} = I_k + \frac{P_R - P_k}{m_k} \tag{2.31}$$

Where the subscript k is the iteration number (e.g. 2 for 2nd point, 3 for 3rd, etc), m_k is the slope of power/current line between k and k-1 point (W/A), P_k and P_{k-1} are the power at the k and k-1 points (W), I_k, and I_{k-1} are the currents at k and k-1 points (A). For design hypercubes with optimal machines, convergence is typically made on the second through fourth point.

The plots in Figure 23 show the convergence of current for one machine, at a single phase angle. The blue lines connect the current settings. The red dashed line is a straight line which passes through (0, 0). The horizontal red line is set at 50 kW (the specified power for that machine). The dashed green lines show the limits of convergence. Point 3 is shown by a small + sign on the left hand plot, at slightly below 50 kW.
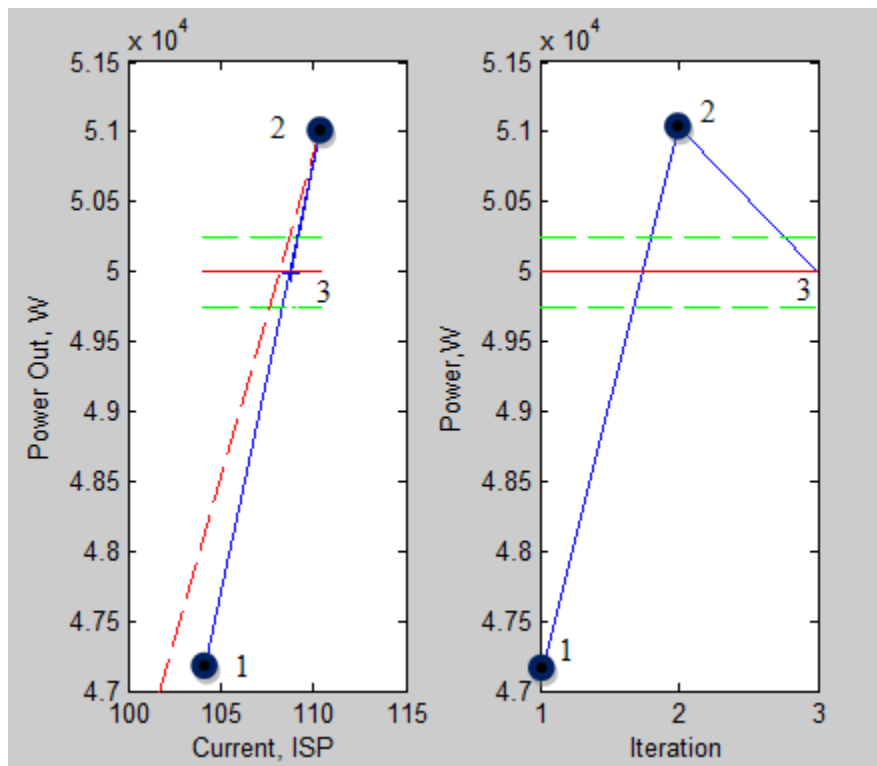
Figure 23, Plots showing convergence by modified Newton's method

The left hand plot shows current and power level. The right hand plot shows the convergence and power level, in chronological order. The first current setting (labeled 1) was at 104 Amps, and produced 47.2 kW. The second point was an estimate using the standard Newton's method, and was too high. The third point used Newton's method, and converged. As can be seen by examining the left hand plot, the curve is fairly straight in this region, which is why Newton's method is an appropriate method for this problem.

3. Determining current using a region elimination method

For some cases, it is not possible to achieve the rated power with the geometry which is created. This situation is shown in the three plots of Figure 24. These three plots are for the same data. All points labeled 1 are the same point.
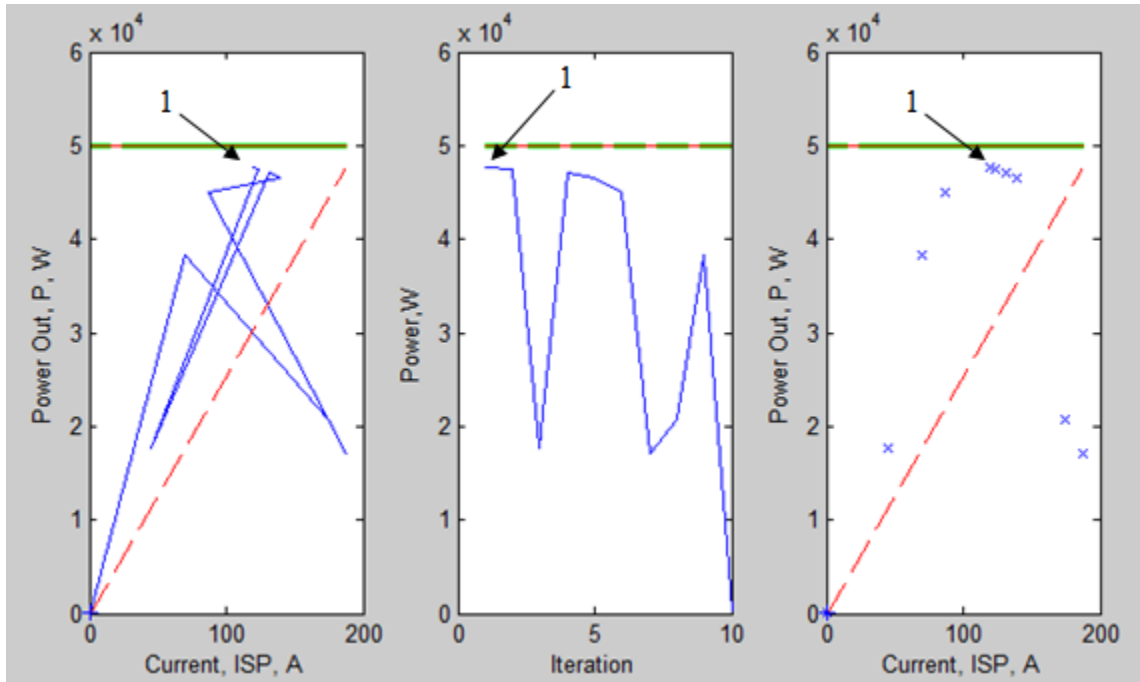
Figure 24, Non-convergence for generator, using Newton-Raphson method

The left and right-hand plots show the current vs. power values. The center plot shows the power achieved at each iteration, and is therefore a chronological plot. The first point evaluated (1) was at about 110 A, and 48 kW, the highest point shown in all plots. The Newton-Raphson method would predict that increasing the current slightly will increase the power slightly. However, the machine is operating in a condition where additional current does not result in additional power. On the left hand plot, the first point is connected by a line to a point at approximately 115 A, but at a lower power level.

Convergence was not achieved, because the geometry was not capable of achieving the rated power. The Newton-Raphson method does not converge to the highest value, but instead oscillates around the maximum value, become lower over time.

The center plot shows the values of the power achieved, for each point, in the order they were evaluated in. The right hand plot shows that the points are actually distributed in a unimodal shape. This performance is typical when rated power cannot be achieved.

For this condition, as mentioned previously, a method to achieve the maximum power possible was adopted. Region elimination methods are appropriate for this situation, such as the golden section or Fibonacci search methods.

4. Modifications to determine the current

Some objective functions may be based on minimizing current, or a combination of current and efficiency. For these cases, where the optimization function shown above was based on efficiency, these would be based on current, or a combined function. Two other possibilities exist; that current will only be part of the objective function at the highest torque requirement, or that current will be a part of this function only for the highest current requirement, which would typically be the highest torque. The method can be modified for these options.

5. Mechanical losses

If the program used for analyzing the electric machine does not analyze (or estimate) the mechanical losses, these may be added as part of the method. The bearing losses will be similar for machines of the same rating (torques and speeds), as there is no reason from the machine specification that the bearing losses would be different. Bearing losses

could be estimated and included in the method, but were not included in the validation work, as they do not affect the relative efficiency of the machines. The bearing losses can be calculated before (or after) the electromagnetic calculations, but do not need to be part of the calculations performed on each run of the machine. They will have a slight impact on the current requirement.

Mechanical loss calculations below come from [37].

Bearing loss

The bearing loss equation used is:

$$P_{\rho,bearing} = 0.5\Omega\mu_f F D_{bearing}$$

(2.32)

where Ω is the mechanical angular frequency of the shaft supporting the bearing (rad/sec), μ_f is the friction coefficient (typically 0.001-0.0050), F is the bearing load (N), and $D_{bearing}$ is the inner diameter of the bearing (m).

Air gap windage losses

Windage losses in the air gap may be calculated from the equation:

$$P_{\rho,w1} = \frac{1}{32} k C_M \pi \rho \Omega^3 D_r^4 l_r$$

(2.33)

where k is the roughness coefficient (for a smooth surface k = 1, usually 1-1.4), C_M is the torque coefficient, ρ is the density of the coolant (kg/m^3), D_r is the diameter of the rotor (m), and l_r is the rotor length (m).

The torque coefficient is dependent on the Couette Reynold's number:

$$Re_\delta = \frac{\rho \Omega D_r \delta}{2\mu}$$

(2.34)

where δ is the air gap length (m), μ is the dynamic viscosity of the coolant (N-s/m^2).

$$C_M = 10\frac{(2\delta/D_r)^{0.3}}{Re_\delta}, \; Re_\delta < 64 \tag{2.35}$$

$$C_M = 2\frac{(2\delta/D_r)^{0.3}}{Re_\delta^{0.6}}, \; 64 < Re_\delta < 500 \tag{2.36}$$

$$C_M = 1.03\frac{(2\delta/D_r)^{0.3}}{Re_\delta^{0.5}}, \; 500 < Re_\delta < 10^4 \tag{2.37}$$

$$C_M = 0.065\frac{(2\delta/D_r)^{0.3}}{Re_\delta^{0.2}}, \; Re_\delta > 10^4 \tag{2.38}$$

Rotor end windage losses

Losses at the end of the rotor (assuming no fan blades) can be calculated from the following equations:

$$P_{\rho,w2} = \frac{1}{64}C_M\rho\Omega^3\left(D_r^5 - D_{ri}^5\right) \tag{2.39}$$

where D_{ri} is the shaft diameter (m).

The torque coefficient is dependent on the Couette Reynold's number:

$$Re_r = \frac{\rho\Omega D_r^2}{4\mu} \tag{2.40}$$

Some viscosities for air at standard pressure are:

$$\mu_{air} \approx 2.2E-5 \; @100C$$
$$\mu_{air} \approx 2.38E-5 \; @140C \tag{2.41}$$
$$\mu_{air} \approx 2.55E-5 \; @180C$$

C_M for this equation of rotor end windage losses is defined as:

$$C_M = \frac{3.87}{Re_r^{0.5}}, \quad Re_r < 3 \times 10^5 \tag{2.42}$$

$$C_M = \frac{0.146}{Re_r^{0.2}}, \quad Re_r > 3 \times 10^5 \tag{2.43}$$

Total windage losses are calculated as:

$$P_{\rho w} = P_{\rho w1} + P_{\rho w2} \tag{2.44}$$

Other windage losses may be present, for example if fins are on the end of the rotor, or oil spray is directed at the rotor. The effects of oil mist in the air, or in the air gap are not included in the above calculations.

J.   Defining the objective function

Objective functions were defined and coded as algorithms. They can include efficiency of the electric machine, or of the system including controller; masses of steel, copper and magnet; or cost, rotor inertia, electrical current, etc.

For validation, two objective functions were used, both of the form

$$F(X) = -\min\big(\eta(N,P)\big) \tag{2.45}$$

where $F(X)$ is the objective function, X is the parameter array, η is the efficiency of the electric machine or the system, N is the speed (rpm), and P is the mechanical or electrical power out (W). For the motor design validation done for this research, the objective function was based on the above equation for 2000 and 8000 rpm, maximizing the efficiency of the machine at two speeds. For generator design, validation was done at approximately 5000 and 7000 rpm. This objective function was used for a number of power levels, from 20 kW up to 200 kW.

For validation, two other objective functions were also used. The first maximized system efficiency at both speeds (the machine and power electronics), the second maximized the efficiency of the machine at two speeds, and at two power levels (N_1, P_1) and (N_2, P_2).

Objective functions can be written before or after machine performance analysis occurs. Analyses must be redone if the required data (power, current, masses, efficiency, etc) was not collected, so a significant amount of data was recorded which was not necessarily required, in case the objective functions were redefined.

K.   Creating the response surfaces

After the 64 machines of the design hypercube are analyzed, response surfaces are created using a least squares fit. The model was of the form:

$$\eta_n = \beta_0 + \sum_{i=1}^{8} \beta_i x_i + \sum_{i=1}^{8} \beta_{ii} x_i^2 + \sum_{i \neq j}^{8} \beta_{ij} x_i x_j + \varepsilon \tag{2.46}$$

or

$$\eta_n = X\beta + \varepsilon \tag{2.47}$$

where η_n is the power at speed n (W), β_i are the coefficients for main effects, β_{ij} are the coefficients for interactions, β_{ii} are the coefficients for quadratic effects, β is the array of coefficients, and X is the array of dimensionless parameters. The model has 45 coefficients, and formed the 8 dimensional response 'surface'.

L.   Optimizing the response surfaces

The optimal design of the response surface was determined using the MATLAB function fmincon, which finds the minimum of a constrained non-linear multivariable function. The bounds of the function were set as the bounds of the local design space. Contour plots were created, so that the response could be visualized.
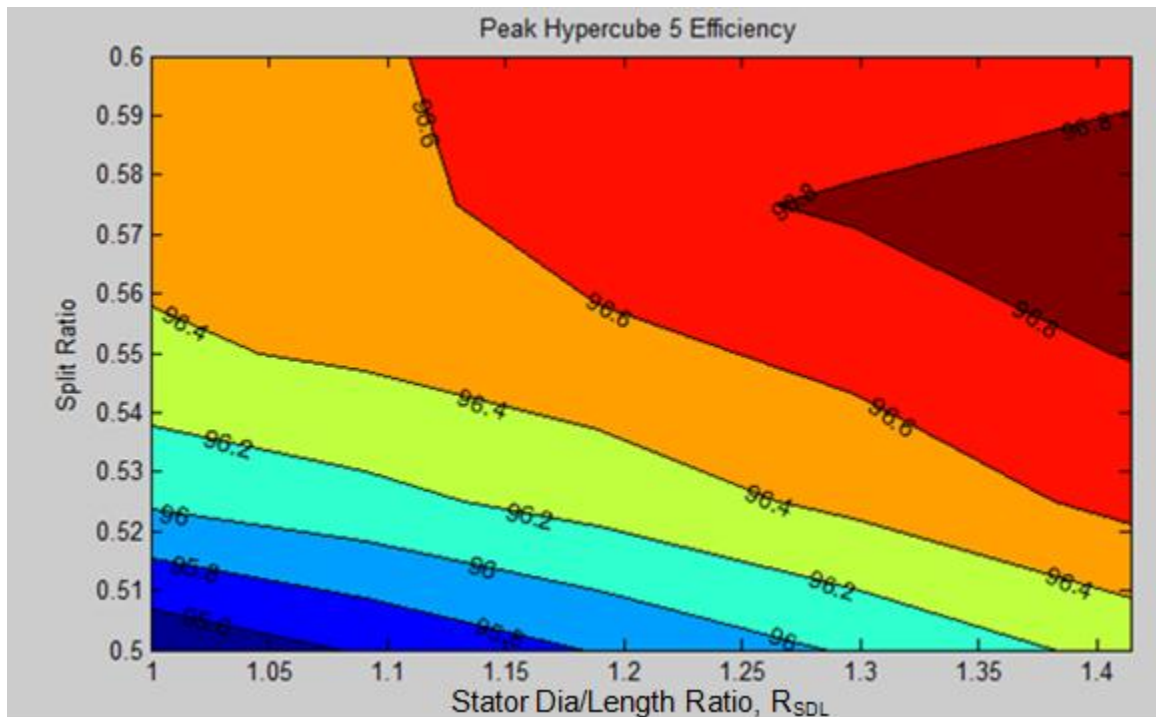
Figure 25, Response surface of one hypercube

For the plot shown in Figure 25, the optimal design is to the right of the hypercube. This plot was made while creating a 'map' of a large portion of the design space, for reference.

When the optimal point is interior to the defined design space, or is on a constraint boundary, convergence has been achieved. The optimal design is then modeled and analyzed, yielding the final design. When convergence is not achieved, the method

determines which direction the optimal design may be found in. A design space is created for this region, and the new design space is analyzed and modeled.

M.   Validating the method – comparison to contracted designs

Two generators (20 kW and 50 kW) had previously been designed and built by an electric machine manufacturer. The materials, specifications and test data were available for those machines. The SPEED models which had been used for their design were also available, giving analytical predictions for the performance of the machines.

The specifications were entered into the data sheets. Previous design work on a 60 kW motor with different operating speeds indicated ranges of parameters which were optimal for the machines. These ranges were used as the initial ranges, with the revised specifications entered.

The same control algorithm was used for the optimized design as had been used for the contracted design, in order to maintain a fair basis for comparison. These results were compared to the results from the SPEED model of the generators, designed earlier using traditional design methods.

N.   Validating the method – comparison to the fmincon MATLAB function

The fmincon MATLAB function finds the minimum of a constrained nonlinear function. In the application of the method developed by this research, the fmincon function is used with DO after response surface models have been created. An alternate method of optimization would be to use the dimensioning scheme created for this research (dimensionless parameters), but not create an RSM. Instead, the optimization could be driven directly by a GA or another optimization method. In order to compare

dimensionless optimization (DO) with other optimization methods, DO was contrasted to the use of the fmincon function.

The method developed for this research was applied to 5 design spaces, for a 25 kW machine. The same dimensionless parameter definitions (R_{Spl}, R_{SDp}, etc) and ranges were used for both optimization methods. The dimensionless parameters for the design spaces are given in Table 9. These design spaces were assumed to be near the expected optimum design. The number of machines evaluated, and the efficiencies of those machines were determined. Parameter ranges which are different from the ranges of design space 1 are shaded.

Table 9, Design spaces used for comparing dimensionless optimization (DO) with fmincon function

Design Space	R_{Spl}	R_{SDp}	R_{SW2}	R_{SW3}	R_{SDL}	R_{Web}	R_{MDp}	R_{MTh}
1	0.55-0.65	0.55-0.65	0.4-0.5	0.45-0.55	2.0-2.82	0.2-0.3	0.1-0.2	6-8
2	0.55-0.65	0.65-0.75	0.4-0.5	0.45-0.55	2.0-2.82	0.2-0.3	0.1-0.2	6-8
3	0.65-0.75	0.55-0.65	0.4-0.5	0.45-0.55	2.0-2.82	0.2-0.3	0.1-0.2	6-8
4	0.65-0.75	0.65-0.75	0.4-0.5	0.45-0.55	2.0-2.82	0.2-0.3	0.1-0.2	6-8
5	0.65-0.75	0.65-0.75	0.4-0.5	0.45-0.55	2.0-2.82	0.2-0.3	0.2-0.3	6-8

O.   Validating the method – machine sizes optimized

To validate the method, this method was implemented using MATLAB algorithms, and a commercially available program (SPEED). Motors and generators were designed using this method from 25kW to 200 kW in power. This method can probably be extended beyond this range, up to the limitations of the analysis program. At certain levels of power and speed, the constraints given in Table 10 are no longer reasonable, so

that voltage and current levels would need to change. At certain levels of speed and rotor

diameter, the bridge thicknesses required may become so large that excessive flux

leakage makes the machines extremely inefficient.

For most of the validation work, the specifications shown in Table 10 were used,

unless otherwise noted.

Table 10, Electric machine specifications for validation

Performance Specifications		Material specifications	
Speed and Power	2000 & 8000 rpm (motors), 5000 & 7000 rpm (generators)	Lamination material and thickness	M19-29 ga [0.35mm]
Overspeed condition	140% of max operating speed	Magnet material	L35UHT NdFeB
Torque density	50 Nm/liter[15]	Maximum material stress allowed	250 kPa
Machine specifications		Geometry Specifications	
3 phases		Stator specifications	
Number of poles	8	Slot shape	round bottom[16]
Slots per pole	6	Maximum diameter	NA
Throw	5	Rotor specifications	
Skew	None	Magnet slot shape	V, with center spoke
Parallel paths in the winding	4	Magnet slot lip	1.0 mm
DC link voltage	700 V	Corner radius	0.4mm
Maximum back-EMF	900 V	Minimum bridge thickness[17]	1%

---

[15] Liters of stator volume envelope. The validation work related to the contracted generator design was done at 30 Nm/liter, identical to the specification for the contracted design.
[16] 'HW' option in SPEED
[17] as percentage of rotor radius

Performance Specifications		Material specifications	
Power level	25, 50, 100, 200 kW		
Environment		Controller definition[18]	
Winding temperature for analysis	140 °C	Drive type	sine
Magnet temperature for analysis	140 °C	Max phase angle [19]	55 °
Min magnet temperature for back EMF	-10 °C		

For validation, a portion of the design space was selected using the GUI. For the initial design space, the program generated and analyzed 64 machine designs. Response surfaces were created, and the optimal design was predicted. The response surfaces were displayed, as well as the deviation of the data points from the response surface model.

The variances of the models at both high and low speeds were reported, as well as a display of the actual vs. calculated efficiencies.

---

[18] The input variables for controllers depend on the type of controller, all are not listed here
[19] For motors, specified to the author to make controllability of the inverter better

CHAPTER III.   RESULTS

The primary goal of this research is to create a rapid method for optimizing IPM machines. This was achieved by creating a method which uses dimensionless parameters; and which allowed rapid setup of the design space; selecting an optimal design which required only 64 machine designs to form a response surface; creating methods to speed up the analysis of those designs; and the use of multiple response surfaces to create the objective functions.

The effectiveness of this method can be measured in two ways; the quality of the designs the method generated, and the number of function evaluations it took to achieve those solutions.

Quantifiable results include the performance of the machine (efficiency, current requirements, etc), the number of function evaluations necessary to analyze each machine, and the number of machines which must be analyzed to achieve an optimal design. Non-quantifiable results include creating a method which considers the structural stresses in the rotor, creating a method which makes it simpler to visualize the designs, creating a method which allows for better initial guesses, and eliminating data entry mistakes.

A.   Efficiency comparison with contracted designs

A specification for 20 kW and 50 kW electric generators had been developed. The specification included performance points, as well as overspeed and transient conditions. These were released to a manufacturer that designed and produced electric machines.

The machines were built and tested. SPEED [38] software models of the electric machines, created by the manufacturer were available.

To validate the method developed by this research, the same specifications and materials were entered into the algorithm written to validate this method.

1. The 50 kW machine comparison

The 50 kW machine had a specified maximum stator diameter, which yielded a stator aspect ratio of 1.5656. As the stator aspect ratio was defined from the specification, this became an upper bound of the stator aspect ratio, $R_{SDL.}$ Boundaries of 1.41 to 2.0 were used, as these boundaries were already available in the validation software. The initial bounds entered into the program are shown in Table 11. These bounds were chosen based on earlier design work of a 60 kW machine with a larger aspect ratio.

Table 11, Initial bounds for 50 kW machine

Parameter	Design space limitation	Design range	Parameter	Design space limitation	Design Range
R_{Spl}	0.55-0. 65	0.10	R_{SDL}	1.41 – 2.0 (specification)	$x_u = x_l \times \sqrt{2}$
R_{SDp}	0.70-0.80	0.10	R_{Web}	00.15-0.25	0.10
R_{SW2}	0.40-0.50	0.10	R_{MDp}	0.20-0.30	0.10
R_{SW3}	0.55-0.65	0.10	R_{MTh}	8.0-10.0	2.0

The 50 kW machine design created by the manufacturer had computed efficiencies of 94.96% at 4913 RPM, and 94.55% at 6937 RPM. After 65 machines had been analyzed, (the 64 machines required to create the response surfaces, and the final optimized design) the machine designed using the method of this research had computed efficiencies of

96.30% and 96.23% at the same speeds. In terms of heat rejection (waste), the change is from 5.04% at 4913 RPM and 5.45% at 6937 RPM to 3.70% and 3.77% at the same speeds. This is a reduction of 26.6% of heat reduction at the lower speed, and 30.8% at the higher speed.

Both machines used the same materials and electronic control parameters (switching frequencies, controller modes, etc.).

The analyses of these 64 machines took 6 hours and 45 minutes[20]. A second design space was not analyzed (the initial guess being good enough). The number of function evaluations for the 64 designs was 3386. The amount of time (in man-hours or computer hours) used by the supplier, or the number of function evaluations executed was not available. Therefore, a comparison in terms of time cannot be made.

Analysis of the optimized machine took 6 minutes, and 59 function evaluations. This specific machine (as well as others in the design space) had phase angles which could not achieve rated power, and therefore took more objective function calls than was typical when designing a motor.

Other comparisons are shown in Table 12. A slightly larger magnet mass was used in the optimized design. While the length and stator diameter were the same, the rotor diameter of the optimized machine was smaller, and the coil slots were slightly larger in every dimension. Therefore, the teeth were slightly narrower.

---

[20] A longer computation time, and a higher number of objective function evaluations was required in analyzing these generators compared to previous work on motor designs.

Table 12, Comparison of the optimized and contracted 50 kW designs

		Contracted design	Optimized design	Change
4937 RPM	Efficiency	94.96%	96.30%	1.34%
	Heat rejection, %	5.04%	3.70%	-26.6% [21]
	Losses, Copper, %	2.90%	2.41%	
	Losses, Iron, %	1.89%	1.04%	
	Current, A rms	114.09	121.60	7.51
6913 RPM	Efficiency	94.55%	96.23%	1.68%
	Heat rejection,%	5.45%	3.77%	-30.8% [21]
	Losses, Copper, %	1.49%	1.23%	
	Losses, Iron, %	3.63%	2.21%	
	Current, A rms	82.91	83.00	0.09
Dimensions and masses	Stator OD, mm	191		
	Stack Length, mm	122		
	Rotor OD, mm	124	113.76	-10.24
	Gap, mm	0.5	0.6235	
	Slot opening width, mm	2.5	1.9119	
	Magnet Thickness, mm	4.7	6.2352	
	Magnet mass, kg	1.1015	1.3816	0.28
	Copper mass, kg	4.3296	5.6527	1.32
	Steel mass, kg	18.8808	16.2098	-2.67
	Rotor mass, kg	9.51	7.95	-1.56

Figure 26 shows the lamination designs for the two machines. An overlay, as well as

FEA figures of the laminations for these two machines is located in the appendices.

---

[21] The change is shown as compared to the total heat rejection
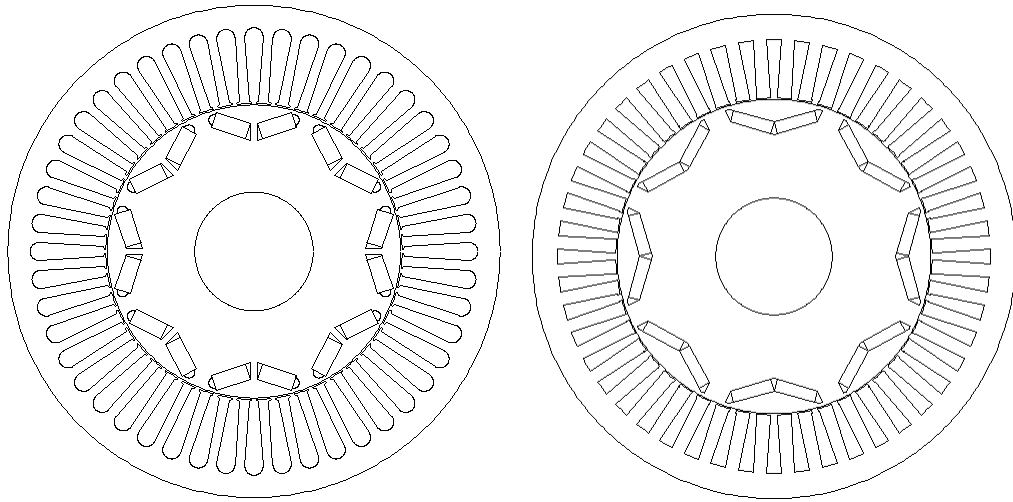
Figure 26, 50 kW optimized design resulting from this research (left) and contracted design (right)

The dimensionless parameters for this design are shown in Table 13.

Table 13, Dimensionless parameters for the optimized 50 kW machine

Parameter	Design space limitation	Parameter	Design space limitation
R_{Spl}	0.5957	R_{SDL}	1.5656 (specification)
R_{SDp}	0.7731	R_{Web}	0.15
R_{SW2}	0.50	R_{MDp}	0.2550
R_{SW3}	0.65	R_{MTh}	10.0

2. The 20 kW machine comparison

The 20 kW machine had a maximum stator diameter which yielded a stator aspect ratio of 3.9139. As the stator aspect ratio was defined from the specification, this became an upper bound of the stator aspect ratio, $R_{SDL.}$ Boundaries of 2.83 to 4.0 were used, as these boundaries were available in the validation software. The initial bounds entered into the program are shown in Table 11.

Table 14, Initial bounds for the 20 kW machine

Parameter	Design space limitation	Design range	Parameter	Design space limitation	Design Range
R_{Spl}	0.55-0.65	0.10	R_{SDL}	2.83 – 4.0 (specification)	$x_u = x_l \times \sqrt{2}$
R_{SDp}	0.70-0.80	0.10	R_{Web}	0.10-0.20	0.10
R_{SW2}	0.40-0.50	0.10	R_{MDp}	0.10-0.20	0.10
R_{SW3}	0.45-0.55	0.10	R_{MTh}	6.0-8.0	2.0

The 20 kW machine design created by the manufacturer had computed efficiencies of 93.47% at 4913 RPM (at 75°C), and 93.23% at 6937 RPM. After 65 machines had been analyzed, (the 64 machines required to create the response surfaces, and the final optimized design) the machine designed using the method of this research had computed efficiencies of 95.25% and 95.87% at the same speeds. In terms of heat rejection (waste), the change is from 6.52% at 4913 RPM and 6.77% at 6937 RPM to 4.75% and 4.13% at the same speeds. This is a reduction of 27.4% of heat reduction at the lower speed, and 40.9% at the higher speed.

Both machines used the same materials and electronic control parameters (switching frequencies, controller modes, etc.).

Analysis of the optimized machine took 7.4 minutes, and 86 function evaluations. Other comparisons are shown in Table 12. While the length and stator diameter were the same, the rotor diameter of the optimized machine was smaller, and the coil slots were slightly larger in every dimension. Therefore, the teeth were slightly narrower.

Table 15, Comparison of the optimized and contracted designs

		Contracted design	Optimized design	Change
4937 RPM	Efficiency	93.47%	95.25%	-2.59%
	Heat rejection, %	6.52%	4.75%	-27.4%[22]
	Losses, Copper, %	3.88%	3.65%	
	Losses, Iron, %	2.64%	1.10%	
	Current, A rms	42.54	33.38	-21.5%
6913 RPM	Efficiency	93.23%	95.87%	-2.64%
	Heat rejection, %	6.77%	4.13%	-40.9%
	Losses, Copper, %	2.01%	1.96%	
	Losses, Iron, %	4.76%	2.15%	
	Current, A rms	30.98	24.47	-21.0%
Dimensions and masses	Stator OD, mm	191		
	Stack Length, mm	48.8		
	Rotor OD, mm	124	107.02	
	Gap, mm	0.50	0.6235	
	Slot opening width, mm	2.70	1.66	
	Magnet Thickness, mm	4.70	4.99	
	Magnet mass, kg	0.49	0.40	-18.4%
	Copper mass, kg	2.86	3.26	+14.0%
	Steel mass, kg	7.51	7.51	–
	Rotor mass, kg	6.33	3.54	-44.1%

For both machines, the efficiencies of the optimized designs were higher than the efficiencies of the contracted designs. Efficiencies were improved at both high and low speeds, and in the copper and iron. Table 16 gives the dimensionless parameters for the optimized 20 kW machine.

[22] The change is shown as compared to the total heat rejection

Table 16, Dimensionless parameters for the optimized 20 kW machine

Parameter	Design space limitation	Parameter	Design space limitation
R_{Spl}	0.5603	R_{SDL}	3.9139 (specification)
R_{SDp}	0.75	R_{Web}	0.1965
R_{SW2}	0.4622	R_{MDp}	0.1818
R_{SW3}	0.55	R_{MTh}	8.0

B.   Comparison of DO to the fmincon MATLAB function

Table 17 shows the number of machines evaluated by each method, and the

efficiencies each method attained. Table 9 (p. 72) shows the design spaces used for this

comparison. The number of machines to evaluate each hypercube design using the

dimensionless optimization method is shown as 64 for each design. The cumulative

number of machines evaluated using the DO method, however, is not 64 X 5, due to the

sharing of data points with adjacent design spaces. The cumulative number of machines

evaluated using the fmincon function is additive, as none of the designs are shared with

adjacent design spaces.

Table 17, Performance of dimensionless optimization (DO) vs. the fmincon MATLAB function

Design Space	Efficiency (DO)	Efficiency (Fmincon)	Machines Evaluated (DO)	Machines Evaluated (fmincon)
1	88.997	88.681	64	113
2	87.247	88.691	64	65
3	89.767	88.810	64	160

Design Space	Efficiency (DO)	Efficiency (Fmincon)	Machines Evaluated (DO)	Machines Evaluated (fmincon)
4	89.710	88.971	64	250
5	89.722	87.431	64	274
Total			213	862

A plot showing the evaluation of each machine for design space 3 (see Table 17) is shown in Figure 27. The plus signs are the efficiencies of the machines at low speed (2000 rpm), which for this design space were always lower than the efficiencies at high speed (8000 rpm).
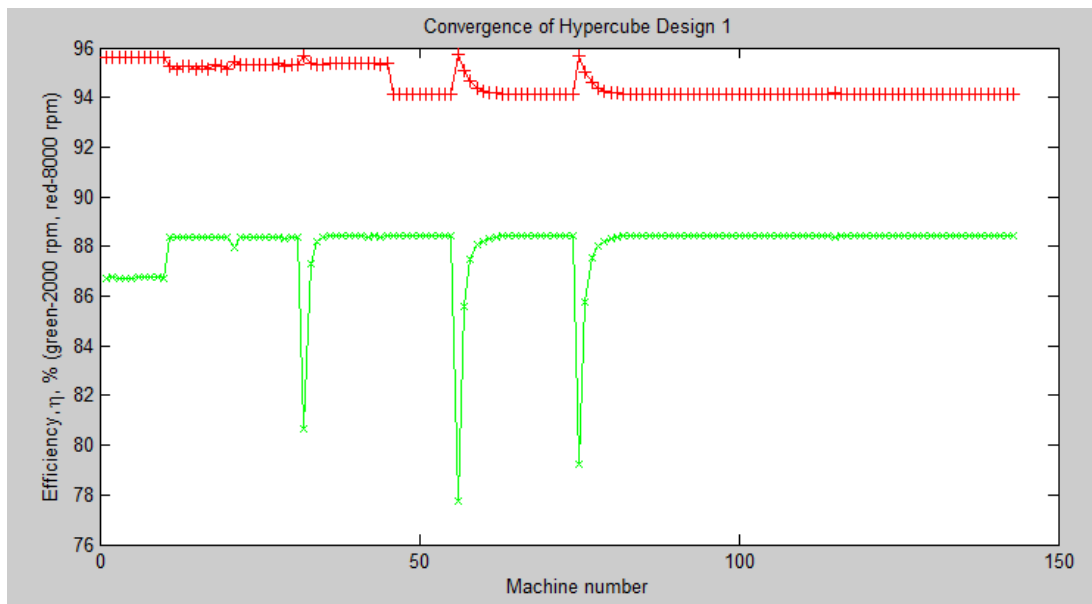
Figure 27, Plot of convergence using fmincon MATLAB function

C.   Variance obtained from a range of designs

Table 18 shows the variance for a number of design hypercubes which were run, for both motors and generators, from 25 kW to 100 kW. The dimensionless parameter value listed in the table is the lowest value in that range. As an example, if the value of R_{Spl} is

shown as 0.55, the value for the range used for that machine would be 0.55 to 0.65. The

hypercube index indicates which design hypercubes were identical, e.g. 25 kW generator

(A) and 100 kW generator (A) used the same hypercube design.

Table 18, Variance of machines designed using this method

Machine description (Hypercube index)	Design Hypercube Dimensionless parameters				Variance Low speed / High speed
	RSpl RSDL	RSDp RWeb	RW2S RMDp	RW3S RMTh	
25 kW generator[23] (A)	0.55 1.41	0.70 0.15	0.40 0.20	0.55 8.0	1.2423 / 0.6346
25 kW generator (B)	0.55 2.00	0.70 0.15	0.40 0.20	0.55 8.0	0.5426 / 0.1667
25 kW generator (C)	0.55 2.83	0.70 0.15	0.40 0.20	0.55 8.0	0.0871 / 0.0347
100 kW generator (A)	0.55 1.41	0.70 0.15	0.40 0.20	0.55 8.0	0.0034 / 0.0101
100 kW generator (B)	0.55 2.00	0.70 0.15	0.40 0.20	0.55 8.0	0.0020 / 0.0056
100 kW generator (C)	0.55 2.83	0.70 0.15	0.40 0.20	0.55 8.0	0.0031 / 0.0114
25 kW motor (D)	0.55 2.0	0.55 0.20	0.40 0.10	0.45 6.0	0.5892 / 0.0006
100 kW motor (E)	0.55 2.0	0.55 0.20	0.40 0.10	0.45 8.0	0.2640 / 0.0255
100 kW motor (D)	0.55 2.0	0.55 0.20	0.40 0.10	0.45 6.0	0.0885 / 0.0319

---

[23] 13 of the 64 machines in this design space could not achieve the rated power, regardless of phase angle and current.

The first 25 kW generator design space (A) had excessive variance, however. 13 of the 64 machines in that design space could not achieve rated power. The design spaces for each machine family (e.g. 25 kW generator) are listed in the order in which they were run.

D.   The rapidity of the method

The rapidity of the method can be measured in terms of time, or in terms of the number of function evaluations. Measurement in terms of time is dependent on the computer and software used to run the algorithms. For this reason, rapidity was measured in terms of the number of function evaluations required. References in this text to physical measurements of time are given to create some understanding for the general amount of time required.

Definition of 'function evaluation'

The term 'function evaluation' can have any of the following meanings:

- Measuring performance of a single design at all performance points
- Measuring the performance of a single design at one performance point
- The evaluation of a machine's performance at one specific current level, phase angle, and speed setting

The last definition leads to a comparison which most directly correlates with the amount of computational time required for the method, and was therefore used for this research. Reducing the number of times each machine must be analyzed at each setting of current, phase angle and speed reduces the total design time. Reducing the number of machines which must be analyzed also reduces the total design time.

1. Reducing the number of designs which require analysis to 193

The initial methods used for this research employed genetic algorithms (GAs), varying 10 dimensions. These 10 dimensions used standard units (millimeters and degrees). The computer program analyzed 2400 designs, and ran for approximately 7 days. These analyses were run at only one phase angle, rather than having the algorithm determine the optimum phase angles and currents as is done using the method developed by this research.

A significant amount of optimization work on electric machines has been done using GAs, but researchers report that a large number of machine designs must be analyzed to find the optimum. This is true even when the design space is significantly restricted. A majority of this research is performed using analytic equations. For an accurate analysis of IPM machines, FEA is required. Because of the need to use electromagnetic FEA as part of the analysis process, it was necessary to choose a method which required fewer machines to be analyzed in the search for the optimum.

The method developed in this research forms a set of response surfaces based on 64 designs. The output of these response surfaces indicates the location of the next set of designs, which at most would be an additional 64 designs. If only one variable must be modified, 43 additional designs will typically be required. The output of the second response surface indicates the location of the third set of designs, if necessary, which could be an additional 64 designs. At the end of this analysis, the range of the design space covered could be 50% of the range of any given parameter, assuming one parameter increased or decreased both times. Therefore, with 192 machine designs, plus

an additional analysis of the proposed design, a good electromagnetic design of an electric machine can be obtained.

A set of 64 machine designs can be analyzed in approximately 3 to 6 hours. This is based on an objective function which is evaluated at two speeds or power levels.[24] If it was necessary to analyze three hypercubes at these two speeds, this analysis could be done in approximately 9 to 18 hours.

The reduction from thousands of machine designs required to use GA compared to 193 is a significant reduction. The 64 machine design space for the 50 kW machine referenced in A. Efficiency comparison with contracted design (p. 75) required 3386 function evaluations, and determined the physical dimensions as well as the current and phase angle requirements at both speeds for optimum performance.

2. Reducing the number of function evaluations

The work above reduced the number of machines to be analyzed. Research was also done on methods to reduce the number of function evaluations required to determine the performance of a given motor design. During the validation portion of the research, a record was kept of the number of function evaluations made on over 900 motor designs at two performance points. There were a total of 26,488 function evaluations made for 1800 performance points, or 14.72 function evaluations per performance point.

Table 19 shows the number of function evaluations during the latter stages of the research. In order to compare the speed of the method, a design space of 64 specific

---

[24] Computer had AMD 6000+ dual core processor, running Windows Vista, and using SPEED PC-BDC with FEA. PC-BDC used only one core of the processor. The settings used have a significant impact on solution speed.

designs was selected. As the method was modified, the number of function evaluations to

analyze these 64 designs was counted. This allowed for a means of comparison.

Table 19, Object function evaluations to analyze 64 machine designs

Method	Object Function Evaluations
For the initial estimate, begin with the optimal current from the previous design[25]	2320
If the current waveform was distorted, reduced the number of turns, and increased the current to achieve equivalent amp turns	2100
Used the reactances and back EMF to estimate the next current value	2425
If phase angle evaluations for three points existed, curve fit the three closest points (γ, I) to estimate the required current at the next phase angle.	2047
Used the current from the previous phase angle evaluated to estimate the first two phase angle points of new designs	2029
If the power was not achieved with the initial current setting (for a given phase angle), for second current setting, use 0.75 of the increase calculated by Newton's method. [26]	1737
If the power was too high on the initial current setting (for a given phase angle) increased the recommended current adjustment by 1.3.[27]	1702

The same methods have been applied to generator design, and additional work is

continuing in this area.

---

[25] The number of function evaluations prior to this modification was not recorded.
[26] This adjustment was used due to the fact that the torque equation has current in the first term, and current squared in the second term Also tried other numbers, such as 0.8, but 0.75 was optimal. This number might be varied, depending on how much reluctance and magnetic torque are in the machine.
[27] Had also tried 1.2 and 1.4, with 1.3 being optimal.

3. Eliminating data entry errors

Part of the method focused on eliminating data entry errors. The boundaries of the design spaces to be searched are not typed into the computer. A graphical user interface (GUI) allows design spaces to be selected by incrementing or decrement variables. These increments were based on the range size, so that the boundaries of the design spaces were always forced to be at 0.05, 0.10, 0.15, etc for most parameters. The magnet thickness had boundaries at 6.0, 8.0 and 10.0; and the stator aspect ratio had boundaries logarithmically spaced, at 0.5, 0.707, 1.0, etc.

The GUI was also written so that new design spaces could be duplicates of previously used design spaces, with selected parameters of the previous design space modified. This system worked effectively during validation.

E.   Structural FEA

In order to design electric machines which are feasible, the rotors must be capable of withstanding the mechanical stresses at the maximum overspeed condition. The MATLAB structural FEA algorithms determined the stresses in approximately 2 second intervals, with the rotor geometry being modified in that time frame. The initial web and bridge thicknesses were structurally adequate for smaller rotors, and did not require modification from the initial values, which were selected as thicknesses suitable for production.

For larger rotors, or very high speeds, the algorithm increased the post size 1mm in width per iteration, and then optimized this width after the width increases had given the rotor sufficient strength. This algorithm could be optimized further, but consumed a

small percentage of the machine analysis time. An example of this convergence is shown in Figure 28. For this case, the bridge converged to about 175 N/sq mm of stress, while the post converged to 260 N/sq mm, which was the yield strength of the material. For the case shown, there was a specific ratio of bridge thickness to post thickness (1:2).
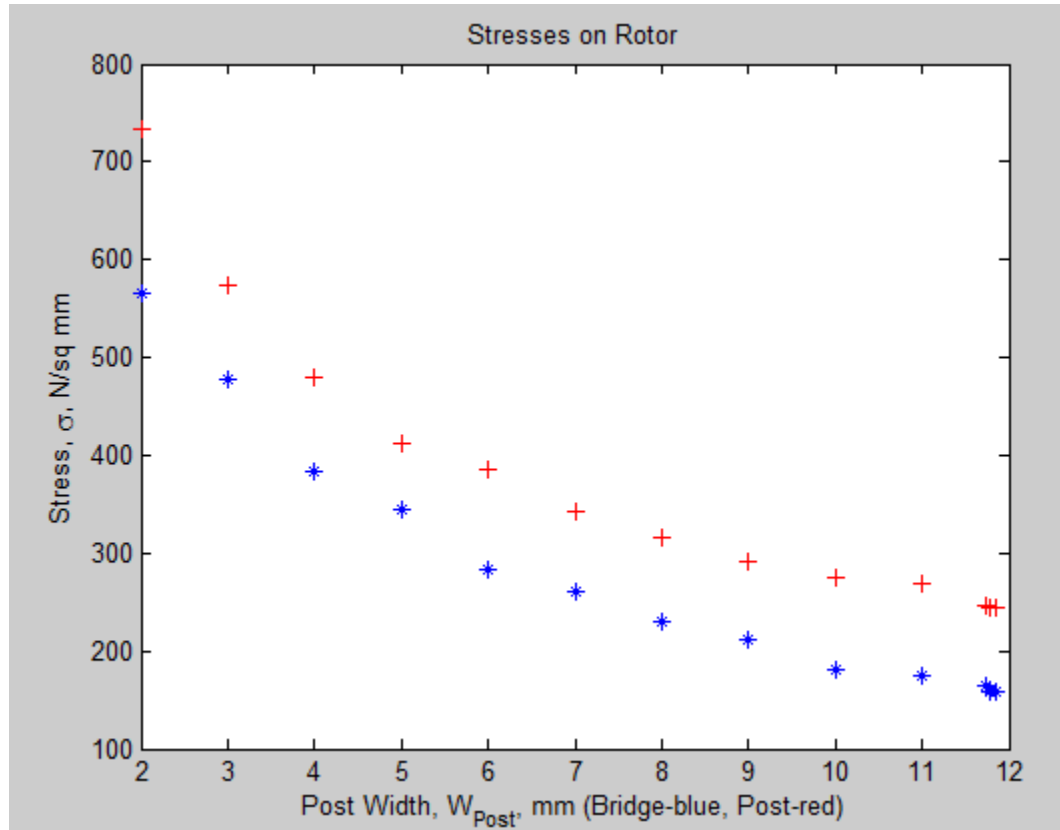
Figure 28, Convergence of bridge and post stresses with increase in bridge and post width

Figure 29 was created by the MATLAB structural FEA algorithm. The high regions of stress are on the post and the bridge, as expected. This rotor had a radius of approximately 58 mm, and was analyzed at 11,200 rpm. The yield stress for the steel was 260 N/sq mm, so this rotor was acceptable with the minimum bridge and post thickness.
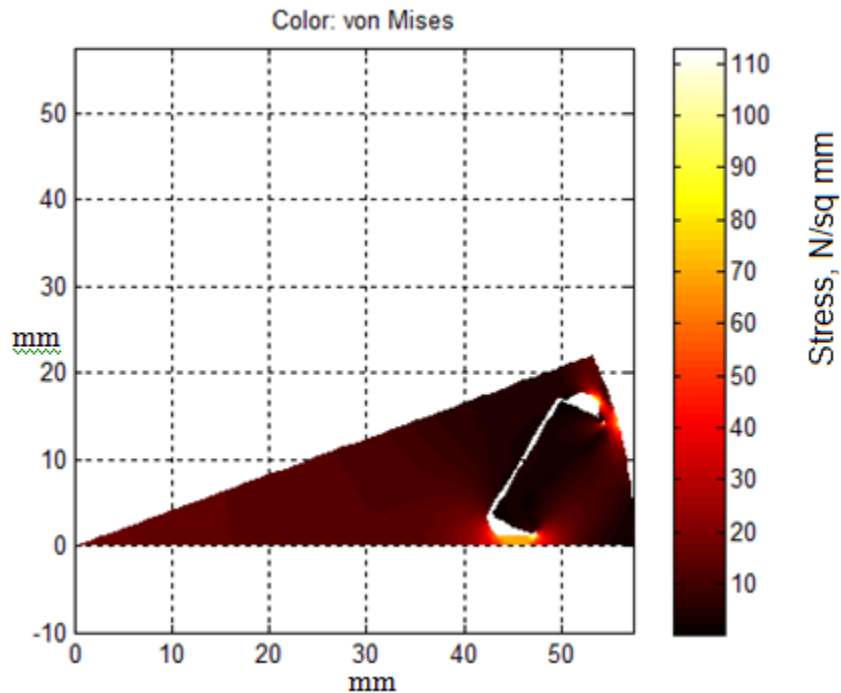
Figure 29, FEA of stresses on rotor

F.   The current required to achieve rated power

In order to analyze the optimal performance of the designs, it is necessary to set the current and phase angle to the optimum value, for the given design and operating conditions. A golden section search method was used, searching the phase angle region between 15 and 55° for motors. The 15° limit was determined after running a number of electric machines, and finding that the optimum current was always above this value. The 55° limit was a specification given by the controls engineers, to maintain stability of the controller.

For each of these phase angle points, the current to achieve the power at that performance point was determined. The following cases are shown:

- The use of Newton's method to determine the current to achieve rated power

- The use of Newton's method, followed by the golden section method to determine the current to achieve maximum power, when rated power could not be achieved

- The use of Newton's method, followed by the golden section method, followed by Newton's method to determine the correct current to achieve rated power

Newton's method, to determine current for rated power
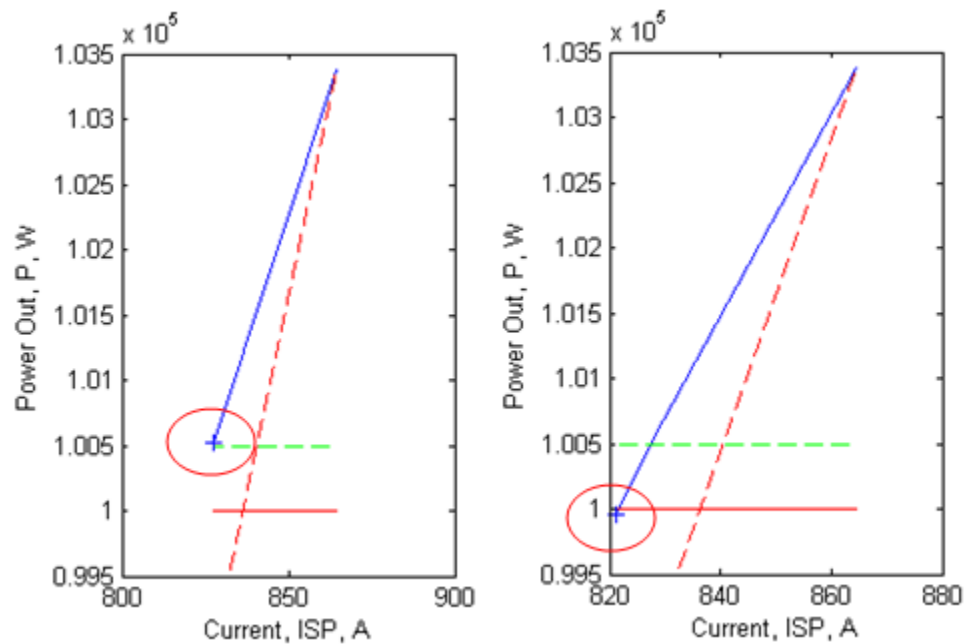
Figure 30, Determining current using modified Newton-Raphson method

Figure 30 shows the convergence to rated power. The left plot shows the first two current settings analyzed, the right plot shows the three current settings required for convergence for this machine. The red horizontal line indicates the power specified. The green dashed lines (the lower dashed line is on the x axis at 0.995×10^5 W) indicate the convergence limits, which are 0.5% above and below the required power level. The blue line indicates the current settings, and the power achieved. The most recent current

setting is indicated with a plus sign at the end of the blue line (circled). The red dashed

line extends from the maximum current/power setting to the origin (0 Amps, 0 Watts).

  After the phase angle was set, the current was set to approximately 870 A for this

specific machine. Power achieved was slightly over 103 kW. The second point (shown

in the left figure, the black plus sign) was determined as explained in Methods

(CHAPTER II.I.2 , p. 60), and was slightly higher than the convergence limit (0.5%

error).[28] The third point, shown in the right hand figure (the black plus sign) falls slightly

below 100 kW, and is within the convergence band.

  The results in Figure 30 and Figure 31 are typical for the method, on either of the first

two phase angle settings. After this, achieving the desired power level typically occurs

on the first or second current setting.[29]
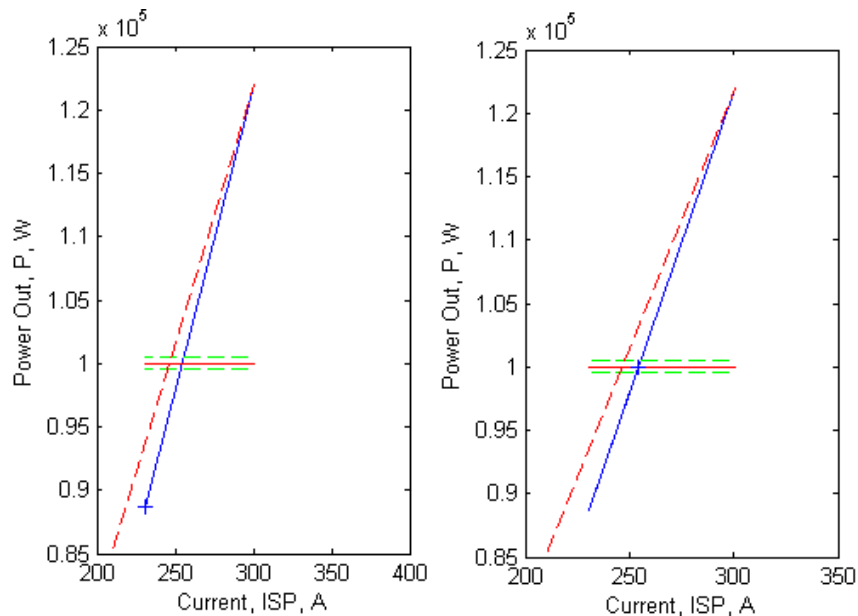
**Figure 31, Undershooting desired power, using modified Newton-Raphson method, after two
iterations (left) and after three iterations (right)**

---

[28] A 0.5% error of the power requirement results in a much smaller error in efficiency.
[29] For motor design.

Figure 31 shows the convergence to rated power for a motor with the same specifications as for Figure 30. The left hand plot shows the first two points, the first point at the upper right of the blue line, and the second at approximately 240 Amps, at the lower left of the blue line, indicated by the plus sign. The initial current setting (point at approximately 300 Amps, 122 kW) exceeded the power specification. The second point produced too little power.

The right hand plot shows convergence on the third current setting, at approximately 255 amps. The first two points are the end points of the blue line, the third point being indicated by the plus sign, and being collinear with the first and second points. The current was determined using the same method as was used for Figure 30, but depending upon the specific machine design, the power achieved may be higher or lower than the rated power.

Again, this method resulted in convergence to within 0.5% in three iterations.
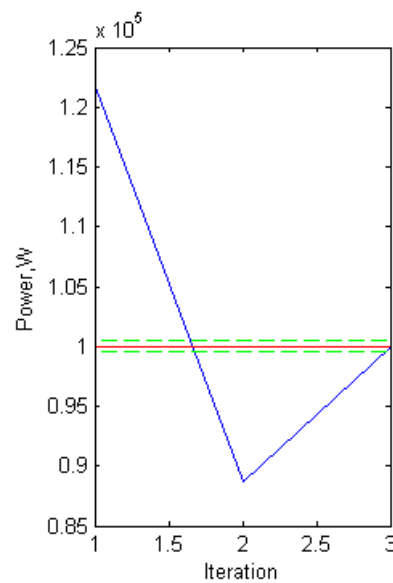
Figure 32, Convergence plot for Figure 31

Figure 32 is a plot corresponding to the data from Figure 31. It shows the convergence in a different manner, were the number of iterations are shown on the x axis. The first setting achieved slightly over 120 kW, the second setting slightly under 90 kW, and the third setting was within the convergence limits. For all cases above, response is fairly linear, indicating the Newton-Raphson method is a suitable choice for this part of the problem.

Figure 33 shows the behavior of the method when the initial current setting was too low. For this case, the initial power was 2% low, and converged with the second current setting. Convergence on the first or second current setting typically happened after the first two points of the golden section search had been obtained.
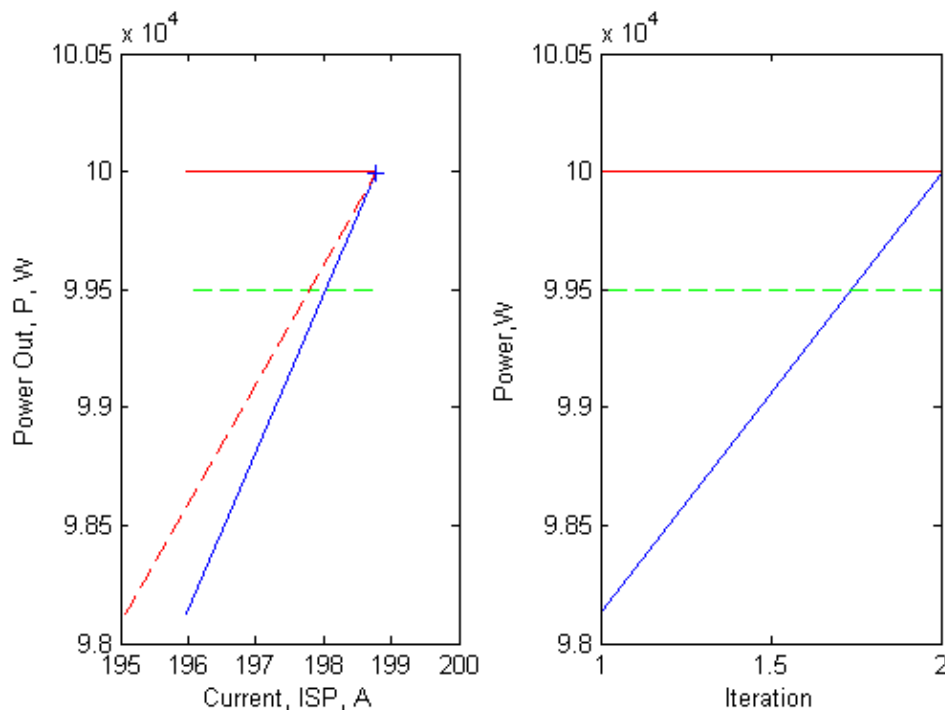
Figure 33, Convergence when initial current is low

Newton's method followed by GS, when unable to achieve rated power
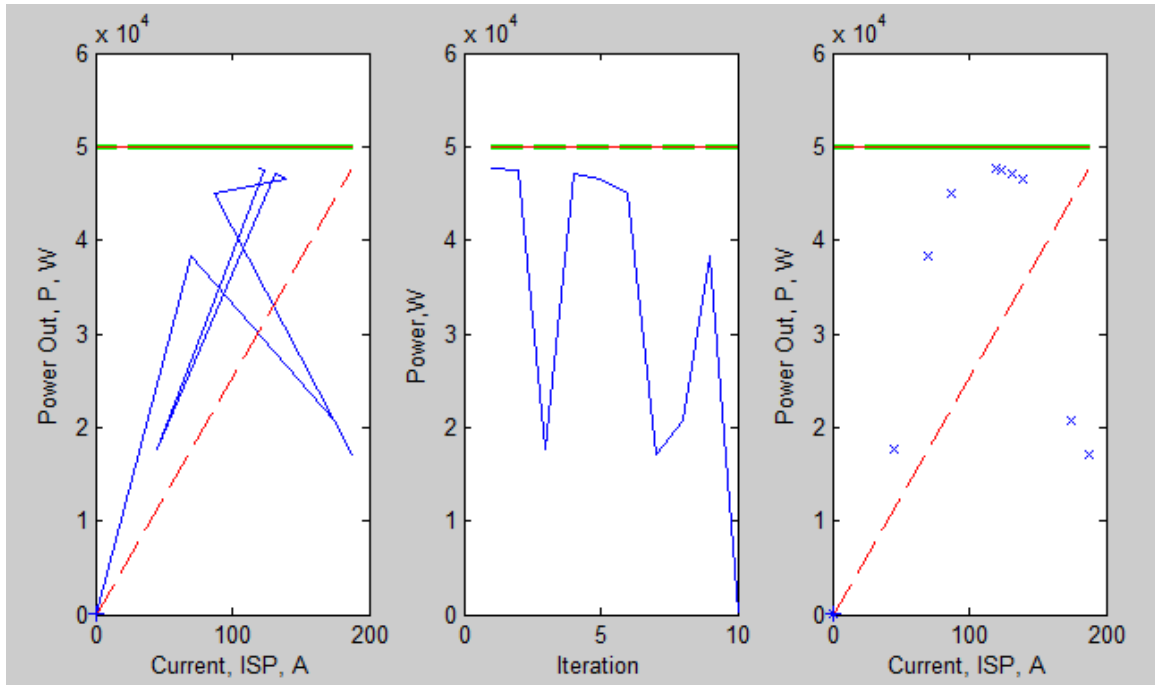
Figure 34, Non-convergence for generator, using Newton-Raphson method

For some machine designs, it is not possible to achieve the rated power with the geometry which is created. This situation is shown in Figure 34. The Newton-Raphson method was used, but convergence to the rated power was not achieved, because the geometry and voltage levels are not capable of achieving rated power. For this situation, the Newton-Raphson method is not appropriate.

The left hand plot shows the order in which points are being evaluated, starting at approximately 100 Amps and 49 kW, and never improving beyond that point. The right hand plot shows that the points are distributed in a unimodal shape.

When rated power cannot be achieved, the method was changed to a golden section search, which achieved the highest power possible for the given machine and specifications (DC link voltage).

Newton's method followed by golden section, followed by Newton's method
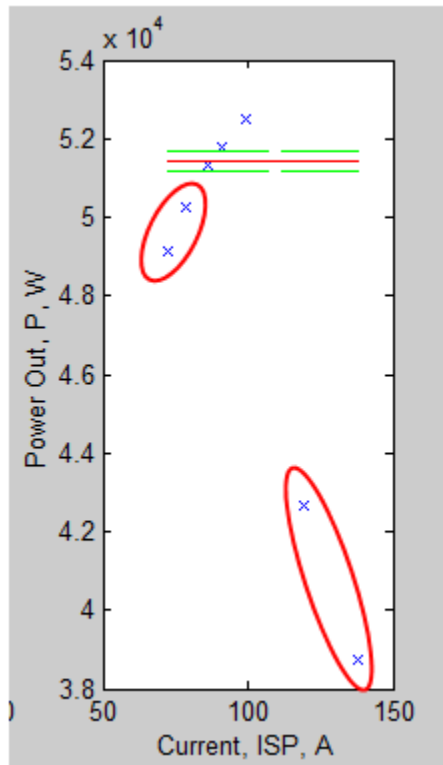
Figure 35, Convergence using golden section and Newton-Raphson methods, initial points circled in red

For some machines, at given phase angles the rated power could not initially be achieved. These points are shown in red ellipses. This is shown in Figure 35. For these cases, the method switched over to a golden section method. The method continued

using the golden section method unless rated power was achieved. If rated power was achieved, the method switched back to using the Newton-Raphson method.

G. The optimum phase angle

Having determined the performance for the first two phase angle settings, the golden section method was followed. For the objective function defined, the peak efficiency at two performance points was needed. Figure 36 shows a typical golden section search for the peak efficiency for a motor at 2000 rpm. Another golden section search was performed on this machine at 8000 RPM (not shown).
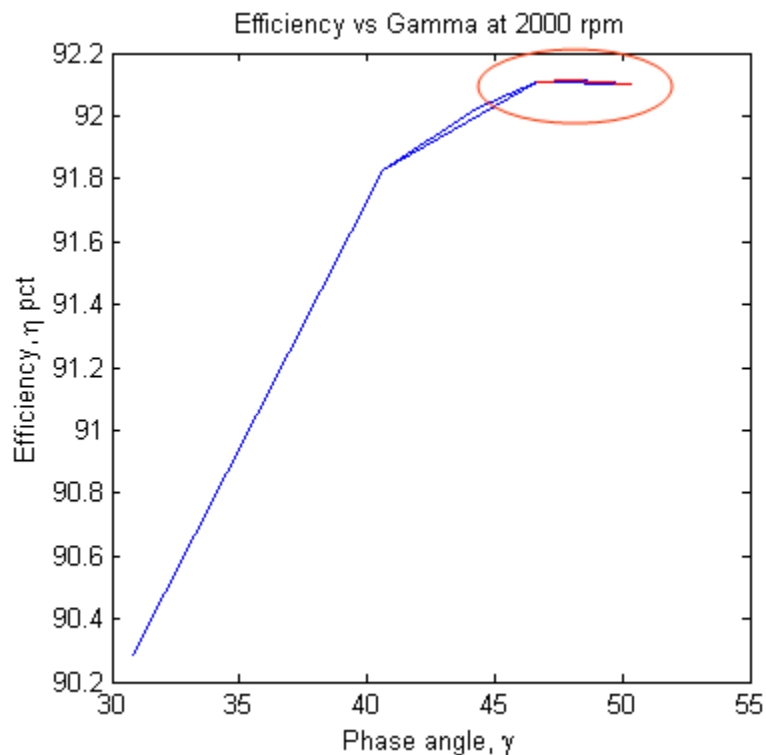
Figure 36, Golden section search for peak efficiency

The vertices of the blue and red lines indicate the phase angles used. The upper two line segments of the plot (circled) are red. The endpoints of the two red line segments

indicate the three last vertices obtained. The highest efficiency obtained is used by the algorithm.

H.   Accuracy of the surface response models

For this validation, the surface response models consisted of two surfaces, the first at 2000 rpm, and the second at 8000 rpm. For each design hypercube, a plot of the predicted response vs. the actual response was created. Figure 37 shows the correlation between the 64 designs of one hypercube, and the predicted response, using a least squares fit.

The upper figure was for the response at 2000 rpm, the lower figure was for the response at 8000 rpm.
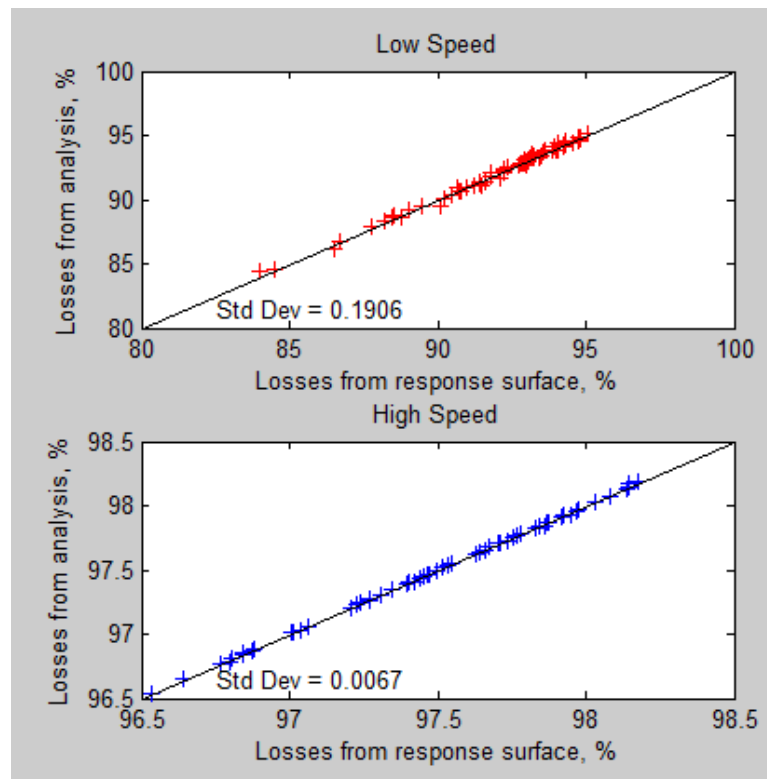
Figure 37, Efficiency from analysis vs predicted efficiency from the response surface

This was a design space which produced efficiencies between 84 to 94% at 2000 rpm, and between 96.5 and 98.5% at 8000 rpm.

Figure 38 is for the same machine specifications, but for a different local design space. The scatter on these plots is more visible, especially at the higher speed. The efficiencies for this plot vary from 96.5 %, to 98.5 %. Because the range of the graph is small, small errors are more apparent. While the standard deviation is higher for this plot than for the first, it is only 0.0416%.
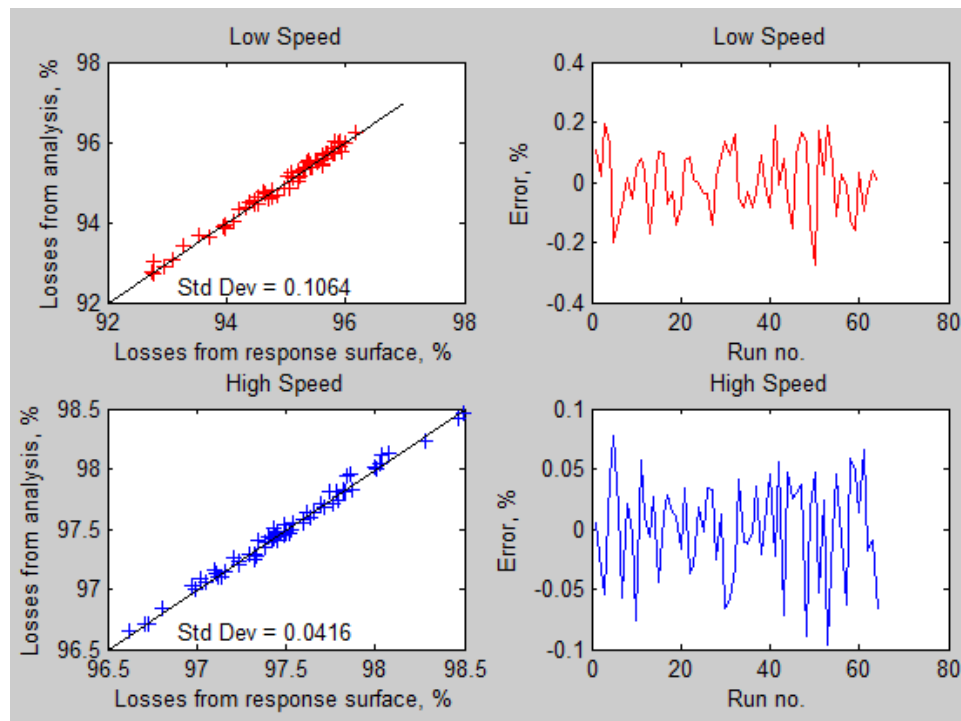
Figure 38, Fit of data for 100 kW machines, for 64 data points in hypercube

In this region of the design space, the response was fairly flat, varying from 96.5 to 98.5% at high speeds. The curves to the right show the error of each design vs. the run number. The peak error at low speed is about 0.2%, while the peak error at high speed is less than 0.1%. The x-axis for the right hand plots is the order in which the machines

were analyzed, and carries no significance, other than allowing for the examination of specific data points after designs have been analyzed.

I.   Surface response maps

Figure 39 (for a 100kW motor) shows a response where the global optimum is to the right of the plot. In this case, the design was limited by a specification constraint

$$R_{SDL} < 0.707 \qquad (3.1)$$

The constraint was placed on the diameter of the stator, due to the space available in the application. The available portion of the design space is on the left half of the plot, the shaded portion of the plot extends beyond the range of the specification.
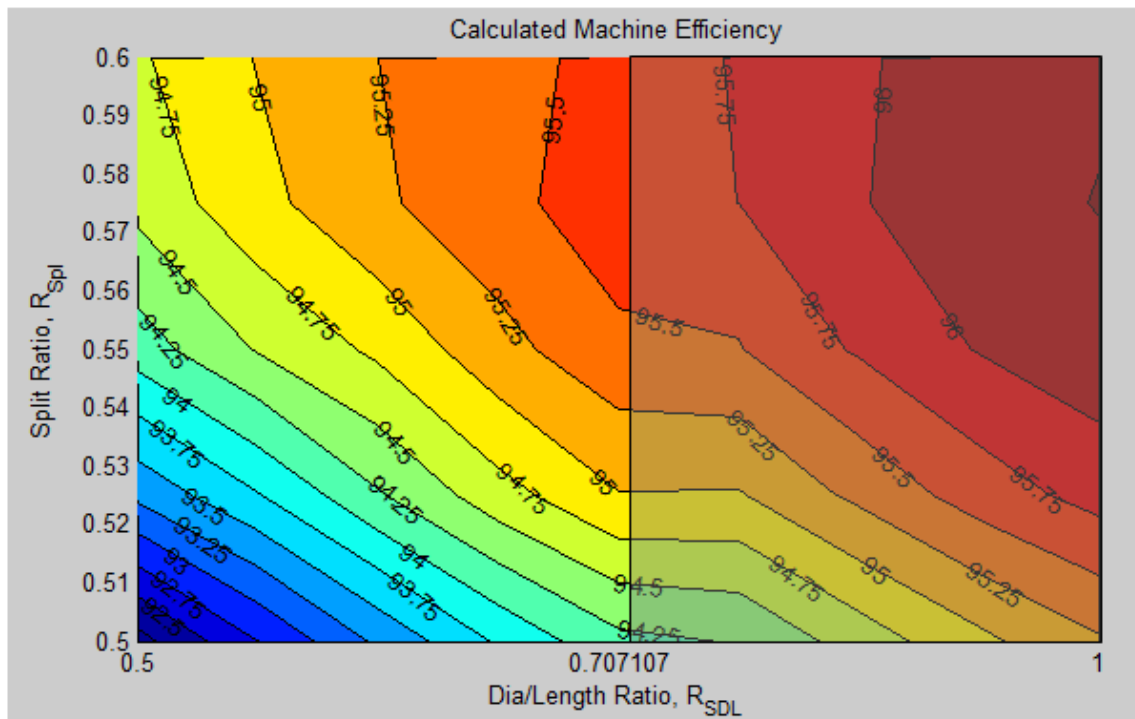
Figure 39, Response surface for a hypercube, in a region with a constraint at R$_{SDL}$ equal to 0.707

A greater efficiency could have been achieved if the stator diameter over length ratio (R_{SDL}) was allowed to increase. This plot shows the region to the right of this constraint, to explore the opportunity to increase the efficiency of the machine. The entire design space has a stator diameter/length ratio ranging from 0.5 to 1.0.

Table 20 is text from the validation program, indicating values which fell within the boundaries of the design space, and values which fell beyond it. After the response surface was created, the MATLAB fmincon function determined the optimum parameter settings for efficiency, for each hypercube.

Table 20, Optimal design estimate from algorithm

```
+/- indicates direction of improvement if on boundary
        1       2       3       4       5       6       7       8
      RSpl    RSDp    Rw2s    Rw3s    RSDL    RWeb    RMDp    RMth
    [0.58]  0.70+   [0.47]  0.55+   1.00+   [0.18]  [0.49]  [7.72]

     0.50    0.60    0.45    0.45    0.71    0.15    0.40    6.00
     0.60    0.70    0.55    0.55    1.00    0.25    0.50    8.00
```

J.   Direction of the optimum design

Figure 39 and Table 20 indicate that R_{SDL} should be increased. Other values (R_{SDp}, R_{w3s}) should also be changed. The table did not indicate how much each value should change, as this is not predictable from the design spaces analyzed.

This table was output whenever a design hypercube was evaluated. This made it possible to determine if the design had been optimized, or to continue to refine the design. This was also used to gain more insight into optimal designs.

The first row indicates the parameter number ($x_1 - x_8$). The second row shows the acronym for that parameter. The third row shows either the optimal value (in square brackets), or recommended changes, shown using + or - symbols. For the example above, all recommended changes were positive. The following two rows show the ranges for each parameter, for that hypercube.

Another response surface was added to the right of Figure 39, which is shown in Figure 40. The optimum is still to the right of this composite response surface.
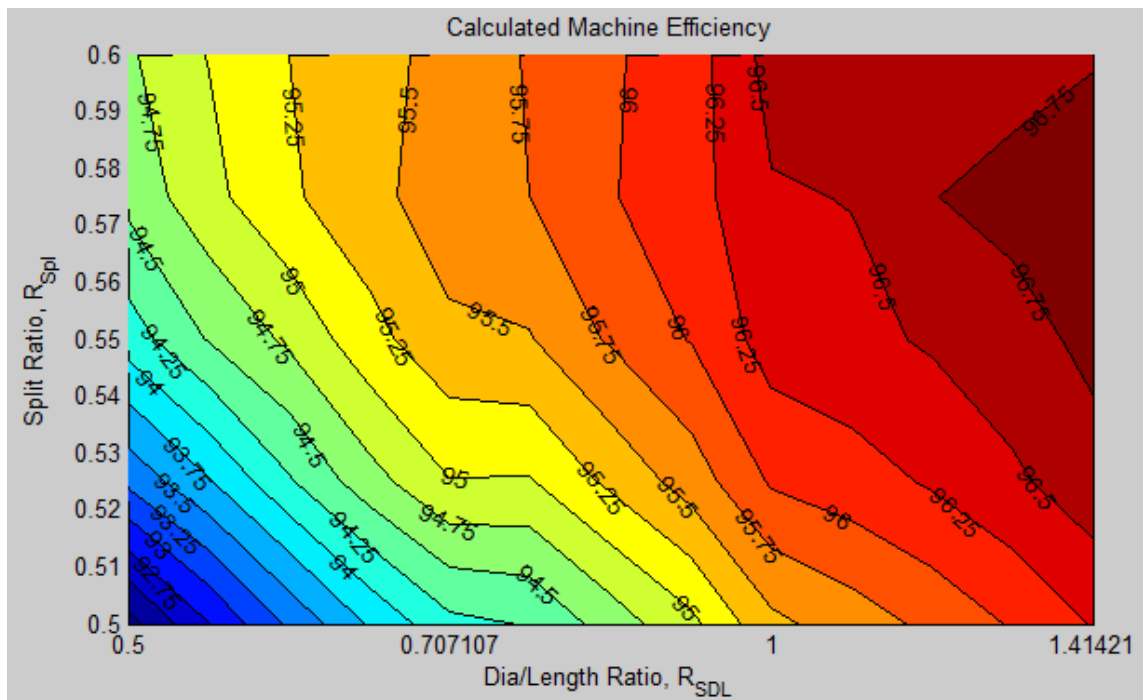
Figure 40, Composite response surface three diameter/length ranges wide

To create the rightmost hypercube (ranging from R_{SDL}=1.0 to 1.414), the algorithm required only 38 additional points. The other 26 points of the hypercube were shared with a previously analyzed design set, the hypercube with R_{SDL} ranging from 0.707 to 1.0.

As can be seen from the above diagram, the optimum is still to the right of the regions analyzed, indicating that R_{SDL} had not been increased enough.
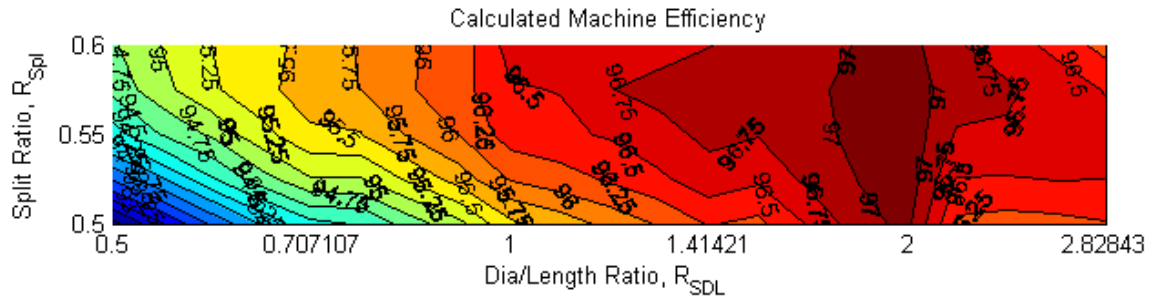
Figure 41, Composite map of efficiencies of 100 kW IPM motors, split ratio vs. diameter/length ratio

To create Figure 41, two additional hypercubes were added to the right of the previously analyzed design space. While the design specification limited this machine to a stator diameter/length ratio of 0.7, the figure shows that while the optimum efficiency in Figure 41 is 97.0%, the optimum efficiency of the machine with a stator aspect ratio of 0.7 is 95.5%. Comparing the heat rejections of one machine with another, the heat rejection of the larger diameter machine would be 3.0%, while the heat rejection of the smaller diameter machine will be 4.5%, an increase of 50% in the heat rejection requirement.

Figure 42 (b) shows the response surface visualized using 3D contour plots. The 3D and 2D contour plots represent the same surface. This specific contour plot, a split ratio vs. stator aspect ratio (stator diameter/length ratio) was often plotted, because the diameter or the length of the machine is often a constraint of the design. By making the tradeoffs of diameter vs. efficiency visible, more information is available for design decisions.
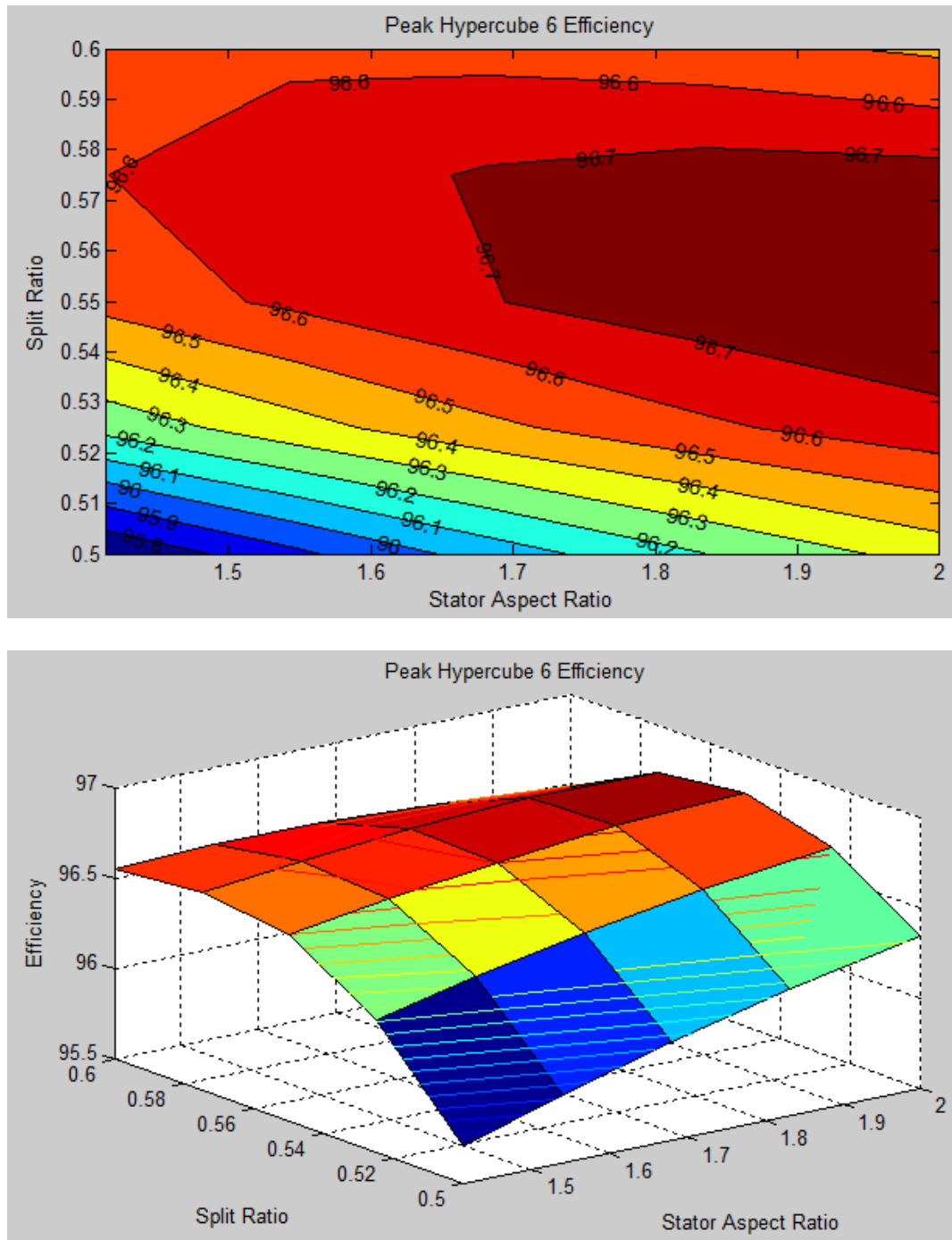
Figure 42 a (above) and b (below), Efficiencies of 100 kW IPM motors, split ratio vs. dia./length ratio, for one hypercube

K.   Conclusions

Two machines had been designed and built by an electric machine manufacturer. The method developed by this research was used to create new designs using the same materials, specifications, and control constraints as the existing machines. The first set of machines were designed using SPEED software, and traditional methods. The second set of machines was designed using the method developed by this research, and analyzed with SPEED software, and had higher performance. Using this method, each of these machines with improved performance was designed in one day.

Structural finite element analysis achieved designs which met the overspeed requirements mechanically.

The number of designs which must be analyzed with this method has been reduced (based on experience with this method) to 193 models or less, if 3 design spaces must be analyzed. The function evaluations include determining the optimal current and phase angle settings for the controller.

Response surface models were created which closely correlated with the 64 designs of the design hypercube.

CHAPTER IV. DISCUSSION

This chapter discusses the method, and the results produced by the method. The following topics are covered:

- Comparison of two contracted designs to dimensionless optimization designs

- Variances of the response surfaces

- Use of dimensionless parameters

- Selection and treatment of design variables

- Creation of the design space

- The method of analyzing the performance of the machine, including determining the optimum current and phase angle for peak efficiency

- Creation of an objective function

- Creating the response surface – specifics of how the response surface method was implemented

- Initial specifications

A.   Comparison of the contracted designs to DO designs

As shown in CHAPTER III.A (p. 75), the designs optimized by this method had significant efficiency improvements over the designs contracted to another company. Table 21 shows performance and dimensional differences between the two designs. Table 22 compares the dimensionless parameters of the 50 kW machine designs.

1. 50 kW machine comparison

Table 21, Comparison of the optimized and contracted 50 kW designs

		Contracted design	Optimized design	Change
4937 RPM	Efficiency	94.96%	96.30%	1.34%
	Heat rejection	5.04%	3.70%	
	Copper losses, %	2.90%	2.41%	-0.49%
	Iron losses, %	1.89%	1.04%	-0.85%
	Current, A rms	114.09	121.60	7.51
	Current density, A/mm^2	10.6714	8.9049	-16.5%
6913 RPM	Efficiency	94.55%	96.23%	1.68%
	Heat rejection	5.45%	3.77%	
	Copper losses, %	1.49%	1.23%	-0.26%
	Iron losses, %	3.63%	2.21%	-1.42%
	Current, A rms	82.91	83.00	0.09
Dimensions and masses	Stator OD, mm	191		
	Stack Length, mm	122		
	Rotor OD, mm	124	113.76	-10.24
	Gap, mm	0.5	0.6235	0.1235
	Slot opening width, mm	2.5	1.9119	0.5881
	Slot area, unlined, mm^2	97.9	156.9	60.2%
	Magnet Thickness, mm	4.7	6.2352	32.6%
	Stator Thickness, mm[30]	33	37.9875	4.99
	Slot opening, mm	2.50	1.912	-0.588
	Magnet mass, kg	1.1015	1.3816	0.28

---

[30] Stator thickness is defined as the distance from the stator OD to the stator ID

	Contracted design	Optimized design	Change
Copper mass, kg	4.3296	5.6527	1.32
Steel mass, kg	18.8808	16.2098	-2.67
Rotor mass, kg	9.51	7.95	-1.56

The most significant performance differences are the improvement in efficiency at lower and upper speeds, and the corresponding reduction in losses which affect the heat rejection requirements of the machine. The reductions in losses may be used to reduce the cooling requirements; or to reduce the magnet temperatures, increasing the performance of the machine.

The losses in the copper and steel decreased at both upper and lower speeds. This is significant in that the optimization did not trade off one type of losses for the other. The current density was reduced in the optimized machine by 16.5%. This impacts how intensely the machine must be cooled.

The contracted design has a smaller air gap than was recommended by our consultant. If this smaller air gap is realistic, the optimized design could have a smaller air gap also, resulting in a lower magnet mass, closer to the magnet mass of the contracted design.

Table 22, Comparison of dimensionless parameters between contracted and optimized designs

Parameter	Contracted design	Optimized design	Change
R_{SDL}	1.5656		NA
R_{Spl}	0.649	0.596	-0.0594
R_{SDp}	0.697	0.773	0.0762
R_{SW2}	0.368	0.50	0.132
R_{SW3}	0.539	0.65	0.111
R_{MTh}	9.4	9.86	0.46

Parameter	Contracted design	Optimized design	Change
R_{MDp}	0.23	0.26	0.03
R_{Web}	0.202	0.15	-0.052

Table 22 allows comparison of the dimensions of the contracted vs. the optimized designs. As implemented in the validation algorithms, typical range sizes are 0.1. If the dimensionless parameters from the contracted design had been used as the center point for the ranges of a design hypercube, only the magnet depth ratio (R_{MDp}) and the magnet thickness ratio (R_{MTh}) would have been in the correct range. The slot widths would not have been in the initial ranges, and in fact are two range settings off.

The stator aspect ratio (R_{SDL}) was a specification of the design, and so was held constant. The split ratio (R_{Spl}) was smaller in the optimized design by 0.0594. This is significant because research by others has shown that the performance of electric machines is sensitive to the split ratio. As mentioned previously, if standard length units (mm or inches) are used, once an initial rotor diameter has been selected, and optimization work has begun, changing the split ratio requires changing most of the other stator and rotor dimensions. This is difficult to do while trying to find the dimensions to achieve the optimum performance.

Using traditional units, when the rotor diameter is changed, the back-iron thickness is also changed. This affects the iron losses in the machine. It may also affect the amount of current required to create the necessary flux, impacting the copper losses. If the rotor diameter is decreased, the copper area is also decreased. At the same time, the widths of the teeth decrease, increasing flux density, and iron losses. When the rotor diameter is reduced, the slot depth should typically be increased (increasing the copper area, to

decrease copper losses), and the slot widths should be narrowed (increasing the tooth width, and decreasing iron losses). These interactions highlight a benefit of using the dimensionless approach, which makes these changes automatically.

The difference in the split ratios resulted in the stator thickness being about 5 mm larger for the optimized design, approximately 38 mm vs. 33 mm. The smaller stator ID was used not to increase the back-iron thickness; but rather to increase the amount of copper area. The slot depth ratio (R_{SDp}) increased from 0.697 to 0.773; increasing the depth available for the copper from 23 mm to 29.4 mm. This (combined with changes in the slot widths) reduced the current density from 10.7 A/mm^2 to 8.9 A/mm^2.

Both slot width ratios, R_{SW2} and R_{SW3} were larger in the optimized design, which partially explains the reduced copper losses. The combined effect of increasing the slot widths, and decreasing the rotor diameter resulted in thinner teeth. This would be expected to increase iron losses in the teeth. However, the slot openings in the contracted design were larger than the optimized design, increasing the flux density in the teeth in the contracted design, probably equalizing the losses in the teeth of both designs.[31]

Images of the FEA simulations are in the appendices. Portions of the teeth for the contracted design are at approximately 2.0 T. Saturation in the bridge region is approximately 2.4 T. The results for the optimized design are similar. In the optimized design, the flux density in the teeth is slightly higher, while the flux density in the back-iron is significantly lower.

---

[31] The losses in specific regions, such as the tooth regions, are not available in the software

2. 20 kW machine comparison

The 20 kW machines showed similar improvements when optimized using DO. Data is given in Chapter III – Results (p. 75). The first 20 kW machine optimized using DO had good performance, but the slot opening was fairly narrow. Changing the range of R_{SW2} to 0.4-0.5 increased the slot opening, and resulted in almost identical performance.

The change in upper slot width ratio showed a major advantage of this method. The response surface models had already been created. To extend the range, new response surfaces were required, which required analyzing 41 additional machines. The 41 machines, plus 23 machines which had already been analyzed were used to create new response surfaces. These surfaces were used to create an optimal machine with a wider slot opening, with minimal effort. Analyzing the additional 41 machines was simple and fairly quick.

B.   Comparison of DO to the fmincon MATLAB function

Table 9 (p. 72) shows the locations of 5 design spaces which were optimized using both dimensionless optimization and the MATLAB function fmincon. Table 17 (p. 82) shows the results of that comparison. The first comparison which may be made is the number of iterations required to perform the optimization. When DO was used, the hypercube design resulted in always having a design space which was determined by 64 machine designs. When the fmincon function was used to optimize the design, modifying the parameters in SPEED, 65 to 274 evaluations were performed. In total the fmincon function created 862 machine designs.

This is in contrast to dimensionless optimization, where five design spaces were evaluated using a total of 213 evaluations. So a significantly greater number of machine designs were required using fmincon (approximately four times greater). It can also be noted that for all of the design spaces except for design space 2, DO produced a design with a higher efficiency. From Table 17 it would appear that design space 2 was a fairly efficient design space, however the variance of that design space was 2.344, indicating that the RSM was not an accurate model. The RSM did indicate the direction of the optimum design space. For all other design spaces, DO created an optimal design which was more efficient than the design created using the fmincon function.

C.   Variances of the response surfaces

In order to use response surface models to find the optimum, the models must accurately fit the data. A number of hypercube designs were used to model machines from 25 kW to 200 kW. Response surface models were created from these hypercubes, and the variances were determined.

Table 18 (p. 84) shows the variances of some of these response surfaces. The variance of the three 100 kW generator designs was between 0.002 and 0.0114, indicating that the RSMs were very good. The variances for the first and second 25 kW generators at low speed are much larger, indicating that their RSMs were not as good.

The first design hypercube for the 25 kW generator had a variance of 1.2423 at low speed, and 0.6346 at the upper speed. The second design hypercube had a variance of 0.5426 at the low speed, and 0.1667 at the high speed, while the third had variances of 0.0871 and 0.0347 respectively.

The only parameter varied between these hypercubes was R_{SDL}, the ratio of the diameter of the stator to its length. For the first design space, the algorithm located the optimum design on the boundary at $R_{SDL} = 2.0$, indicating that this parameter was too small. For the designs in that hypercube, 13 of the 64 machines could not achieve rated power, some falling significantly short. The response surface models are more accurate when the designs are capable of achieving rated power.

The second hypercube design was more accurate, but again had some machines which did not achieve rated power. In contrast, the third hypercube produced a very low variance, and all machines in that design hypercube achieved rated power. These results demonstrate the importance of being able to achieve rated power, and the importance of verifying the curve fit.

The 100 kW generator hypercube designs all produced models with low variance. The only difference between the 25 kW hypercube designs and the 100 kW hypercube designs was the power designation; the dimensionless parameters (and therefore the design hypercubes) were the same. The 100 kW generator hypercubes were analyzed first, and the 25 kW hypercubes were modeled using the same hypercube designs. The torque density for both of these machine analyses was the same. Reducing the torque density of the 25 kW machines would have improved their performance.

The 25 kW motor hypercube design (D) and the 100 kW motor hypercube design (D) had the same hypercube design. The variance for the 25 kW machine is much larger than for the 100 kW machine. To improve the variance, the ranges for this hypercube could be reduced, however the machines in this hypercube had higher losses than desired. In

general, larger variances indicate that there are larger losses in the hypercube, and that the optimum is in a different hypercube.

For this part of the verification, the goal was not to find the optimum design, but to determine if the response surfaces accurately model the design space. Scaling of the machines by this magnitude (4:1) did not produce response surfaces with the same variance. It can also be seen that by adjusting the design spaces, better variances were obtained.

The RSM for the 200 kW motor had a higher variance at the low speed, 0.5057. For this design hypercube, all of the machines met rated power. At this power rating, the diameter is larger, and therefore the bridges and post must be thicker. The bridge leakage makes the response more non-linear. To reduce the effect of non-linearity, the ranges of some of the parameters can be reduced. Reducing the range of R_{SDL} or R_{SDp} would have the greatest effect, as these two affect the rotor diameter the most.

D.   Dimensionless parameters

The uses of dimensionless units in engineering include establishing similarity between experiments or designs which are dimensionally different, and in communicating ratios. Dimensionless parameters are used for both of these benefits in this research.

Dimensionless units are not new to electric machine design. Electrical engineers make extensive use of the per unit system in designing and analyzing the performance of electric machines, as well as in measuring efficiency and percentage of rated power.

However, dimensionless units are not used extensively in the design of the geometry of electric machines.

1. The challenges of using traditional units in machine design

During the process of optimizing an electric machine, the dimensions are constantly being changed. In electric machine optimization performed by engineers, as contrasted to optimization performed by algorithms, two primary methods are scaling of similar machines, and the "trial and error" method. When scaling is used, design begins with a similar machine, and is scaled as the initial step of creating the design. This may include lengthening the machine, as well as changing all of the lamination dimensions by a scaling factor. This is typically followed by trial and error methods.

Using the trial and error method, the outer diameter and length of the stator are often modified first, based on the experience of the machine designer and the specifications. The rotor diameter and air gap are also determined based on experience and design guidelines. After this, dimensions are tweaked, and the effects of the changes are used to determine subsequent dimensional changes.

Machine dimensions other than the diameters and length are typically optimized by varying one dimension at a time. The depth of the slot might be optimized, then the width of the slot, then the depth of the slot might be returned to. For IPM machines, these adjustments are made based on a machine analysis program that includes FEA. So the basic design steps are to analyze the machine, evaluate the results, adjust one or two dimensions, and analyze the machine again. This process is repeated until the specifications are met, or the design is considered to be optimized.

As the machine is being designed, the focus shifts between the rotor geometry and the stator geometry. Modifying the coil slot dimensions is fairly simple. Deepening a slot can typically be done without modifying other stator geometry, as shown in Figure 43.
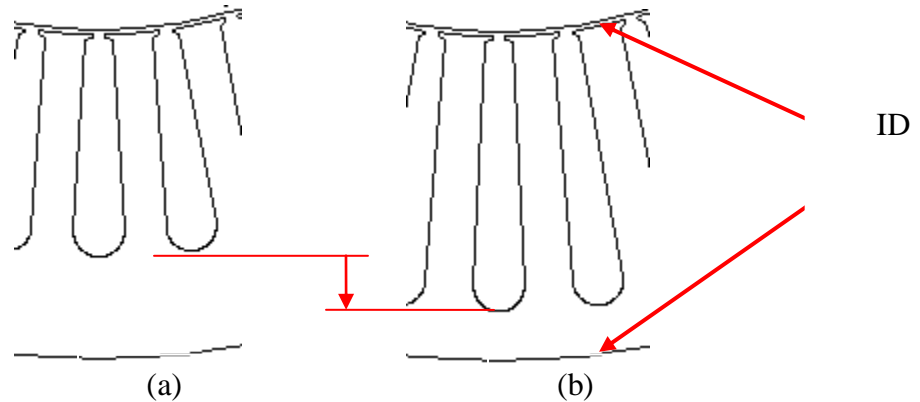
Figure 43, Deepening the slot geometry

The designers make decisions based on intuition, one dimensional curve fits, spreadsheet calculations, etc. As the slots are made deeper, the geometry appears reasonable. However, there are no physical dimensions shown on this figure.

If the distance between the stator inside diameter (ID) and outside diameter (OD) is 50 mm, the designers recognize that they cannot make the stator depth 60 mm; the slot would cut through the stator. For the geometry shown in Figure 44 (a), if the slots are to be shortened similar decisions can be made to arrive at a design like that shown in Figure 44 (b). The designers would typically recognize that these slots appear to be excessively shallow.
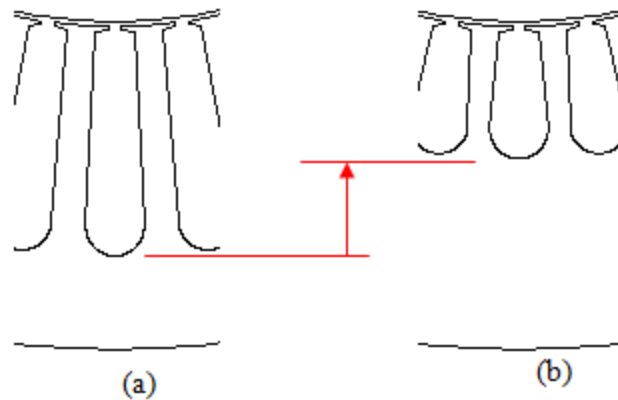
Figure 44, Reducing the depth of the stator slot

At some point, as the stator slots become shallower, the tooth geometry does not look reasonable. FEA results would show that the flux in the back-iron is low compared to the flux in the teeth, and the copper losses would increase due to the increased current density in the slots. For some stators this depth may be 20mm, for others, this may be 100mm. Therefore, the physical dimensions to be modified are constantly being evaluated. The question is 'what percentage should this dimension be changed?'

At the same time, calculations are made to decide how much of an adjustment to make on a given dimension. Typically, this may be a marching method or a region elimination method similar to the golden section (GS) search method, though not as disciplined. Use of the GS method requires typing in a number of digits, when approximations are accurate enough at early stages of the design.

Computer aided design

If an algorithm rather than a designer is used to optimize the design, and standard dimensional units (mm, inches, degrees, etc) are used, rules can be added to the algorithm to simulate the thinking process of the engineer. Those rules are often based on ratios,

such as 'the slot depth must be less than 90% of the distance between the stator OD and ID', or 'the minimum thickness of the back-iron for a machine of this size would be 20 mm'.

Optimizations of electric machines are often done successfully on computers. These optimizations often have limitations like the rules above, and these rules are basically ratiometric. However, the dimensions are not created using ratios, rather some designs are eliminated using these ratios. Using GA or PSO algorithms, with standard units, failures like the one in Figure 45 can occur.

(a)   (b)
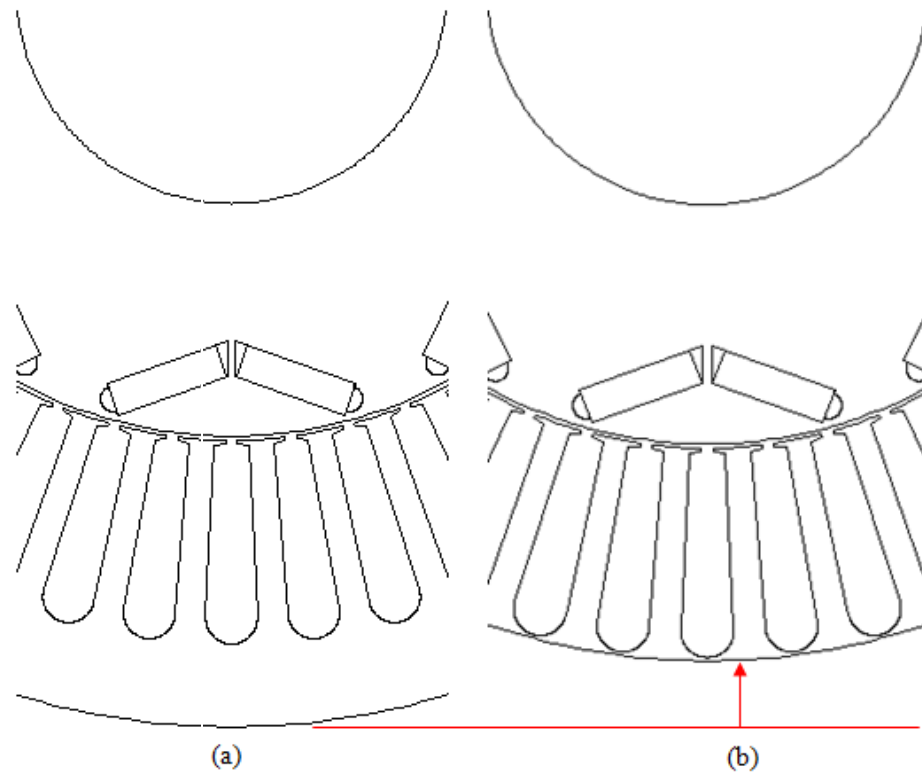
Figure 45, 11% reduction of the stator outer diameter

Figure 45 shows two views of a rotor and stator lamination, before and after modification. Figure 45 (a) is of the laminations before modification, Figure 45 (b) is of the laminations after modification. The machine design of Figure 43 was to be modified by reducing the stator OD by 11%. The stator slots maintain the same depth, and the stator slot nearly goes through the back-iron of the stator. This stator is neither electromagnetically nor mechanically sound. For this minor change of diameter, nearly every significant dimension (slot depth, upper and lower slot widths, rotor diameter, magnet lengths, magnet depth, web widths) needs to be modified.

When human driven optimization is performed, with standard engineering units (mm, inches, etc.) there is a tendency to fix the stator and rotor diameters, rather than allowing them to vary in the optimization process. Consequently, the benefits of changing the stator or rotor diameters are often unknown. When computer driven optimization is performed, situations such as the above will occur. The algorithm will analyze this machine, even though it is obvious to a human that it is not manufacturable.

Minor changes to designs

For the case above, if the stator OD was to be reduced by an engineer, the laminations would typically be scaled, and perhaps some of the optimization for the coil slots or rotor would be repeated. However, if the change is not considered significant, the slots might simply be shortened until an optimum is found. This would be a sub-optimal design. While scaling of the machine is a good initial step, designs benefit from optimization.

Dimensionless parameters do not eliminate the need to optimize this machine again. However, they simplify the work of scaling the machine, and then of modifying its dimensions. They eliminate the need to change the dimensions in a specific order.

2. Types of dimensionless parameters

There are at least two types of dimensionless parameters. The first is a ratio of identical units. An example of this is the Mach number, which is the speed of an object moving through a fluid, divided by the speed of sound in that fluid.

The second type of dimensionless parameter is a ratio of more than two variables, where the units cancel. An example of this is the Reynolds number, which is:

$$Re = \frac{\rho V D}{\mu} \tag{4.1}$$

Where ρ is the density (kg/m^3), V is the velocity (m/s), D is the diameter (m), and μ is the dynamic viscosity (kg/m-s).

While it is not immediately obvious that the dimensions cancel, the Reynolds number allows similarities to be observed between objects of differing sizes, traveling at differing velocities, through differing fluids.

Dimensionless parameters as ratios

As applied for this research, the dimensionless parameters are similar to the Mach number. Dimensionless optimization (DO) is applied by taking many of the physical dimensions of the electric machine, and rendering them into dimensionless ratios. Rather than specifying the stator inner diameter as 67.34 mm, the stator inner diameter ratio is specified as 0.564 (the ratio of the stator ID to the stator OD).

Similitude and dimensionless parameters

Dimensionless parameters can be used to establish similarity between experiments or designs relating machines of different power levels, different constant power speed

ranges, different torque densities, etc. Trends in dimensionless quantities, as power levels, etc. are varied can be used to predict the optimum operating point of a machine, before optimization is begun on a specific machine. Based on an accurately predicted starting point, the design space to be searched can be smaller, and optimization can occur more rapidly.

Using dimensionless parameters is not new to electric machine design; however the use of physical dimensionless ratios has focused primarily on the split ratio, which has been studied by a number of researchers. Dimensionless parameters have not been used as a tool to understand the relation of the physical dimensions of the machine to its performance, or to other machines.

Design guidelines

The use of dimensionless parameters in communicating ratios makes it possible to set limits on the dimensionless parameters. This is used to establish manufacturability, in the case of slot openings; or to make certain that the geometry is feasible. This last case is shown, for example, when the slot depth ratio is equal to, or larger than 1.0. When R_{SDL} is 1.0, the geometry is not feasible, as the bottom of the slot would cut through the outside of the stator.

3. The benefits of dimensionless parameters to manual design

Rendering the geometric parameters of an electric machine dimensionless has significant benefits, even if the optimization is done manually by the engineer. An example of the benefits of using dimensionless parameters is the ability to vary the stator diameter independently of the other dimensions. If the rotor diameter is proportional to

the stator diameter, then when the stator diameter is decreased, the rotor decreases

proportionately. At the same time, the slot depth adjusts to the difference between the

rotor diameter and the stator diameter, and the magnet slots become smaller. This

alleviates a significant amount of tedious work on the part of the engineer, and reduces

the likelihood of data entry errors. Similarly, when the stator becomes larger, the slots

become deeper, and the slot widths and openings also become larger, automatically.
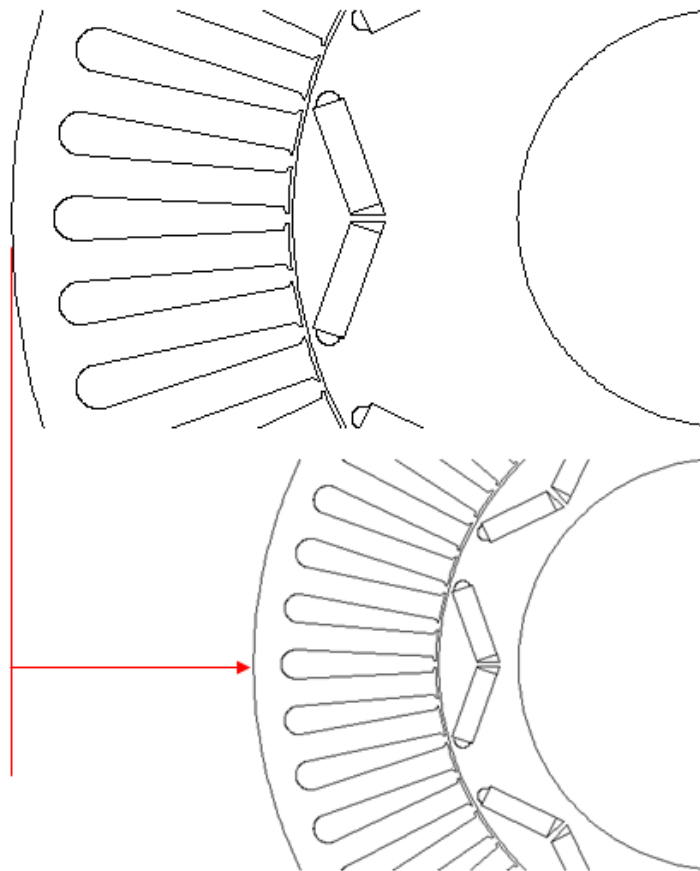
Figure 46, Scaling of machines by varying the stator diameter

Exceptions to this typically depend on mechanical or manufacturing considerations,

for instance the shaft torque and material determine a minimum shaft diameter. In Figure

46, the bottom machine is 67% the size of the top machine. The rotor, stator and all slot

geometries were scaled automatically by the dimensionless parameters. However, the

shaft (inner diameter) remained the same size. If the shaft can be made smaller, further

reductions in size are possible. If the shaft is at its minimum diameter, the design has

reached its limit as far as scaling the stator diameter down. This is not a limitation of the

method, but a limitation of the constraints of the machine.

Another benefit to the use of dimensionless parameters is that rotor magnet

dimensions and stator slot dimensions can be optimized independently. When standard

units are used, the machine designer typically optimizes one or the other first, going back

and forth between the two. It would be rare for a designer to adjust the stator slot depth

before the rotor diameter. For these two dimensions, the rotor diameter must be set first.

With dimensionless parameters, the engineer can make changes in any order, focusing on

regions that appear critical, perhaps due to high flux densities, high current densities, etc.

Therefore, the benefits of dimensionless design are:

- The models are more robust, (do not crash as a result of conflicting dimensions)
  For most of the parameters, the parameters range between 0.0 and 1.0. Any setting
  between 0.05 and 0.95 can generate geometry, though the design may not be efficient.

- Dimensionless parameters eliminate the need to create additional rules in
  computerized optimization algorithms (DO, GA or PSO), which emulate the
  engineer's thought processes. The need for these rules leads to what the author calls
  'over-complexificational behavior', the choice of a complex method, when a simple
  method is available.

- Regions of the design space can be more easily eliminated. Typically, only a small portion of the design space contains efficient designs. For example, for an efficient design, the rotor diameter will probably be between 0.4 and 0.6 the diameter of the stator. If the program is initially set up to restrict variations of this parameter between 0.4 and 0.6, a large portion of the infeasible design space will not need to be searched.

- Dimensionless variables make it simpler to see similarities between systems which are different in size, speed, power, etc. If the parameter values are stated in terms of millimeters or other common engineering units, it is difficult to estimate the effect of a change to the machine's engineering specification.

  An example of this is that if the torque level of an electric machine is doubled, and the machine is simply scaled, all dimensions would increase by the cube root of 2. Understanding trends of machine dimensions using DO allows an estimate of how the optimal machine dimensions change with the new torque requirement.

- The region of the optimum ratio can be estimated beforehand. This is one reason for the number of papers written on the optimum split ratio. This method allows designers to create design guidelines. Since the speed of optimization often depends on an initial 'good guess', the use of this data accelerates optimization. These educated guesses, based on previous data, can be embedded into the optimization code, or drawn from a database.

- An engineer with knowledge of the ratiometric values and trends as specifications change gains an increased understanding of these machines.

- Dimensionless parameters enable a greater understanding of the interactions among various parameters. There are significant interactions between the parameters of an

electric machine. It is not obvious what the impact on slot width will be if the rotor diameter increases from 95 to 105 mm. However, from the interactions figures developed during the research, the change on the slot width based on a rotor ratio change from 0.45 to 0.50 can be estimated.

For the above reasons, dimensionless parameters are part of the design method.

4. The benefits of dimensionless parameters to optimization

Dimensionless parameters have benefits when applied to both engineer driven, and computer driven optimization.

Computer driven optimization

An alternative to the trial and error approach is to use optimization techniques which allow the computer to vary the dimensions of the machine. For the example above, this allows the stator or rotor diameter to change independently of the other dimensions. Therefore, a larger portion of the design space can be more easily searched.

The problem with this approach is that the computer algorithm may generate designs which cannot be manufactured. This was seen in the literature, where the 'optimal' design was not manufacturable. In that research, only seven of 20,000 designs randomly created could be manufactured. The authors modified their study by selecting a similar production design, and deviating only minimally from that design. This made more of the designs feasible, but there were still designs which were not manufacturable, one of which was the 'optimal' solution.

A comparison between the two methods (the use of standard engineering units and the use of dimensionless parameters) is difficult to make. An example can be created for

a machine which would have the dimensionless boundaries specified for an 8 pole, 48

slot machine producing 90 Nm of torque, and 30 Nm/liter, using the searchable design

space from CHAPTER II.D. Table 22 is a duplicate of the table from that chapter.

Table 23, Parameter bounds of searchable design space

Parameter	Design space limitation	Design range	Parameter	Design space limitation	Design Range
R_{Spl}	0.40-0. 70	0.10	R_{SDL}	0.5 – 4.0 (logarithmic)	$x_u = x_l \times \sqrt{2}$
R_{SDp}	0.40-0.80	0.10	R_{Web}	00.05-0.35	0.10
R_{SW2}	0.25-0.65	0.10	R_{MDp}	0.05-0.55	0.10
R_{SW3}	0.35-0.65	0.10	R_{MTh}	6.0-10.0	2.0

The volume for this machine will be 3 liters, or 3,000,000 cu mm. If standard units

are to be used, and the genetic algorithm must be able to search at least the design space

listed above, some of the maximum and minimum dimensions shown in Table 24 result.

Table 24, Stator geometric boundaries using dimensionless parameters

	Minimum (mm)	Maximum (mm)
Length (from R_{SDL})	61.97	247.88
OD Stator (from R_{SDL})	124.27	248.27
OD Rotor (from R_{Spl})	49.65	173.79
Slot depth (from R_{SDp})[32]	*	59.59
Top slot width (from R_{SW2})	0.81	7.39
Bottom slot width (from R_{SW3})[33]	1.14	15.27

---

[32] Slot depth is calculated based on the thickness of the back-iron, and R_{SDp}. For some combinations of dimensions, the back iron was negative.
[33]

It can be seen from this table that the diameter of the largest rotor which is possible is 50 mm larger than the outer diameter of the smallest stator. A machine with these dimensions cannot possibly be built, as Figure 47 shows.

If the dimensions are limited to the dimensions above, and are randomly distributed, this situation occurs approximately 8% of the time. However, these are the probabilities for the rotor to be larger than the stator. This is not the probability for the rotor to be larger than the hole in the stator, which is what is shown in Figure 47, and which is required.
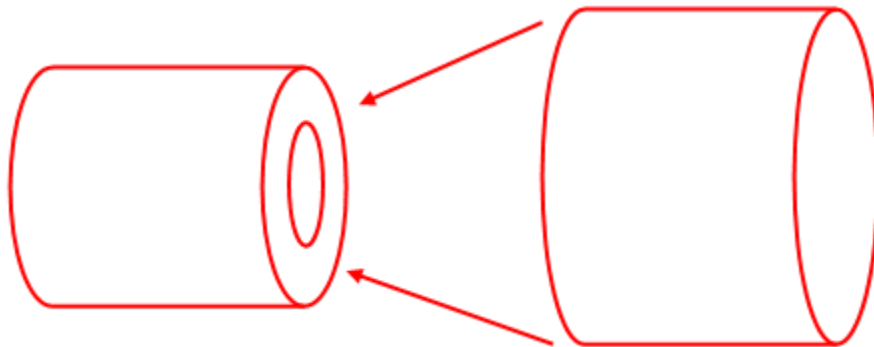
Figure 47, The largest rotor and smallest stator

Another situation which can occur using randomly generated dimensions is that the bottom of the slot will pierce through the outside of the stator, as mentioned before, and as shown in Figure 48.
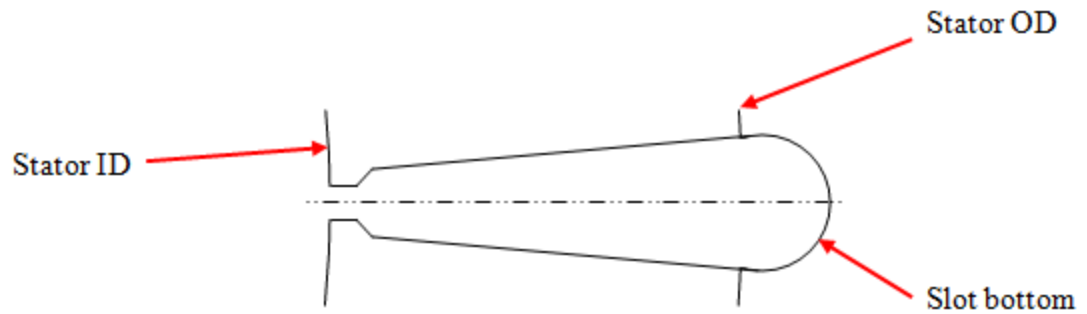
Figure 48, Bottom of slot piercing through outside of stator

With the constraints given, an additional 71.6% of the designs have this problem.
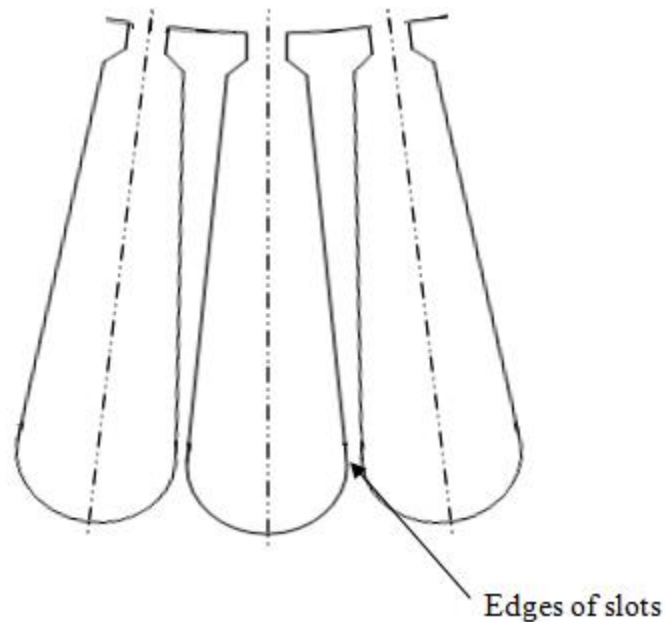
Figure 49, Region where edges of slots can touch

The width of the slots at the bottom can also become large enough that the edges of the slots intersect. An example of very thin teeth, which is where this problem would occur, is shown in Figure 49. The problem of the teeth actually having no width occurs an additional 9.3% of the time, given the constraints above. One or more of the above three problems occurs 88.8% of the time.

The remaining 11.2% of the designs are not necessarily feasible, and many of them have interferences in the rotor lamination slots, which are not discussed here. A significant number of the designs which do not have inferences will be extremely poor designs, and will not achieve rated power. If all eight parameters which have been rendered dimensionless are included, the proportion of acceptable designs is very small.

The adoption of the dimensionless parameters used in this research, by itself, produces benefits for methods such as genetic algorithms, particle swarm optimization and others. It greatly reduces or eliminates the creation of geometry which is not manufacturable.

E.   Selection and treatment of design variables

As mentioned, the method of optimization developed used eight geometric variables. These were selected based on their impact on performance, and how well they define the geometry, while creating models which will not 'crash'.

Dimensions were broken down into the following classes:

- Variables used to create the response surface (8)

- Parameters calculated from the above 8 variables

- Parameters determined by the performance of the machine

- Parameters which were not optimized by the method

1. Parameters selected to form the response surface

Figure 50 shows a view of the rotor in dark gray, surrounded by the stator in light gray. The pink and blue portions are magnets, the pink magnets having their flux flowing

outward, and the blue magnets having their flux flowing inward. Being pink and blue, they are naturally attracted to one another.

Some parameters were rendered dimensionless, but were not used as parameters to be optimized. These were not varied because the optimum value of that parameter was known. Other parameters were not varied because the parameter had a minimal effect on the performance of the machine, and had a ratio which can be determined for other reasons, e.g. manufacturing.
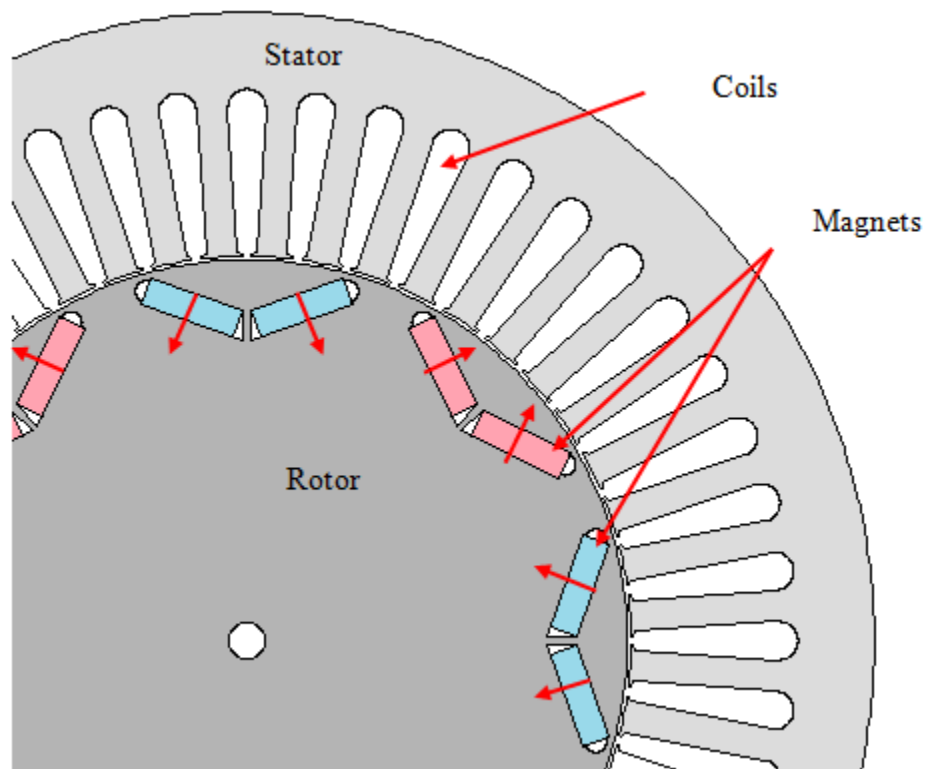
Figure 50, Portion of motor, showing rotor, stator and magnets

In the machine analysis program used [38], with the shape of the stator and magnet slots chosen, there are approximately 40 dimensions that can be varied. The reasons for rendering specific parameters dimensionless follow.

Stator aspect ratio, R_{SDL}

Figure 51 is a photo of the 2010 Toyota Prius motor [39]. The diameter and length of the stator are visible. The stator aspect ratio (diameter divided by length) appears to be on the order of 4:1 or more. The stator appears to be shorter than the previous Prius motor, indicating they have changed the stator aspect ratio.

Figure 51, 2010 Toyota Prius motor

The length and diameter of the stator are fundamental dimensions of an electric machine. In earlier research by the author, using genetic algorithms, three 60 kW machines were optimized with stator aspect ratios of 2:1, 1:1 and 0.5:1. The most efficient machine with a stator aspect ratio of 2:1 had losses of slightly less than 3000 Watts, while the most efficient machine with a stator aspect ratio of 0.5:1 had a loss of over 5000 Watts (see Figure 53). This indicates that the stator aspect ratio has a significant impact on performance, and is a parameter which should be optimized.

If the diameter and length are both parameters of the algorithm, and the number of variables is limited to eight, only six additional parameters can be varied. By requiring

the torque density to be a specification, the stator diameter and length become related. The torque density is primarily determined by the cooling methods used in various types of machines (aerospace, industrial, etc). Higher torque densities can be achieved when cooling methods are aggressive (liquid cooling, spray cooling, etc). Machines of the same class and cooling method tend to have similar torque densities. Therefore, torque density is a reasonable specification to require.

Given that the torque density and maximum torque are specified, the volume of the stator envelope is known. The stator's length determines the diameter, or vice versa. Therefore, the stator aspect ratio was the first dimensionless parameter defined, and it is defined as:

$$R_{SDL} = \frac{D_{sta}}{L_{sta}} \tag{4.2}$$

where R_{SDL} is the stator aspect ratio, D_s is the stator diameter (mm), L_s is the stator length (mm, see Figure 52).

For some electric machines, the stator and rotors have differing lengths. For the validation examples, the stator and rotor lengths were the same.

Split ratio, R_{Spl}

As mentioned earlier, given the diameter of the stator, the split ratio determines the diameter of the rotor. Figure 52 shows the stator length (L_{sta}), the stator diameter (D_{sta}) and the rotor diameter (D_{rot}). The split ratio is defined as:

$$R_{Spl} = \frac{D_{rot}}{D_{sta}} \tag{4.3}$$
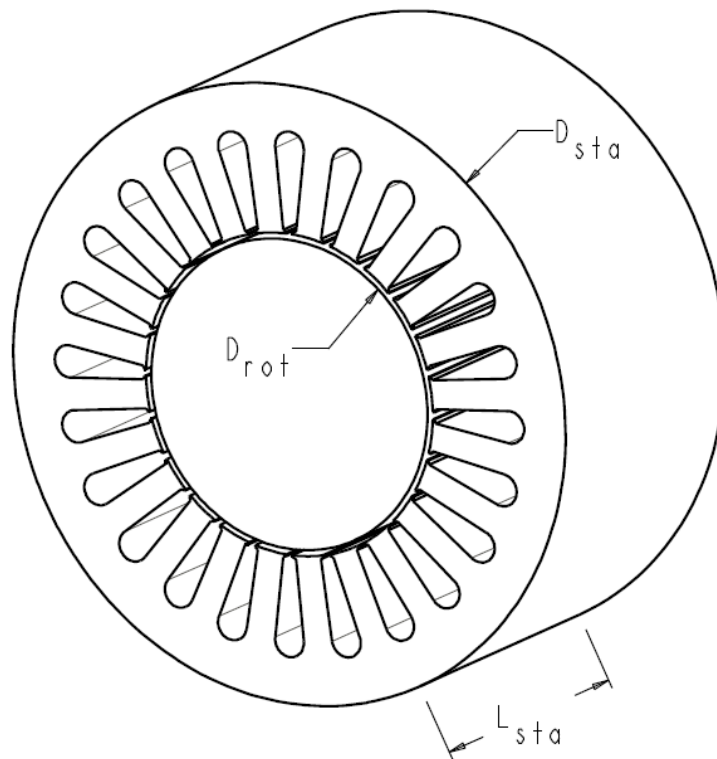
Figure 52, Stator aspect ratio (R_{SDL}) and split ratio (R_{Spl})

In earlier research by the author, using genetic algorithms, the scatter plots in Figure 53 were produced. These plots are for the stator aspect ratios indicated, and are the result of analyzing approximately 2400 designs.

The green line is a convex hull polygon. The red line is a quadratic curve fit to the convex hull. For these specific designs, the split ratio has an optimum of slightly over 0.6. These early plots showed the impact of many of these variables on efficiency. The convex hulls for many of them approximate the shape of a quadratic curve. This indicates that a response surface will consist of main effects and quadratic effects, at a minimum. Other research indicated that interactions must be included, as expected.
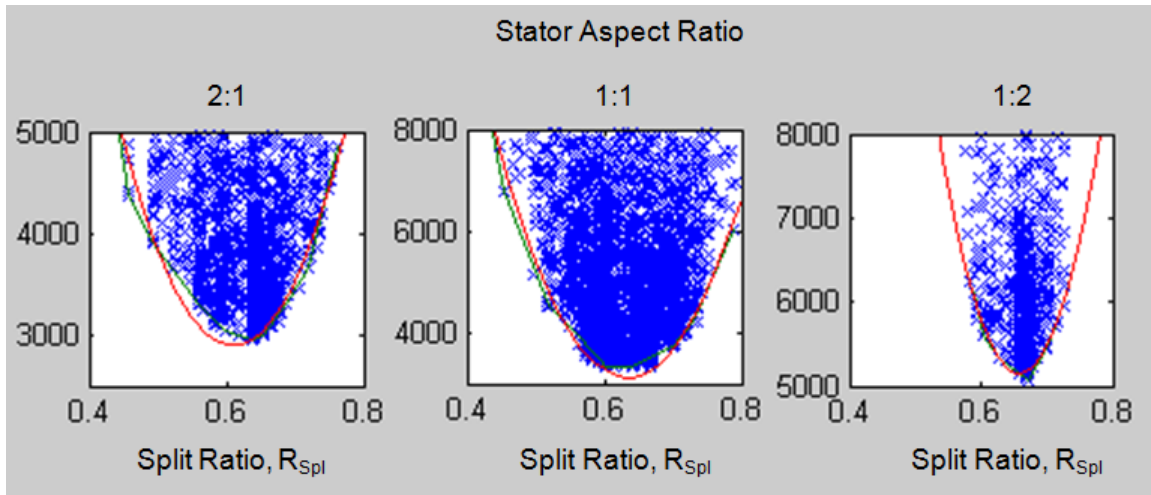
Figure 53, Results of GA optimization of 60 kW IPM machine, the stator aspect ratio and split ratio

The efficiency is very sensitive to the split ratio. For this reason, the split ratio was chosen to be one of the parameters which would be optimized.

Slot depth ratio, R_{SDp}

The stator slots contain the copper coils, which conduct electrical current. As the slot depth increases, with a fixed number of turns in the coil, the resistance of the windings decreases. At the same time, as the slot depth increases, the back-iron thickness is reduced, and the flux density in the back-iron increases. This makes it more difficult to push flux through the steel, increasing the iron loss.

Figure 54 shows the slot depth (H_3) and the slot depth at which the slot would become tangent with the outer surface of the stator (H_{3max}). The slot depth in that figure is approximately 0.65.
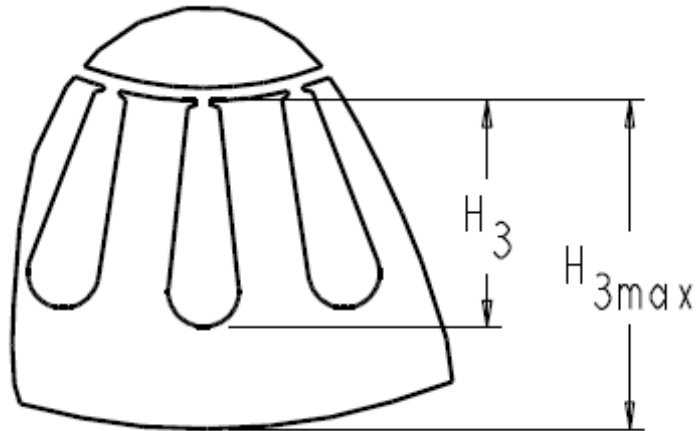
Figure 54, Variables required to calculate the slot depth ratio (R$_{SDp}$)

The slot depth ratio is defined as:

$$R_{SDp} = \frac{H_3}{H_{3\max}} \tag{4.4}$$

$$H_{3\max} = r_{SOR} - r_{SIR} \tag{4.5}$$

where r_{SOR} is the stator outside radius and r_{SIR} is the stator inside radius
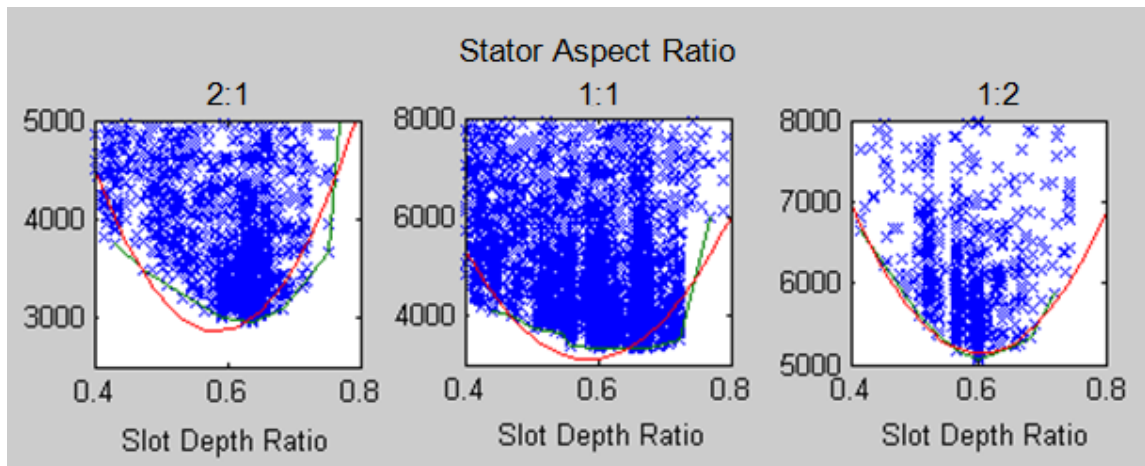
Figure 55, Stator aspect ratio and slot depth ratio effect on losses for 60 kW IPM machine

The scatter plots of the GA work of slot depth ratio vs. losses done earlier are shown in Figure 55. The figures show the significant effect of the slot depth ratio, therefore this ratio was chosen to be included in the optimization.

Slot shapes

The slot width ratios are two ratios which determine the upper and lower widths of the slot for this slot shape. Other slot shapes were considered, including those shown in Figure 56.

(a)   (b)   (c)   (d)
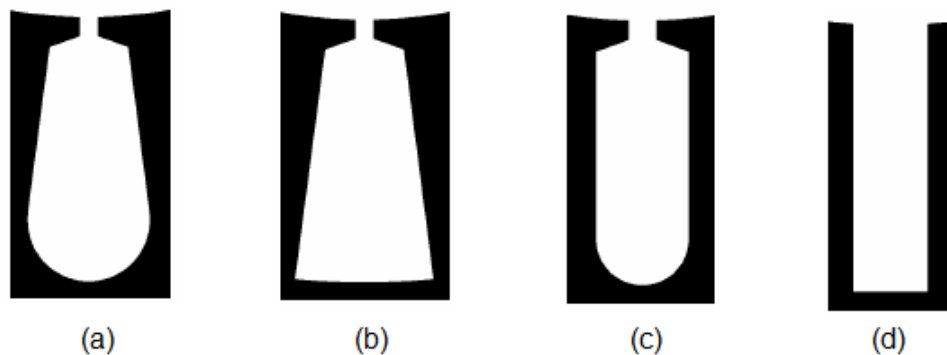
Figure 56, Alternate slot shapes considered for the validation algorithms [38]

Slot shape (a)

The method is not dependent on the slot shape, however to validate the method, one slot shape had to be chosen. The first slot shape, Figure 56 (a) is similar to the slot shape chosen. For slot (a) the tooth sides are parallel. Slots with parallel teeth are common in electric machine design, however it is desirable to not constrain the teeth to be parallel. This is because the method is designed for a large range of machine requirements. It was found early in the research that the optimum designs did not always have teeth which were parallel.

The effect of specifications, such as speed ranges, overspeed requirements, power level, etc. is not always known. While slot shape (a) may be an efficient choice for many machine requirements, allowing the algorithm to determine whether the teeth should be parallel provides a higher degree of certainty that the design would be optimal.

Slot shape (b)

Slot shape (b) is similar to slot shape (a), except that the bottom of the slot is not round. Radii are allowed in the lower corners, though they are not shown. The teeth have parallel sides, rather than the slot walls. This slot shape could be optimized by the method, using design rules to determine the radius in the corners, or allowing the tooth width ratio (an alternate ratio), and the lower slot radius ratio (a second alternate ratio), to replace R_{SW2} and R_{SW3}. If a lower number of slots is required, or if concentrated coils are specified, slot shape (b) would be preferred, as a slot shape with a round bottom is not physically realizable with a low number of slots.

Slot shape (c)

Slot shape (c) has the walls of the slots parallel to each other, rather than having the teeth have parallel walls. Like slot shape (a), this reduces the number of optimization parameters by one. It is known that this will not always be the optimal slot shape, as optimal designs typically have teeth which are more nearly parallel. Therefore, this slot shape was not used.

Slot shape (d)

Slot shape (d) also has parallel walls for the slot. This slot shape would be used for form-wound coils. This is used on some IPM machines, specifically in some hybrid vehicles. This slot shape could be an alternative to the one selected, if form-wound coils

are specified. The validation algorithm written was targeted at meeting the needs of IPM machines which might be used in automotive vehicles. Most of those are currently random wound, and have a round bottom to the slot. Slot shape (d) was, however, used in the early development of the GA based algorithms mentioned above.

Because of the widespread use of a slot shape similar to (a) in hybrid vehicles, a slot shape similar to (a) was chosen for the validation research, where the widths at the top and bottom of the slot could be adjusted.

For the slot shape selected, the top and bottom widths of the slot can be varied independently. Figure 57 shows the upper portion of the slot, and how the upper slot width ratio, R_{SW2} was determined. The figure shows an R_{SW2} of 0.33.
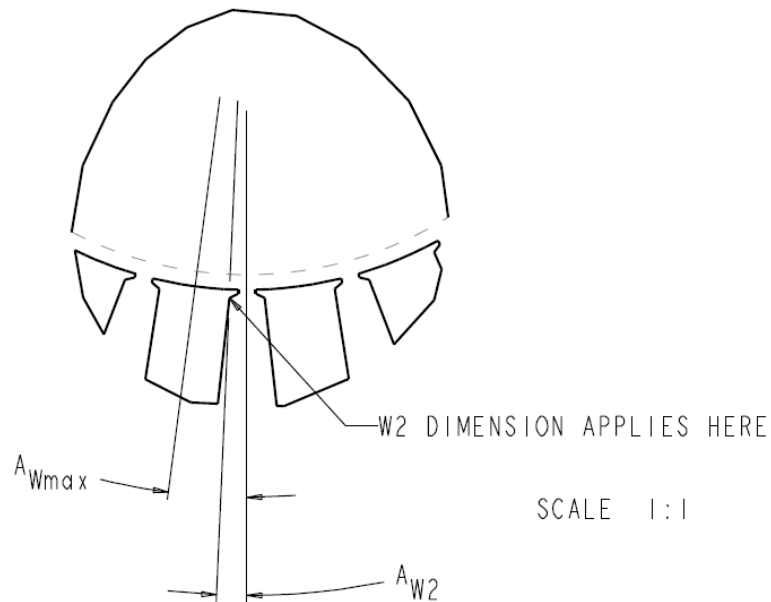
Figure 57, Variables required to calculate slot width ratio R_{SW2}

The ratio for width at the upper shoulder for the slot is:

$$R_{SW2} = \frac{A_{W2}}{A_{W\max}}$$

(4.6)

where A_{W2} is the angle from the center of the slot to the upper corner of the slot, and

A_{Wmax} is the angle from the center of the slot to the center of the adjacent tooth.
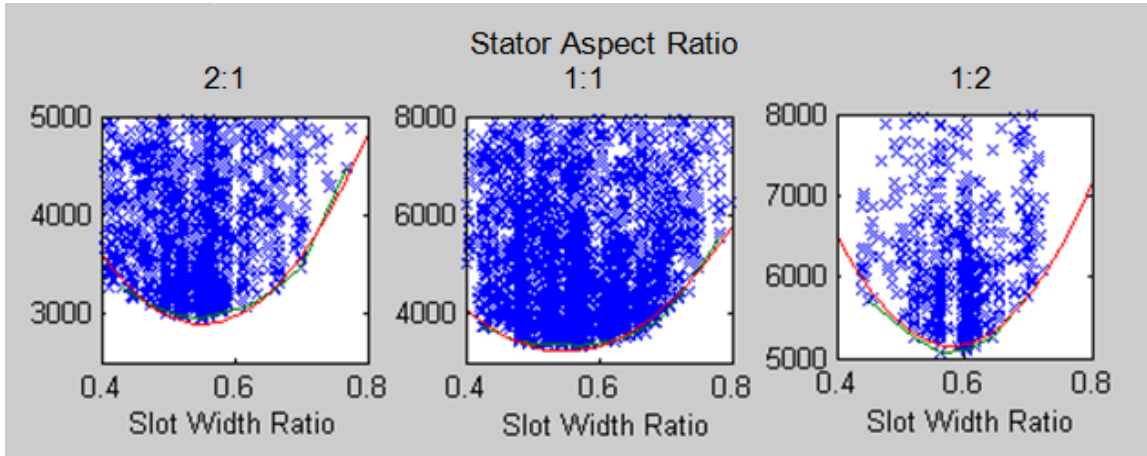
Figure 58, Stator aspect ratio and slot width ratio effect on losses for 60 kW IPM machine

The plots in Figure 58 are from earlier GA research. The slot width ratio has a very

strong effect on efficiency. It also appears in these plots, that the stator aspect ratio R_{SDL}

has an interaction with the slot width ratio. This was true in many of the other plots.

As the slots become wider, there is more area for the copper, and therefore the

resistance of the coils decreases. At the same time, as the slots become wider, the teeth

become thinner, the flux density increases, and the steel begins to saturate. Therefore a

higher current is required to push the same flux through the teeth. The power lost in the

copper is determined by the equation

$$W_{cu} = I^2 R \qquad (4.7)$$

Where W_{cu} is losses in the copper windings, per coil (Watts), I is the current in the

windings (Amps), and R is the resistance of the windings (Ohms). Along with this, as the

flux density in the steel increases, there are losses in the steel. Therefore, there is a

compromise between increasing the area for the copper, and increasing the area for the steel.

Slot width ratio R$_{SW3}$
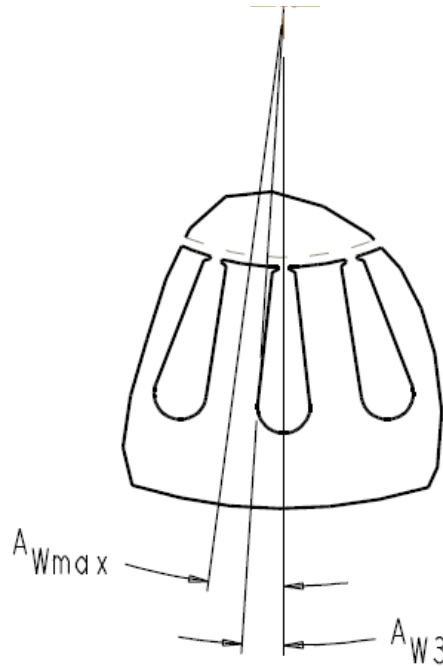
Figure 59, Variables required to calculate lower slot width ratio (R$_{SW3}$)

Figure 59 shows the dimensions which define the lower slot width ratio (R$_{SW3}$); a ratio of 0.5 is shown. The slot width ratio at the lower end of the slot is defined as:

$$R_{SW3} = \frac{A_{W3}}{A_{W \, max}} \qquad (4.8)$$

where A_{W3} is the angle from the center of the slot to the tangent point of the bottom of the slot. The lower end of the slot has the same trade off as the upper and of the slot, trading off copper losses for steel losses. However, as the lower end of the slot becomes larger, the area for copper increases much more significantly than when R$_{SW2}$ is increased.

Web width ratio, R_{Web}
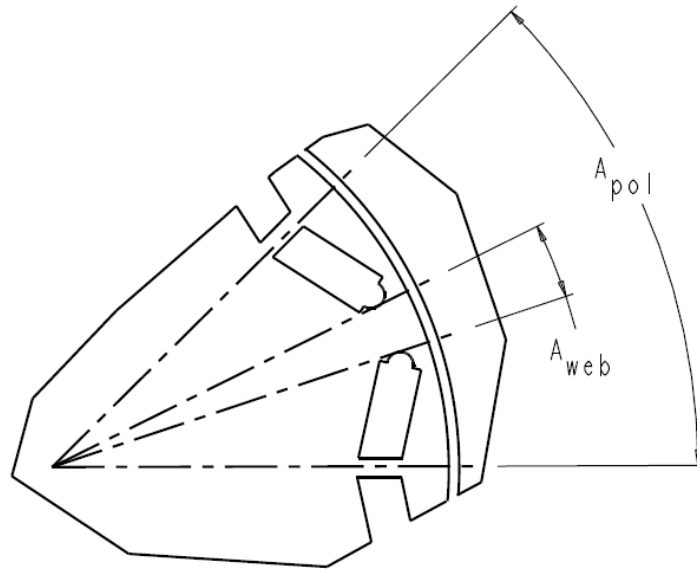
Figure 60, Variables required to calculate web width ratio (R_{Web})

Figure 60 shows the rotor lamination, and details the dimensions required to define

the web width ratio (R_{Web}). A ratio of 0.17 is shown. The web width ratio is calculated

as:

$$R_{Web} = \frac{A_{web}}{A_{pol}} \qquad (4.9)$$

where A_{Web} is the angle formed between the magnets of opposite poles (degrees), and

A_{pol} is the angle formed between the centerlines of the poles. A_{pol} is defined as

$$A_{pol} = 360 / P \qquad (4.10)$$

Where A_{pol} is the angle between pole centers (degrees), and P is the number of poles.

Earlier GA research by the author had not used the web width, but instead used the

'magnet width', measured in degrees. This can be calculated from:

$$MagWid = 180\left(1 - R_{Web}\right) \tag{4.11}$$

where *MagWid* is the magnet width in degrees. The two parameters are related, however the use of R_{Web} is consistent with the other dimensionless parameters, as it keeps the ratio in the same order of magnitude as the other parameters. A plot from this research is given in Figure 61.
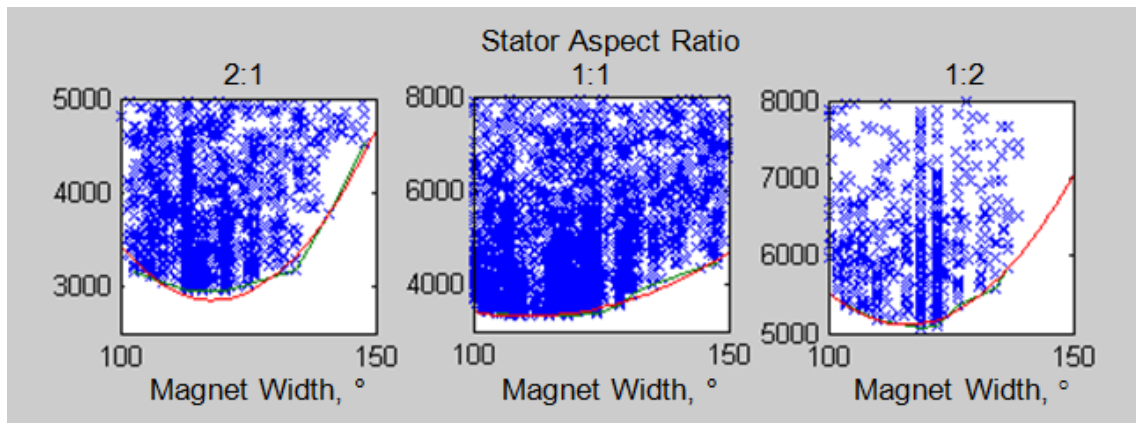
Figure 61, Results of GA optimization of 60 kW IPM machine, the stator aspect ratio and magnet width

The shape of the convex hull polygon of the data points is approximately parabolic, indicating a quadratic effect. The change in magnitudes between the plots indicates an interaction between the magnet width and the stator aspect ratio.

Because of the arc at the end of the magnet slots, at some value less than 1.0, the magnets will have zero length. A large value of R_{Web} results in a larger q-axis inductance, and therefore a higher component of reluctance torque. Therefore, it is expected that optimal values of R_{Web} will differ for machines with differing CPSR specifications.

R_{Web} has a second interaction with rotor size and speed. At high speeds, the centrifugal forces in the rotor increase. As R_{Web} decreases, the magnet width becomes longer. This increases the mass of the slug which the bridge and post must support. The increased mass raises the stresses in the bridges and post. To reduce the stresses, the post and or the bridge must become thicker. This increases flux leakage in the machine, which wastes magnet material.

In high speed machines, it is expected that optimal machines will have higher values of R_{Web} than low speed machines. Based on the plots of Figure 61, the efficiency of the machines is sensitive to R_{Web}.

Magnet depth ratio, R_{MDp}
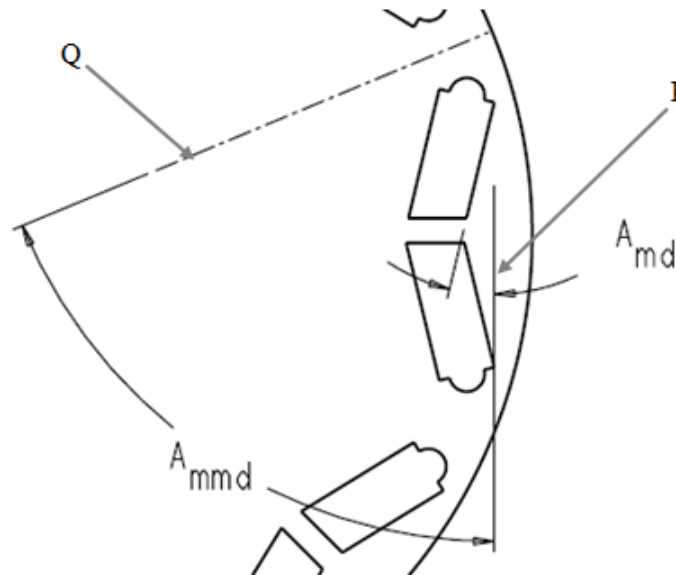
Figure 62, Variables required to calculate the magnet depth ratio (R_{MDp})

The magnet depth ratio is calculated as:

$$R_{MDp} = \frac{A_{md}}{A_{mmd}} \qquad (4.12)$$

where A_{mmd} is the angle between lines P and Q (which is a line from the center of the rotor between two adjacent poles), and A_{md} is the angle between line P and the outer face of a magnet, as shown in Figure 62. In that figure, a ratio of 0.2 is shown. Line Q is a line from the center of the rotor which lies between the poles. Line P is a line perpendicular to the pole.
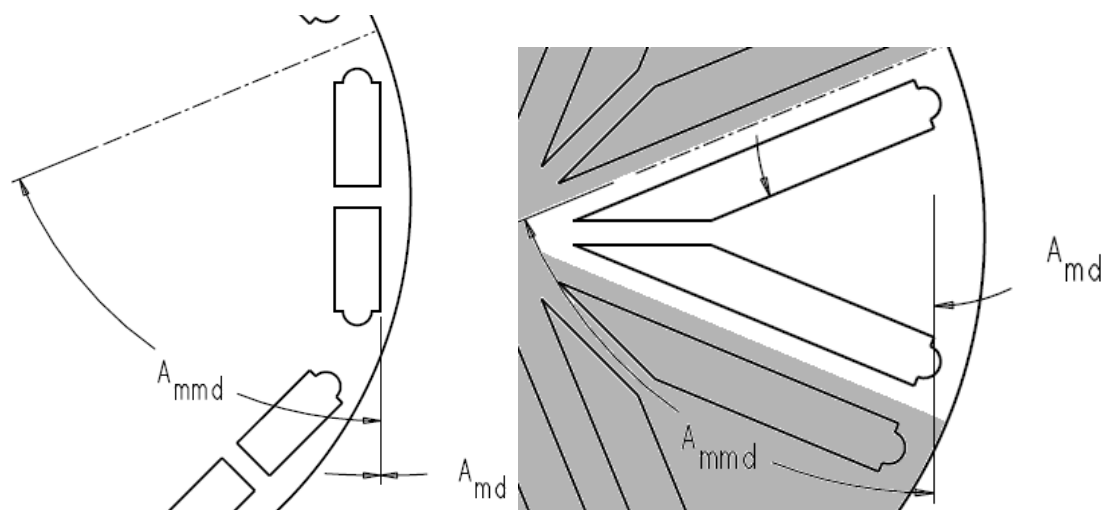
Figure 63, Magnet depth ratios of 0 (left), and 1.0 (right)

The magnet depth ratio is therefore a measure of the angle of the magnet, which determines the magnet slot depth into the rotor. Figure 63 shows magnet depth ratios of 0.0 (on the left) and 1.0 (on the right). The earlier GA research with the magnet depth ratio used a different measure of the magnet depth, based on the radius of the rotor, and how close the magnets came to the center of the rotor. This ratio was more difficult to understand than a ratio based on the angle of the magnet. Plots of the earlier GA work are shown in Figure 64.
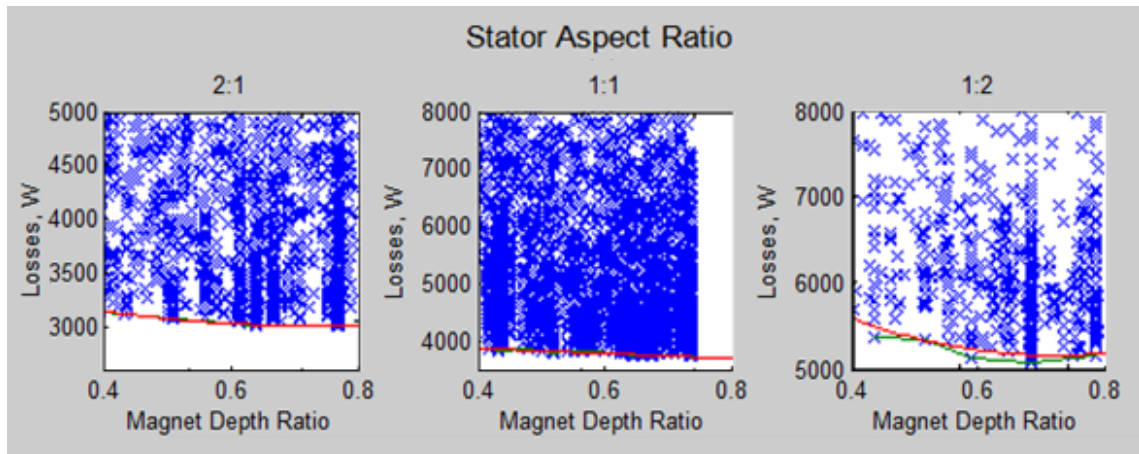
Figure 64, The stator aspect ratio and magnet width effects on a 60 kW IPM machine

The effect of the change of depth is less than previously mentioned ratios, however there is an effect. As the magnet depth increases, at least three things happen. First, the magnet length increases, and therefore the expense increases. Second, the surface area of the magnet to the direction of flux increases. This increases the amount of flux from the rotor to the stator, which may allow for a smaller rotor, and therefore a reduced rotational inertia of the rotor, and more area in the stator for coils, or more area for back iron. Third, the mass of the magnets and the steel 'outside' of the magnets increases.

The increased mass creates larger centrifugal forces away from the center of the rotor. These forces are carried by the post between the two magnets which form a pole, and the bridges on the outside edges of the magnets. The steel outside of the magnets is sometimes called a slug. As the mass of the magnets and slug increases, the thickness of the post and/or bridges must increase. Typically, this material is magnetically saturated, and takes flux away from the magnets. Therefore, there is a point of diminishing returns, related to the magnet depth. As the magnet depth is increased, the added magnet length

generates more flux; but the magnet mass increases, the magnet cost increases, and flux leakage is increased.

For the initial GA work, there was no post, and all stresses were carried by the bridges. At that time, mechanical FEA had not been implemented, and the method did not include increasing the post and bridge thicknesses to compensate for these added forces. When the decision was made to include mechanical FEA in the analysis, it was decided that the bridge and post thicknesses would be determined by stress analysis. These are the portions of the rotor which see the highest stresses.

Figure 65 shows the bridge of an IPM machine, when the magnet depth ratio is 0. For rotors which do not experience extreme stresses in the bridge (stresses near the yield strength of the material), it is sometimes possible to eliminate the post. This is true for lower speed machines, or smaller machines. This special case is not taken into account by the method created by this research.
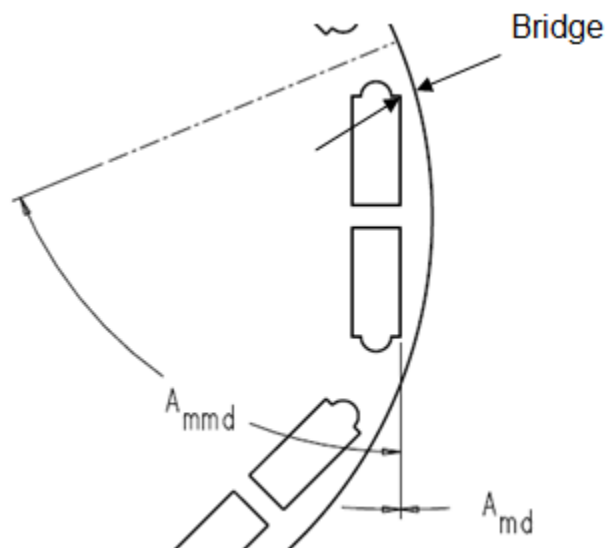
Figure 65, Bridge of IPM machine

Figure 66 is a scatter plot from the earlier GA research on IPM machine design. At this time, bridge thickness was varied, without regards to the strength requirements of the bridge. This figure shows the effect of bridge thickness on efficiency. The effects become greater as the bridge thickness increases, and as the stator aspect ratio increases. While the bridge thickness was studied in the GA based research, it is not used as a variable for the method of the current method. The bridge thickness is determined by the mass of the magnets and the 'slug' outside of the magnets, and the overspeed specification. Therefore, the bridge thickness, magnet thickness, magnet depth and web width are now interrelated.
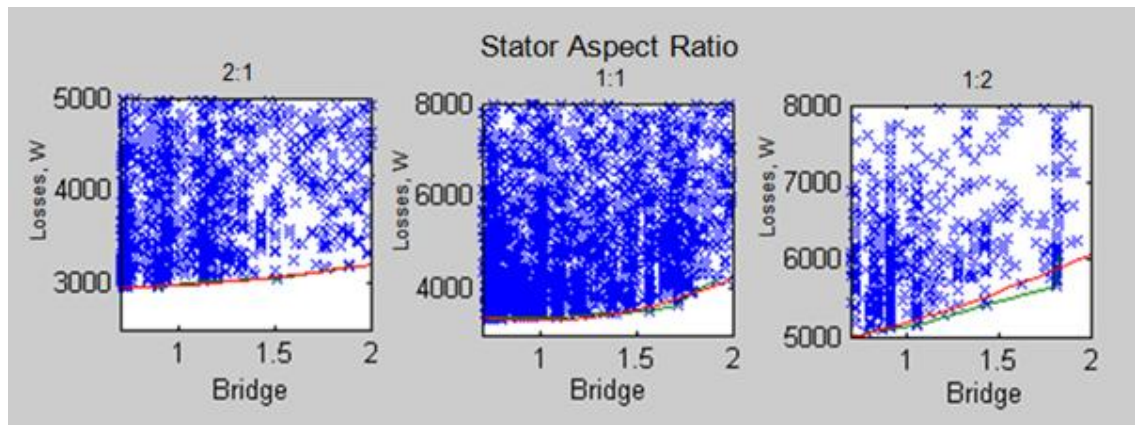
Figure 66, Results of GA optimization of 60 kW IPM machine, the stator aspect ratio and bridge

Magnet thickness ratio, R_{MTh}
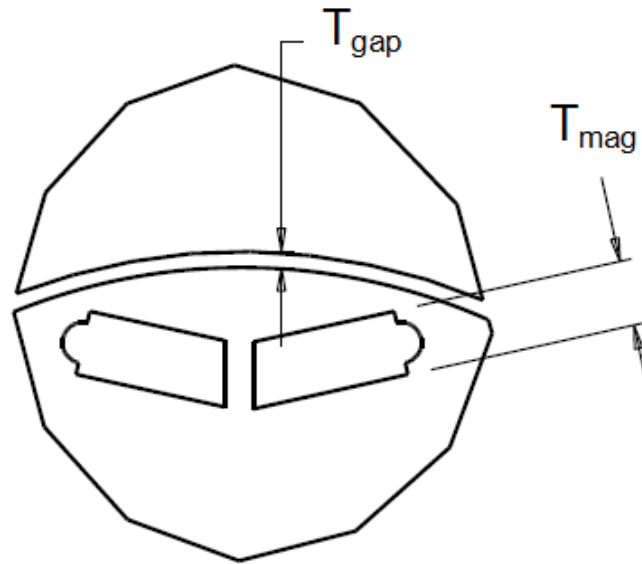
Figure 67, Variables required to calculate the magnet thickness ratio (R_{MTh})

The magnet thickness ratio is calculated as:

$$R_{MTh} = \frac{T_{mag}}{T_{gap}} \tag{4.13}$$

where T_{mag} is the magnet thickness, and T_{gap} is the air gap thickness, (the distance between the rotor and the stator), as shown in Figure 67. This ratio is different from the other ratios in two ways. First, its magnitude for efficient machines will be larger than one. Second, it is a ratio of something inside the rotor (the magnet thickness) to something outside the rotor (the air gap between the rotor and stator). This ratio has a significant effect on the magnetic circuit, especially when the machine is not saturated.
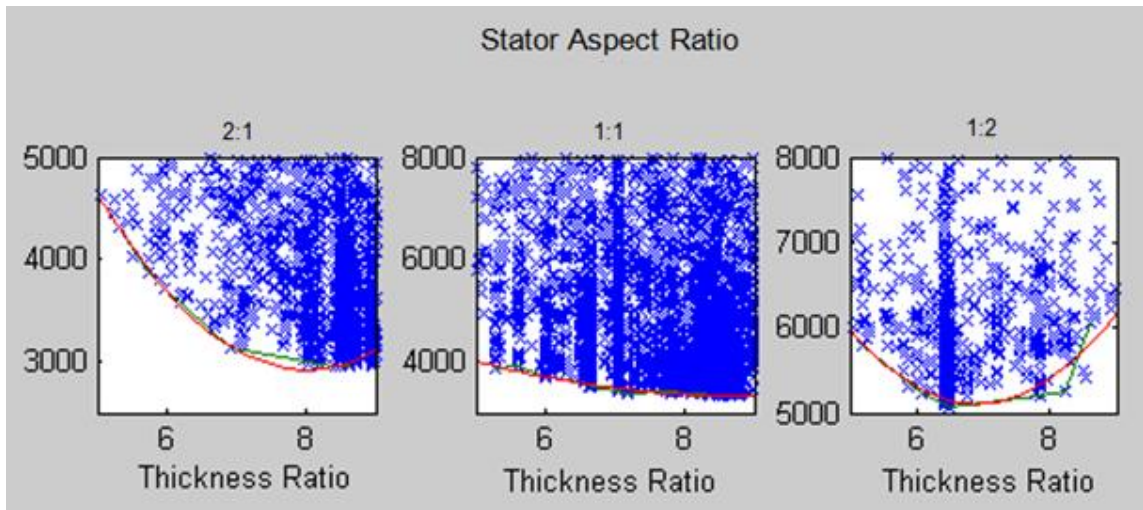
Figure 68, The stator aspect ratio and thickness ratio effect on a 60 kW IPM machine

There is a very strong effect of thickness ratio on efficiency seen in Figure 68. Again, it appears to be quadratic in nature. It can also be seen that it has a much greater effect at some stator aspect ratios than others.

In simplified magnetic circuits, with infinitely permeable steel, the flux passing through the gap has a linear relationship with the thickness of the magnet and the thickness of the air gap.

As can be seen in Figure 69, the slope of the load line is determined by the lengths of the magnet and air gap (T_{mag} and T_{gap}), the areas of the magnet and air gap (A_m and A_g), the leakage coefficient (k_1), and a loss factor (k_2).

$$slope = \mu_0 \frac{-k_1 A_g T_{mag}}{k_2 A_m T_{gap}}$$
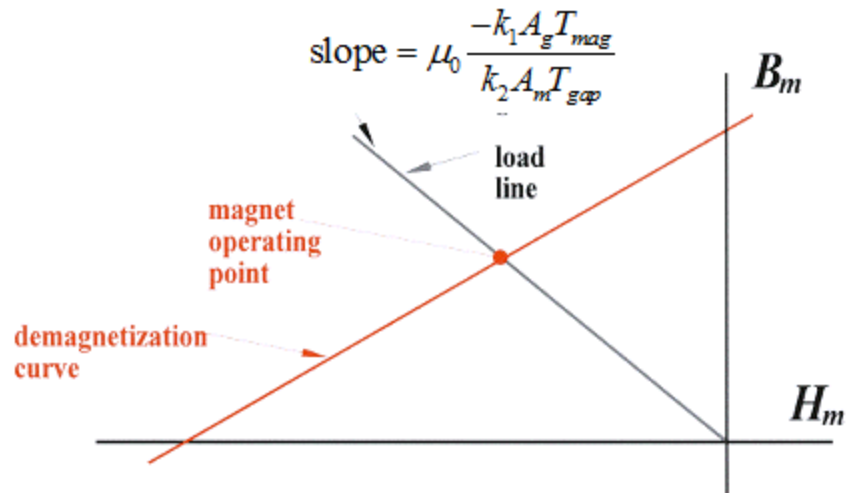
Figure 69, Operating point for magnetic circuit [40]

Figure 70 shows a portion of an IPM machine. This figure focuses specifically on the magnet, the post, and the bridges.
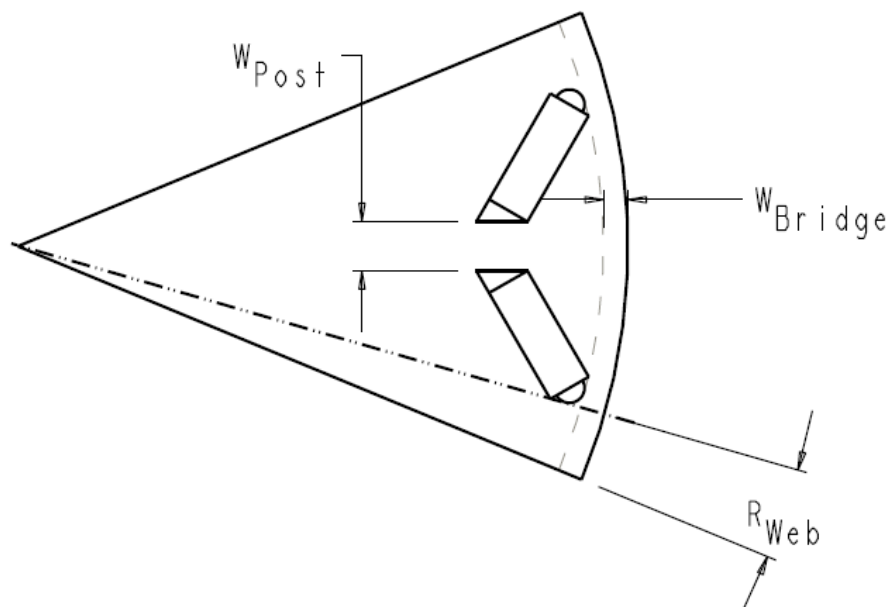
Figure 70, Rotor detail showing the leakage paths of the post and bridges

The leakage path for the magnetic flux goes through the bridge and post areas. The width of the leakage path is:

$$W_{Leakage} = W_{Post} + 2W_{Bridge} \tag{4.14}$$

where W_{Post} is the width of the post (mm), and W_{Bridge} is the width of the bridge (mm). The thickness of the post is determined by the equation:

$$W_{Post} = R_{Post} W_{Leakage} \tag{4.15}$$

where R_{Post} is the post ratio, and $W_{Leakage}$ is the leakage width (mm).

R_{Post} can be specified as part of the algorithm, or can be part of an optimization of the FEA. The leakage width is the total width of lamination which would be saturated magnetically when the stator is not energized. The leakage width (to an extent) determines how much of the magnet's flux does not cross the air gap and enter the stator.

A number of machine configurations were run varying R_{Post}, to minimize the leakage width. As R_{Post} was varied, structural FEA was run to determine the corresponding post and bridge thicknesses. It was determined that a post ratio, R_{Post}, of 0.5 typically gave the minimum leakage width.

The ratio A_g/A_m (from Figure 69) is one of the factors which determines the load line, and is accounted for by the magnet depth ratio and the web width ratio. The magnet thickness ratio is:

$$R_{MTh} = T_{mag} / T_{gap} \tag{4.16}$$

where T_{mag} is the magnet thickness, and T_{gap} is the air gap thickness, the distance between the rotor and the stator.

In general, the efficiency of the machine increases as R_{MTh} increases. There is a limit to this increase, as the bridges become thicker, etc. The magnets in automotive IPM machines are typically NdFeB magnets, which cost \$40 to \$75/kg (perhaps more) in 2009. The cost is influenced by purchasing volumes, etc. Magnets are a significant portion of the machine's cost, and some objective functions may include magnet and other material costs.

2. Parameters calculated from the response surface variables

The magnitudes of some variables are determined by manufacturing considerations as well as by the performance of the machine.

Air gap

In general, a smaller air gap results in higher electrical efficiency. This is because less electrical current is required to force a given amount of flux across the air gap, so electrical $\left(I^2 R \right)$ losses are reduced by a smaller air gap. An air gap which is too small increases eddy current and windage losses. The smaller air gap however can increase surface losses in the rotor caused by harmonics in the stator [37]. The thickness of the air gap is typically determined based on manufacturing considerations. The rotor is spinning inside the stator, and has manufacturing tolerances, as well as rotor dynamic considerations, therefore the air gap will not be uniform. Larger rotors have larger air gaps. For the validation algorithms, the equations used to determine the air gaps were

$$Gap = 1.0; \quad D_s > 355mm \tag{4.17}$$

$$Gap = 0.6777 * \ln \left(D_s \right) - 2.9771; \quad 203 < D_s < 355mm \tag{4.18}$$

$$Gap = 0.1832 * \log(D_s); \quad D_s < 203 \qquad (4.19)$$

The above are based primarily on manufacturing considerations. The air gap in the machine designed by an outside company had a slightly smaller air gap than the above equation would indicate (0.5 mm vs. 0.625 calculated per the above equations).

3. Parameters which were not 'optimized'

Some variables in the design of the machine have optimum values which are known, or which have minimal impact on the performance of the machine. Parameters with minimal impact on performance may be varied to reduce cost, or for other reasons. A description of the parameters, and the reasons they were not optimized is given below.

Web angle

Figure 71 is taken from [38]. SPEED was the analysis program used to validate this method.
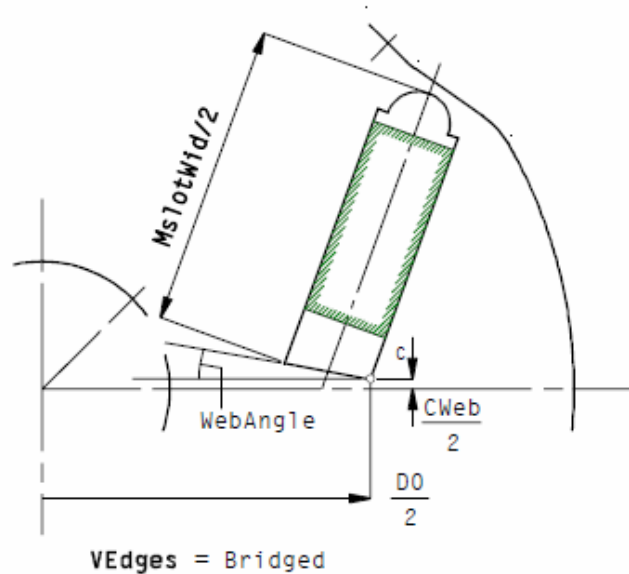
Figure 71, SPEED Type1 rotor, showing the Web Angle parameter

This program has the option of setting the 'web angle', as shown in Figure 71. The area between the magnets will typically saturate, as shown in Figure 72. Saturated areas are shown in red. The amount of flux flowing through these areas is determined primarily by the type of steel, and the width of the saturated area. The rotor steel shown below saturated at 2.2 T. When the web angle was maximized, so that the slot ends touched the sides of the magnets, the rotor saturated at a slightly higher level in this area, 2.5 T. This resulted in more flux going through the center web (the post), and therefore taking flux away from the face of the rotor.
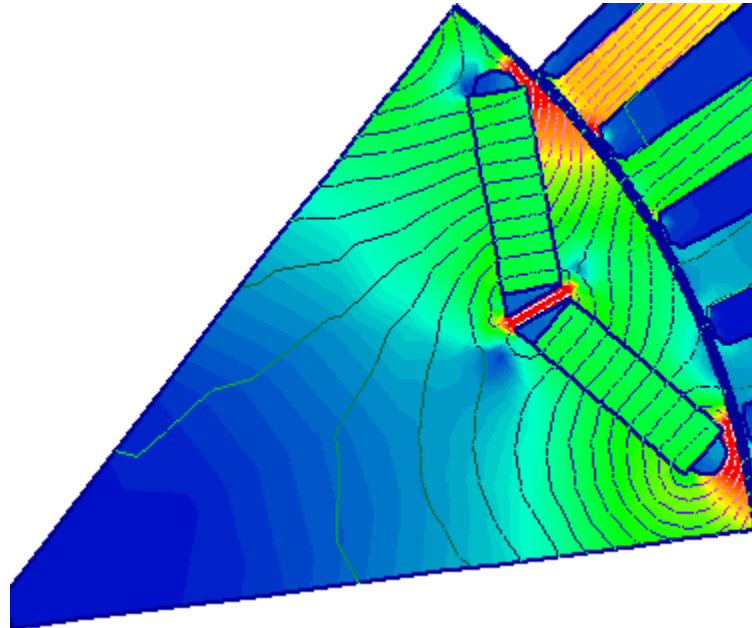
Figure 72, FEA of electric machine, showing saturation

For this reason, the geometry was designed as shown in Figure 72, with the post having parallel walls.

Magnet length

The magnet in Figure 71 (shown with green hash marks on its boundaries) cannot be longer than the slot; however the magnet is sometimes shorter than the slot, as shown in that figure. In earlier research, magnet lengths were varied. In that research, the highest efficiencies were gained by having the magnet length as long as the slot, when the objective function was based solely on efficiency. If cost were to become part of the objective function, or if demagnetization is included in the algorithm, this might no longer be true.

Stator skew

Theoretically, the rotor or the stator can have skew. Skew in the stator refers to the laminations in the stator being angularly offset from one another, as shown in Figure 73. This is typically done to reduce cogging torque, or to improve the shape of the back EMF. In the rotor, if the rotor is skewed, the magnet must either have skew, or if the machine has external magnets, the magnets are sometimes magnetized with skew. This has not been seen in IPM machines.
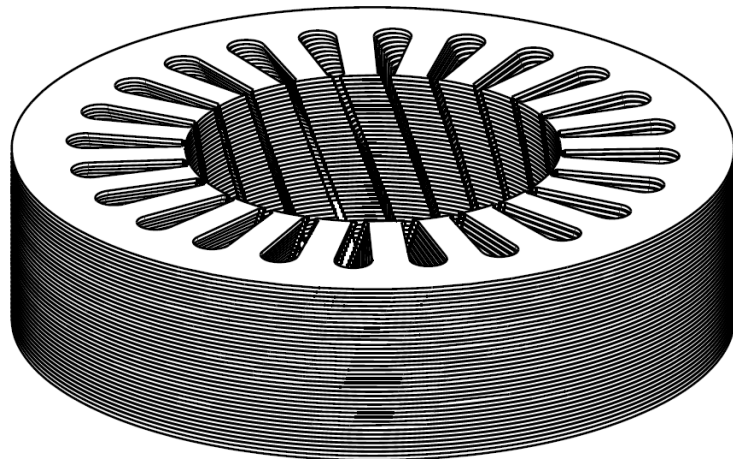
Figure 73, Stator with skewed laminations

When GA research was being done, stator skew was one of the parameters which was varied. As the method was developed, it was found that skew typically decreases the efficiency of an electric machine. While skew is sometimes desirable for reasons that are not part of the objective function chosen, skew was not selected as one of the eight variables.
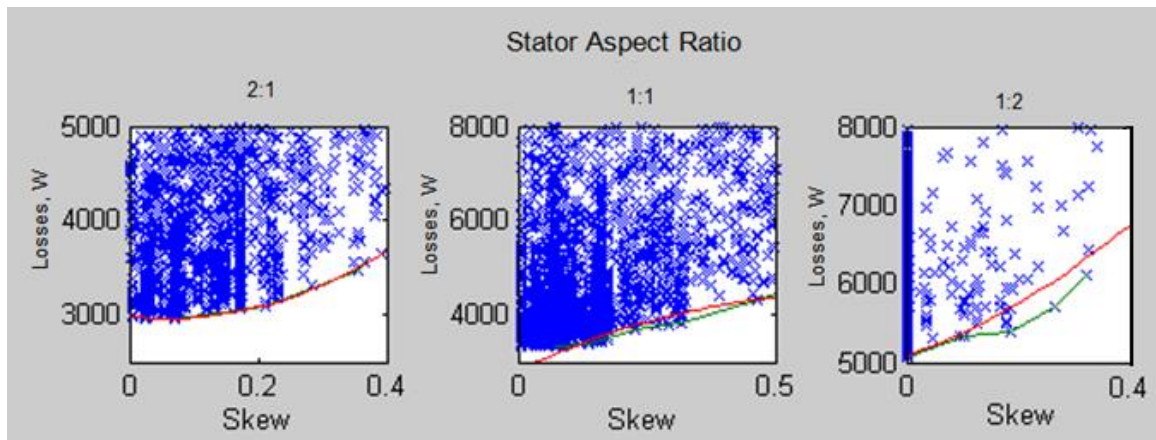
Figure 74, The effect of skew on performance

As shown in Figure 74, the greatest efficiency is achieved with no skew. For this reason, skew was set to zero for the validation algorithms. If cogging torque had been part of the objective function, skew could be added as a variable, or a fixed amount of skew could be part of the specifications.

4. Parameters determined by the performance of the machine

Some variables were determined based on the machine's performance. This specifically includes the number of turns in the winding (which are determined from the back EMF of the machine), and the bridge and post thicknesses (determined based on the mechanical stresses the rotor sees at high speeds).

Turns per coil

For a given electric machine, the speed, the number of parallel paths, and the number of turns per coil determine the back EMF. As the speed increases, the back EMF also increases. At the overspeed condition (which for the validation examples was set at 140% of the maximum operating speed) the back EMF will be highest. At this point it must not exceed the maximum voltage specification. This voltage requirement is based on the requirements of the power electronics.

The first time the machines are analyzed, the back EMF is determined at the overspeed condition. The magnets in the validation example were NdFeB magnets. These magnets have a negative temperature coefficient for B_r, meaning that they put out more flux at low temperatures than at high temperatures. For this reason the temperature was set to the low value in the specification.

The temperature should be determined as a realistic value. The question is; at what temperature will the machine ever run at the maximum overspeed condition? If, in order to get to the maximum overspeed condition, the machine must have been running for a significant amount of time, the temperature should not be set as cold as if the machine had not been running. The magnets in an electric motor will probably heat up fairly rapidly from their lowest temperature, due to losses in the rotor, etc.

For the validation example with an eight pole machine, the number of parallel paths was set to four. This reduces the back EMF to one quarter of what it would be if there were no parallel paths. As the number of parallel paths increases, the ability to adjust the number of turns so that the back EMF is close to the maximum voltage is better.

Each design was analyzed once with minimal current[34] to determine the number of turns per coil. If the voltage at the maximum overspeed condition was too high, the number of turns was reduced. If the voltage at the maximum overspeed condition was less than the maximum voltage allowed, the algorithm increased the number of turns, if possible. This reduced the current requirements for the power electronics.

During the analysis of the machines, some machines could not achieve rated power because of a high back EMF, or possibly due to the inductance of the coils. The number of turns was also reduced for this case.

Bridge and post thicknesses

Meeting the strength requirements of the rotor, while minimizing flux leakage in the rotor, is a significant challenge. This is an area of machine design where the mechanical and electrical engineering fields interface with one another.

The bridges and the post hold the rotor together. For some applications, either with a lower speed, or with a smaller rotor, the post between the magnets which form a pole is not required. This is primarily when the thickness of the bridge to sustain the centrifugal forces is not significant, and therefore a post is not required. In most cases the elimination of the post significantly increases stresses in the bridge area. Through finite element analyses, it was determined that the leakage is usually minimized when posts are used. This is reasonable, as the post is in tension, while the outer bridges experience bending stresses.

As mentioned previously, the bridges and post act as magnetic 'short circuits' in the rotor, as seen in Figure 72. If the electrical steel saturates at 2.4 T, and the magnets have

---

[34] The software used required that the current setting be above 0.0 amps.

a remanence of 1.6T, every 1.6 mm of bridge or post requires 2.4 mm of magnet. This portion of the magnet does not contribute power to the machine, and is therefore only meeting a requirement of the magnetic circuit. Minimizing the widths of the bridges and post therefore minimize the magnet mass.

As described in Chapter II - Methods (p. 51), an algorithm was written in MATLAB to determine the stresses in the rotor. This algorithm returned the highest stresses in the bridge area, and in the post area. These stresses were required to be lower than the yield strength of the material, which for most validation research was 260 N/mm^2. The yield strengths of steels vary significantly, as the examples in Table 25 indicate.

Table 25, Yield strengths of electrical steels

Company	Grade	Yield Strength (MPa)
AK Steel (formerly Armco)	Non-oriented silicon steels DI-MAX M15 FP DI-MAX M36 FP DI-MAX M47 FP	358 290 269
ArceloMittal (formerly Arcelor Steel, Groupe Arcelor)	High permeability and thermal conductivity M 330P-35 A, M 350P-50 A M400P-50 A, M470P-50 A M 530P-50 A, M 600P-50 A	260-310 270-320 250-300
	High Frequency (100-5000 Hz) D24	320-360
	Fully Processed M 235-35 A, M250-35 A M 270-35 A M 300-35 A, M 330-35 A	420-460 330-370 310-350

Neither the bridge nor the post are allowed to experience stresses beyond the yield strength of the material. This can be achieved in a number of ways, by having the post carry the majority of the stress, having the bridges carry the majority of the stresses, or having the stresses more evenly shared between the two. The method does not specify how this is accomplished. For the validation, two methods were used.

The first was to have the load primarily carried by the post, with the bridge having a minimal thickness as required by manufacturing. This usually minimizes the total width of the leakage path for the flux, when the machine is in a non-excited state, which is similar to what it will see when in high speed operation.
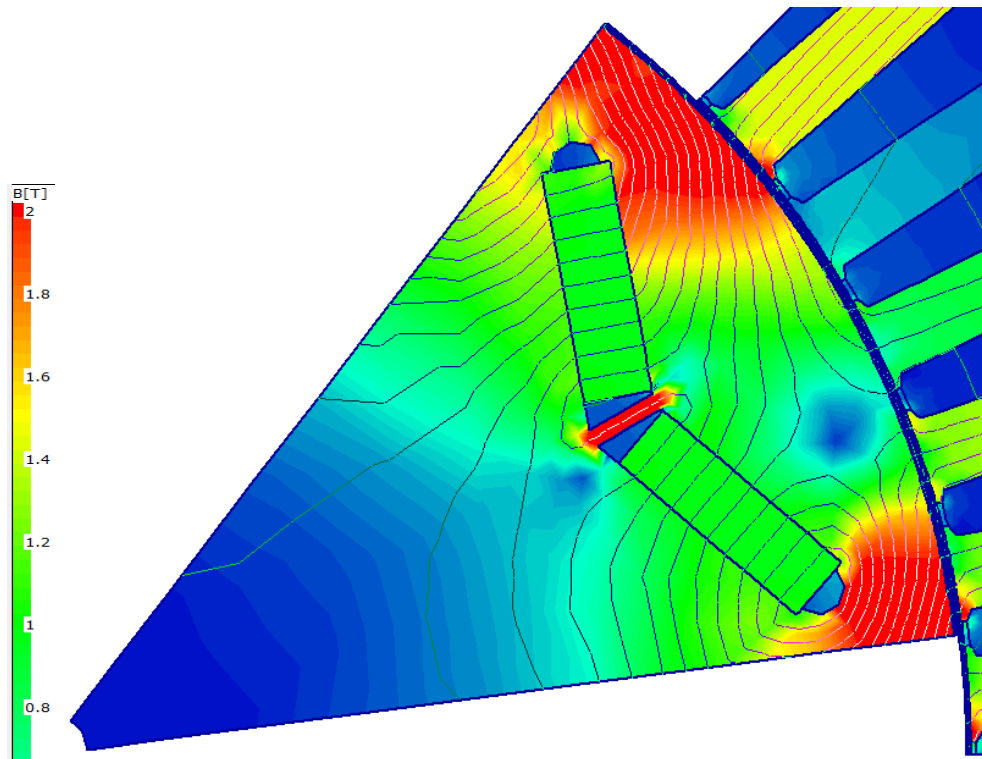
Figure 75, FEA of magnetic flux, at 400A, 45 degrees, approx 2 T in red area, 173 kW

The second method used was to maximize the magnet's 'useful surface area'. This is shown in Figure 75 and Figure 76. Figure 75 shows the flux when the machine is

delivering rated power. Portions of the rotor are saturated (indicated in red), which is typical for an IPM machine. The red region in the upper right of the figure is saturated, but the flux in that region crosses the air gap. There is a second red region in the lower right of the figure, which is saturated. Approximately half of the flux in this saturated region does not cross the air gap, but simply flows from one side of the magnet to the other. This is typical of IPM machines, but should be minimized. This flux is generated by the magnet, and represents a wasted volume of the magnet.

This wasted volume is indicated in Figure 76, where a portion of the magnet and lamination has been shaded white. If the flux lines are followed, one of two things happens. The flux may pass through the magnet, circle through the rotor and re-enter the magnet; or the flux may pass through one magnet, flow through the post, and then pass through the second magnet. This second flux path passes through the air gap eventually, but passing through the magnet a second time does not increase the amount of flux passing through the air gap. Therefore, both of these paths should be minimized.

In Figure 76, it can be seen that the amount of magnet which was 'wasted' near the post was about 1.5 times the width of the size of the post. This was because the remanence of the magnet was approximately 2/3 of the steel's saturation level. Every millimeter of addition leakage path required 1.5 mm of magnet.
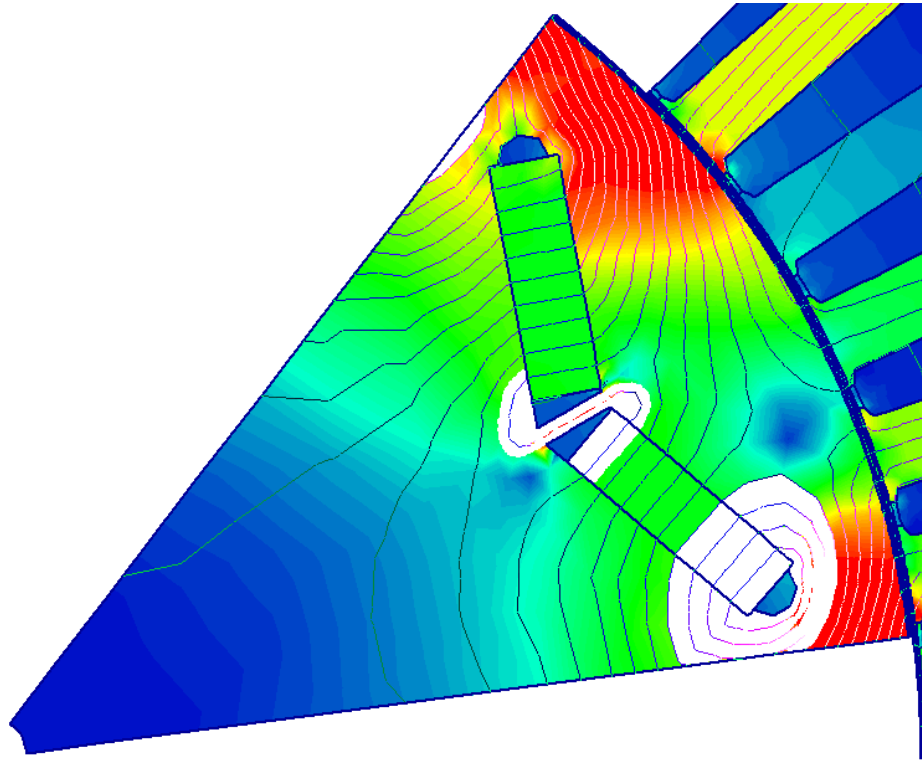
Figure 76, Region of magnet which does not contribute flux to the air gap

If these paths could be made so that they had a high reluctance, the efficiency of the magnets would be higher. This would require either selective heat treatment, or other physical altering of the laminations in the bridge and post area.

Figure 77 shows the two dimensions which were modified for the bridge and post calculation. For a given design (determined by the set of parameters) the corner of the magnet lies along the line dimensioned R_{Web}, based on that dimensionless parameter setting. The equation for the width of the post is:

$$W_{Post} = R_{Post}W_{Leakage} \qquad (4.20)$$

where R_{Post} is the post ratio, and $W_{Leakage}$ is the leakage width (mm).
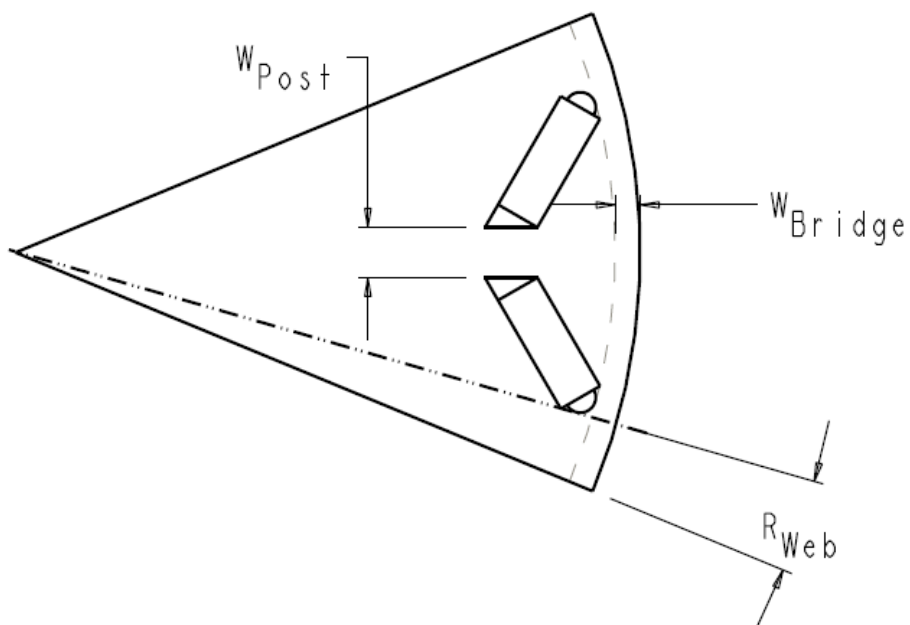
Figure 77, Dimensions for bridge and post thickness calculation, at R$_{Post}$ = 0.5

For the validation research, R_{Post} was set to 0.5, so that the total flux leakage through the bridges was the same as the flux leakage through the post. This value was chosen because at a setting of 0.5 (typically), the maximum magnet width can be achieved, increasing the flux from the magnet.
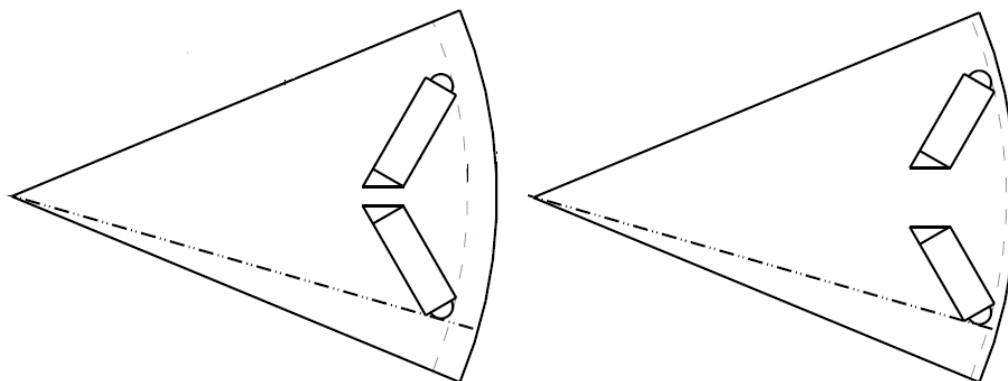
Figure 78, Rotors having post ratios of 0.25 (left) and 0.75 (right)

Figure 78 shows portions of two rotors, with post ratios of 0.25 and 0.75. As can be seen, a post ratio of 0.25 yields a narrow post (the region between the two magnets) but wide bridges; while a post ratio of 0.75 yields a wide post, but narrow bridges. Figure 79 shows a very wide post, which might be required in a high-speed machine. Note the significant amount of flux from the magnet which either does not pass through the air gap, or which passes through the magnet twice. As before, the regions of the magnet shown in white produce flux which does not cross the air gap.
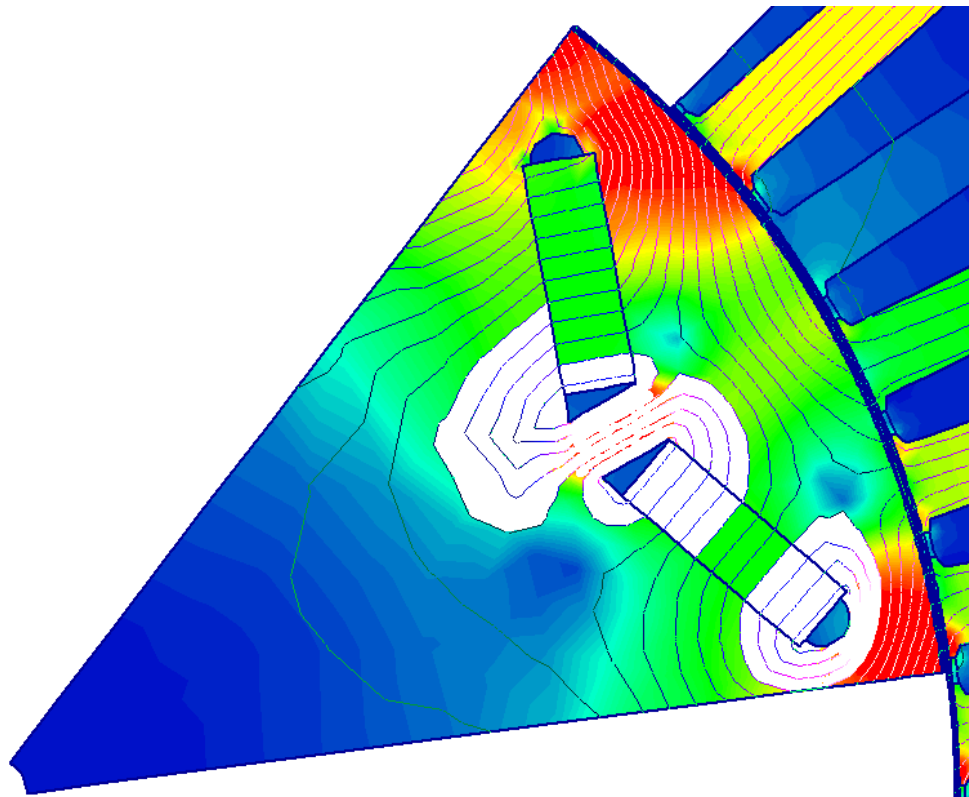
Figure 79, 171.5 kW machine, region of magnet which does not contribute flux to the air gap

5. Parameters determined by manufacturing considerations

The slot opening width was not used as a variable for the method. The slot opening width and the slot overhang angle were determined by manufacturing considerations. The

slot opening width, tooth tip thickness, overhang angle and fillet radius are shown in Figure 80. The slot opening width was calculated as one half of the distance between the shoulders where the A_{W2} dimension applies, as can be seen in Figure 80. The slot tooth tip overhang angle (A_{toh}) was set to 25°. This was based on manufacturing consider-ations, as well as the ability for magnetic flux to enter the teeth without over-saturating this portion of the tooth. This angle can vary between 20 and 30°, without having a significant effect on efficiency.

Slot opening width, tooth tip thickness, overhang angle and fillet radius
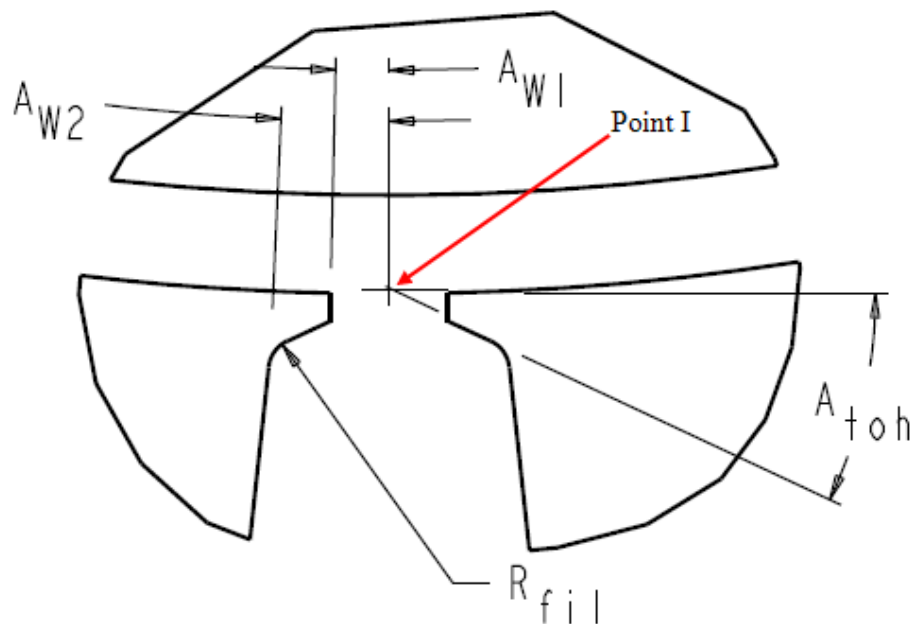
Figure 80, Tooth tip overhang angle and thickness

The tooth tip thickness was determined by the overhang angle, and a requirement (for this method) that the bottom of the tooth tips intersect as shown in Figure 80. Extensions of the lines which form the bottom of the tooth tip intersect on the bore of the stator at

Point I. This requirement resulted in acceptable flux densities in geometries analyzed to validate the method.

Slot overhang angle and opening width were mentioned previously, and are based on manufacturing needs. A slot which is too narrow makes it difficult to put wire into the slots. The typical recommendation is that the slot be 2 to 3 wire diameters wide, so that if the wires happen to be crossed when they are pushed into the slot, they do not 'pinch' in the slot, and become damaged. If the slot opening is extremely narrow, this either requires more assembly time and greater care during assembly, or smaller wires. Smaller wires reduce the amount of slot fill (the percentage of copper in the slot), which results in higher current densities in the remaining copper, and increased temperatures. If thinner wires are required, there is also a higher percentage of wire insulation (varnish) in the slot, reducing heat transfer to the stator. This increases the copper temperature, raising its resistance and increasing the associated power losses.

The tooth fillet radius (R_{fil}) should be set to the thickness of the laminations, at a minimum. This is the minimum radius possible, based on punching considerations. This number could be larger, but will have a small impact on efficiency, and may in a few cases result in the model 'crashing', if the setting for the top slot width is extremely small. This is not likely for machines with reasonable geometry, but in order to avoid this problem, for the validation research, the radius was made small or neglected. Another method would have been to make this radius as large as the wire radius plus the thickness of the slot cell insulation. This is the smallest radius which a strand of wire can fit into.

6. Parameters not varied in the study

Some parameters are known to have an effect on efficiency, but were not varied in the optimization of the machine. The reasons for each are covered in the explanations below.

Lamination thickness

The thickness of the laminations was not varied by this method. The thickness of the laminations has an impact on the performance of the machine and including the thickness would be a useful addition to this method. However, the thickness of the laminations is based on the electrical frequency of the machine at a given condition (perhaps maximum operating speed), and an optimum thickness can typically be chosen before the design is optimized. Laminations are available in a limited number of thicknesses, so that the thickness is not a continuous variable. If this method is rapid enough, additional optimizations with thinner (or thicker) steel can be evaluated quickly. The validation algorithm evaluated the efficiencies both at the base speed, and at the upper speed. If higher losses are seen at the upper speed than at the lower speed, a reduction in material thickness could be investigated. If higher losses are seen at the lower speed than at the higher speed, an increase in thickness could be investigated.

Stator envelope volume and torque density specification

For this method, the stator envelope volume is determined by the maximum torque specified as an input, and by the specified torque density. Therefore, all machines with the same torque requirement have the same stator envelope volume. This means that the stator raw material (the material used to construct both the rotor and the stator) will have basically the same mass. Since they have the same mass, the raw material cost for the laminations should be approximately equal. Punching costs may be higher for the

smaller diameter stators, as a larger number of laminations is required for a longer machine.

Number of poles

The method is not restricted to a specific number of poles, but validation of the software was done on 8 pole machines. If other pole counts are to be examined, this requires additional runs of the algorithm at those pole counts. As is well known, if iron losses at high speeds are seen, reduction in pole count will reduce the electrical frequency of the machine, and reduce those losses. The performance of the speed-torque responses would be affected.

Winding configuration

Winding configurations were not optimized. The basic configuration can be changed, but the method does not optimize these. Winding configurations have an impact on harmonics and losses. For validation analyses, the machines were sine wound.

The number of phases

The number of phases can be changed, but the method does not optimize these. Three phase machines are by far the most typical, and were used for validation.

The DC link voltage

The DC link voltage is included as part of the specification, and is determined by the power electronics. An appropriate DC link voltage must be chosen for different power ranges of electric machines.

Maximum overspeed rating

The maximum overspeed is part of the specification, and was fixed at 11,200 rpm for most of the validation research (140% of the maximum operating speed, 8000 rpm). Increasing the overspeed requirement reduces the number of turns per coil. This requires more current to drive the machine. Overspeed specifications which are higher than necessary increase the cost of the drive electronics.

Shaft radius

For the validation research, the shaft radius was kept small. Initially, the shaft radius was calculated based on the maximum torque rating, which was a machine specification. For the machine designs considered in this research, the shaft radius had minimal impact on machine performance, and made mapping of the extreme dimensions of the design space difficult.[35] While the extreme dimensions did not yield high efficiencies, the shaft was made small to make mapping a larger area of the design space feasible. In validating the final machine design, the shaft radius was set to a reasonable value for the torque required.

Stator laminate shape

The stator laminate shape was circular. Circular stator laminations tend to be the most manufactured form. The method does not specify the lamination shape, but did not vary the shape during the optimization.

---

[35] Mapping a large portion of the design space had been the goal of earlier research.

Temperature and thermal design

The temperatures of the magnets and coils were included in the specifications, which are an input to the algorithms. The thermal design of the machine was not included in the optimization, as thermal design requires a significant amount of judgment and tradeoffs.

F.   Selection of the experimental design

Response surface methods use designs derived from design of experiments methodology. These designs have fixed levels for the machine's design parameters, typically three or five, and the spacing of these levels is systematic. Other methods, such as genetic algorithms (GA) and particle swarm optimization (PSO), define the boundaries of the design space, but the specific machine dimensions evolve throughout the optimization process. Following initial research on electric machine optimization using GA methods, and after reviewing the literature, the choice was made to investigate the use of response surface methods.

The three primary criteria for the experimental design are that it should allow the method to converge rapidly, that it should require a minimum number of machines to be evaluated, and that the design will yield an accurate mathematical model of the design space selected.

1. Response surface method

The response surface method (RSM) is commonly used for systems which have a high (or infinite) number of possible designs. RSM takes a number of data points, and mathematically fits a surface to those points. The surface is the response to the input variables and is usually determined by the objective function. For the validation examples

used for this research, the response was the efficiency of the electric machine or of the electric drive system, at each performance point. The algorithms written allowed for more than two performance points, however only two points were used for validation.

As the design space modeled becomes larger, the models become less and less accurate. For most systems, the entire design space cannot be modeled with a single response surface; the design space must be broken up. This is true for modeling electric machines also. Each model from a portion of the design space either holds the optimum design, or indicates the direction of subsequent design spaces. If the global design space is large, and the approximate location of the optimum value is not known, other search methods can be used prior to creating the response surface design space.

Methods such as a conjugate direction technique, a simplex technique or simply a marching technique are feasible. The method proposed by this research assumes that the locations of optimal regions of dimensionless parameters for electric machines are available. Once the method has narrowed down the region where the optimum is located, RSM can be used to determine the optimum parameter values.

Experimental designs

Design of experiments typically use designs which have 2, 3 or 5 possible values in each dimension. 2 values are used when the response to a given dimension is expected to be linear, and for the initial portion of the search, when a search direction is being determined. In forming a response surface, however, the main effects, quadratic effects, and interactions are all needed. For this reason either three or five values are modeled.

For Box-Behnken designs (see Figure 81 page 178), the design variables in the hypercube have 3 values. For Central Composite Designs (CCD, see Figure 82, page 180), the design variables have 3 or 5 values.

When RSM is applied to experiments that consist of physical tests, or have a stochastic nature, the center point may be repeated to determine experimental error. In those tests, even when the input variables have exactly the same values, the results may differ due to experimental variations. For this research, the results are based on the finite element method (FEM), and give identical results when identical variables are input. For this reason, duplications of the central point were not used.

2. Factorial designs

A factorial experiment is an experiment where factors are tried in various combinations. The number of data points, and the parameter values used for these combinations are called factorial designs. A full factorial design includes the combination of all parameters at all levels. This is neither necessary nor possible at times, and it is much more efficient to use a smaller number of points to determine the response surface.

One method of selecting these data points is to use fractional factorial designs. A full factorial design for eight factors, with three levels for each factor, would require 3^8, or 6561 data points. If the main effects, quadratic terms, and two level interactions are included, it is possible to generate a mathematical model for the same design space with as few as 45 data points. Added data points increase the accuracy of this model, and provide a method to measure the variance of the model.

3. Number of factors

As the number of parameters is increased, the number of simulations required to model the response surface increases, increasing the complexity of the response surface model. In order to create a rapid method, it is desirable to limit the number of parameters varied. At the same time, those parameters critical to machine performance must be identified and included. A significant amount of optimization research has been done on electric machines using fewer than eight parameters; however these focus on optimizing either the stator or the rotor, or add constraints to the design. If both the rotor and stator are to be designed simultaneously, seven to eight parameters are required. The decision was made to render 8 parameters dimensionless, based on the dimensions required to create rotor and stator geometry which led to efficient machine designs.

Having selected 8 specific parameters, it was found possible to successfully optimize electric machines, though some parameters (pole count, magnetic material, etc) were not included in the optimization. These limitations have been outlined above.

Table 26, Experimental designs for response surface modeling (RSM)

Number of Factors	Minimum Number of Runs for Box-Behnken and/or Central Composite Design	Design Type Box-Behnken (BB) or Central Composite Design (CCD)	I-Optimal Number of Runs
4	25	BB or CCD	15-16
5	41/27	BB or CCD	21-32
6	49/45	BB or CCD	28-32
7	57/61	BB or CCD	36-64
8	113/81	BB or CCD	45-64

Table 26 shows the increase in the number of analyses required as the number of factors grows. It also shows that fewer runs are required using an I-optimal (or D-optimal) design as compared to a Box-Behnken or CCD.

As mentioned, the CCD can have either three or five levels. An additional reason for choosing I-optimal or D-Optimal designs rather than a five level CCD is that the three level designs share more data points with adjacent design spaces, if a design space needs to be expanded.

Initially for this research, GA was used, and 10 parameters were varied. It was determined that some of these parameters did not need to be optimized. After investigation of RSM, it was decided to begin with 8 parameters and verify if this yielded optimal designs in a reasonable time. Depending on the computer analysis settings used, the present method results in machine designs in between three and nine hours of computer time.[36] This is acceptable, compared to manual alternatives often used in industry, or other optimization methods found in the literature. These time frames assume that the optimum design is within the hypercube selected. Successive adjacent hypercubes require additional time, but if the hypercubes share data, they require less time than the original design space.

Reducing the number of parameters to 7 could be done by forcing a ratio between the top width of the slot and the bottom width of the slot, as these tend to be related, or by selecting slot configurations which have parallel teeth. As Table 26 shows, the reduction in runs from eight factors to seven factors is between 0% and 20%.

---

[36] Algorithms were run on an HP Pavilion Media Center m8200n, with an AMD Athlon 64 X2 dual core processor, 6000+, with 3GB RAM, available in 2008. The operating system was 32 bit Windows Vista. The software ran on one core of the processor.

Table 26 shows that as few as 45 runs can be used to create an I-optimal experimental design. At present 64 runs were used, in order to determine the variance of the model more accurately. By understanding the variance of the model, it is possible to determine the accuracy of the model, and when the ranges of some parameters can be increased. This allows larger portions of the global design space to be modeled with a single experimental design, resulting in more rapid convergence.

4. Selection of the experimental design

The requirements for the experimental design are that it produce an RSM that is accurate, and that it produce this surface rapidly (minimizing the number of machine designs required, and therefore minimizing the objective function evaluations). Once the surface is created, the optimum point on the surface can be found rapidly.

Hypercubes

A simple description of a hypercube is that a hypercube is an extrapolation of what a cube might be, if it had more than 3 dimensions. Each variable for this research had 3 values for each dimension of the hypercube. These values are often coded as -1, 0 and 1. The coded values are then mapped onto the range of the specific design space being evaluated. Using designs of experiments, an interval from 0-1 might indicate an interval such as 0.126 millimeters, or a ratio such as 0.05 of the range of a dimension. The design of experiments (DOE) tables provided by JMP or other programs; which are coded as -1, 0 and 1, are a starting point for determining the actual parameter values.

Factorial designs

If a response varies in 3 dimensions, with two levels for each dimension, eight data points yield a response surface for a region of the design space. If the models are non-linear, and contain interactions and quadratic effects, there must be three levels for each factor, which increases the number of data points required. Table 27 shows the number of data points required if the model will be based on all possible combinations of each variable, at three levels.

Table 27, Data points required for full factorial designs

Number of variables	Number of data points required for 2 levels	Number of data points required for 3 levels
1	2	3
2	4	9
3	8	27
4	16	81
5	32	243
6	64	729
7	128	2187
8	256	6561

As the number of variables increases, the number of data points required increases exponentially. For this research, eight variables were modeled at three levels. If all possible combinations of variables and levels were modeled, 6,561 data points are required for each response surface.

These 6,561 data points model only a portion of the design space small enough that it can be modeled accurately. This model includes the main effects, the interactions, and the quadratic effects. If the data points are spaced apart by 10% of the design space, and if the design ranges from 0-100%, there would be 11 levels for each variable. The number of data points required to completely model the design space would be approximately 11^8, or 2.1×10^8.

Most of the design space consists of combinations of variables which yield electrical machines which cannot achieve the required power, or are highly inefficient. These regions of the design space should be eliminated.

Box-Behnken, Central Composite, D-optimal and I-optimal designs were evaluated for their usefulness for this research. The I-optimal design was selected.

Box-Behnken designs
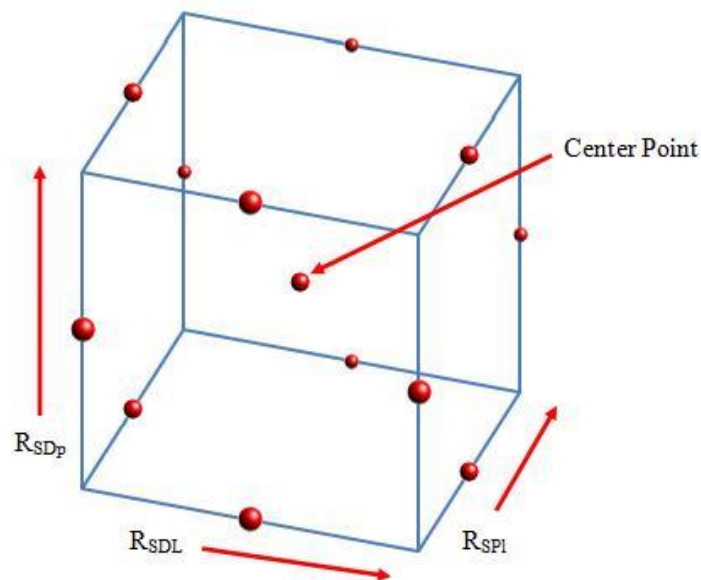
Figure 81, 3 dimensional Box Behnken design

Figure 81 shows a Box-Behnken[37] (BB) experimental design having three parameters. The BB design has points which are regularly spaced, and this three-dimensional design has points which are 1.414 coded units from the center. Design points are midway along the edges of a 'box'. For 3 parameters, this requires 13 points, without replications. The points shown represent the variations of R_{SDL}, R_{Spl} and R_{SDp} which would be analyzed.

As an example of the use of this design, the values of R_{SDL} might vary from 0.8 on the left to 1.2 on the right, having a range of 0.4. The ranges do not have to be the same, and so the values for R_{Spl} might vary from 0.50 in the front, to 0.58 in the back, having a range of 0.08. The values for R_{SDp} might vary from 0.68-0.80.

Box-Behnken designs are used in RSM, and have been used to model up to 21 variables. A Box-Behnken fractional factorial design used for modeling 8 variables is available which requires 113 points, including the center point, without replication. As with other 8-variable RSMs, this would have 45 coefficients in the quadratic model.

Central Composite Designs

The Box-Behnken design required 113 points, which means that 113 machine designs would have to be analyzed for each design space. Central composite designs (CCD) have either three or five levels, and for eight factors, can have as few as 81 points. To allow for reuse of the maximum number of designs, if the design space is to be extended, the axial points should be on the faces of the hypercube.

---

[37] Developed by George E. P. Box and Donald Behnken
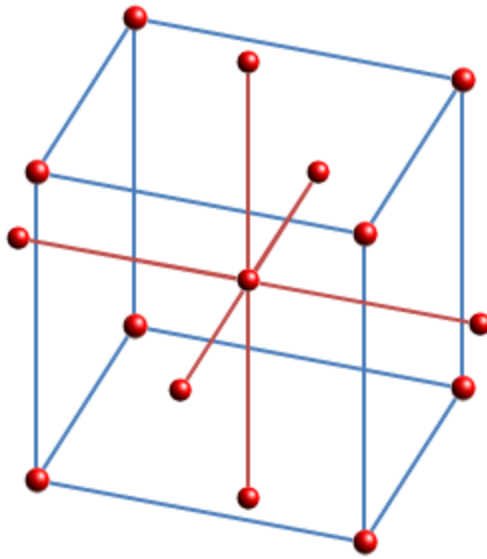
Figure 82, 3D central composite circumscribed design

Like many other programs, JMP codes the values for the levels of the corner points of the box as -1 and 1. Figure 82 shows the circumscribed design, which has axial points which fall outside of the volume of the cube. If an additional design space were to be created adjacent to this one, the four points on the shared face of the two designs would already have been analyzed. All axial points would have to be analyzed, as none of these points are shared between the two design spaces.

The values of the axial points (shown connected by red lines) are determined by starting at the center point of the CCD, which for an eight-dimensional design space would be coded (0, 0, 0, 0, 0, 0, 0,0). The axial points are then placed a fixed distance from the center.

All of the values for the axial points except for one must be zero, i.e. they lie on an axis. An example is that one axial point could be located at (2.055, 0, 0, 0, 0, 0, 0, 0), which is a distance of 2.055 from the center in the x_1 direction. Circumscribed designs

are good at predicting responses over the entire design space (the space inside the cube), which is what the method proposed by this research requires. There are two problems with a CCD. The first is if an optimal point is near a boundary of the design space. For many of the ratios, the feasible values fall between 0.0 and 1.0. If an optimum point happens to fall near 0.0 or 1.0, the CCD requires that the axial point be greater than 1.0, or less than 0. An electric machine with these dimensions cannot be modeled.

A second problem for the CCD is that if an additional portion of the design space needs to be evaluated, fewer of the data points already evaluated apply to the new region. For CCDs which have only three levels, more of the design points can be part of the new design space. For designs with 5 levels, none of the axial points are shared, and therefore all axial points of the new design need to be evaluated.
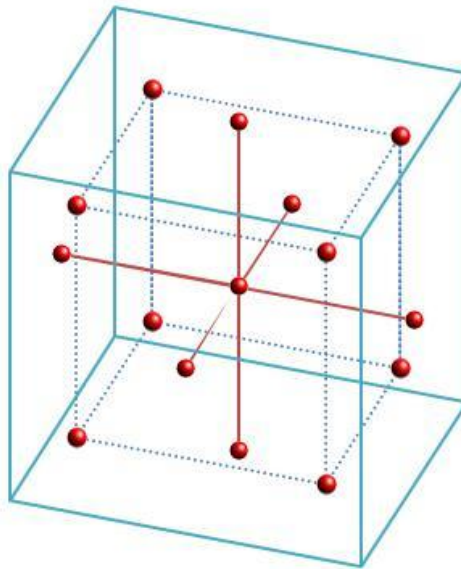
Figure 83, 3D central composite inscribed design[38]

---

[38] Mathworks.com

Figure 83 is for an inscribed design. It does not have the problem of having points

which fall outside of the feasible design space. However, it is not accurate when

predicting responses near the corners of the cube. As both of the designs above have

limitations, if a CCD had been used in this method, the axial points would have been

placed on the faces of the hypercubes. In other words, the axial points would have been

at a distance of 1.0 from the center.
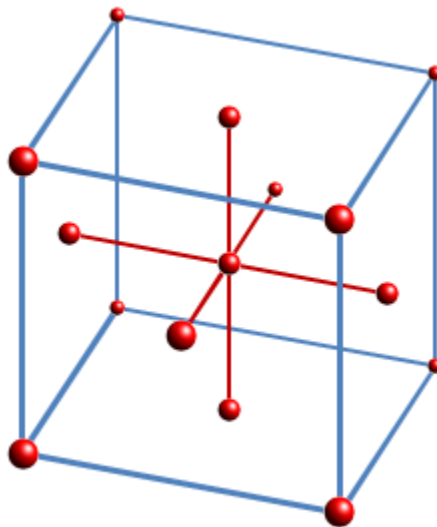
Figure 84, 3D central composite faced design

Figure 84 is an example of a central composite design which is faced. It can be easily

seen that if the design space were to shift in any axial direction by 2 units [moving from

coded values of (-1 to 1), to coded values of (1 to 3)], the five points on any side could be

re-used in determining the response of the next region of the design space. This concept

can be extended to the use of designs which have eight factors.

Any of these CCDs with eight factors can be coded with 81 points, an improvement over the Box-Behnken design. Like the Box-Behnken design, this design will produce a model which includes all main effects, 2 factor interactions and quadratic terms, and will have 45 coefficients. There are no replications at the center point.

I-optimal vs. D-optimal designs

Both D-optimal and I-optimal designs have been used for the creation of response surfaces. I-optimal designs were created to have less variance than D-optimal designs have, and are recommended where the prediction of the response needs to be accurate. D-optimal designs are recommended when screening is being done, rather than for prediction. Figure 85 from [16] shows this difference in variance. These figures are based on the predicted variance for a design with only two factors.

On these plots, red and orange are desirable, while green is undesirable. Figure 85 (a) shows the variance for a D-Optimal design. There are only three regions which have a variance below 0.3, and these regions are fairly small. Figure 85 (b) is a plot of the variance for an I-optimal design. There is a large region where the variance is less than 0.3. The results for this two factor design are similar to what is seen for an eight factor design, though the contrast between the performances of the two designs is even more significant as factors are added.
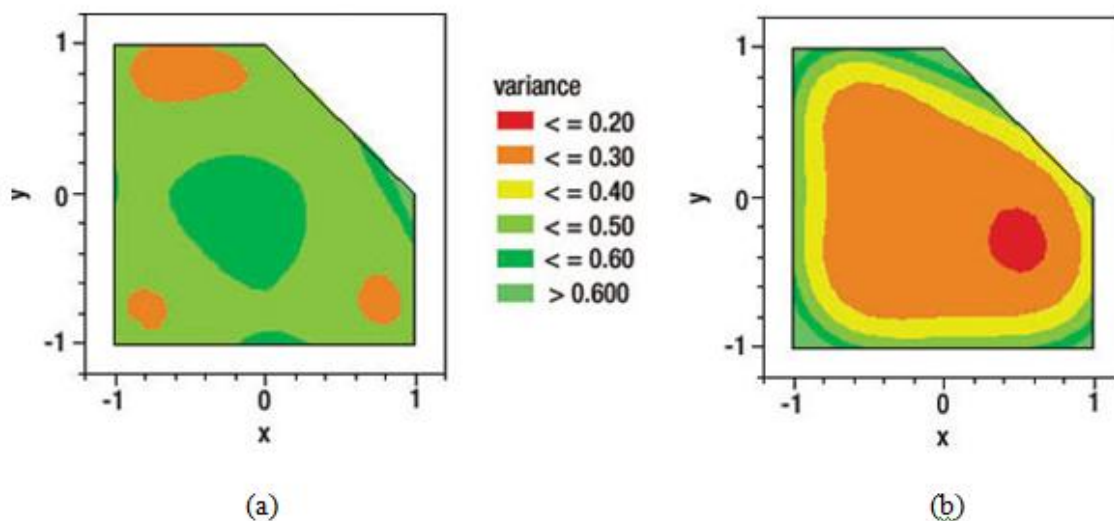
Figure 85, Variance of D-optimal (a) and I-optimal (b) designs. Red and orange are preferred areas

A second comparison (Figure 86 and Figure 87) shows the differences in variance between D-optimal and I-optimal designs when eight factors are modeled. In these two figures only the first four factors are shown. In Figure 86 it can be seen that the variance profile for the D-Optimal design ranges from approximately 0.7-0.8. For the I-optimal design the variance ranges from approximately 0.15-0.25. Therefore I-optimal designs are significantly more accurate than D-optimal designs for prediction in eight factor designs.
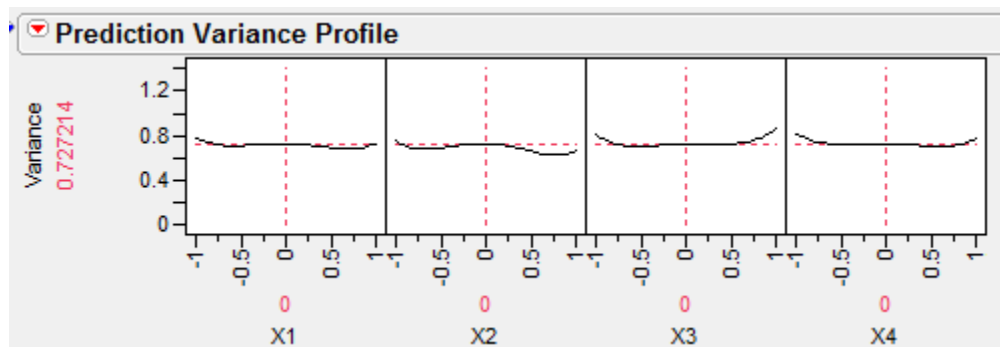
Figure 86, Prediction variance profile for eight factor D-optimal design [16]
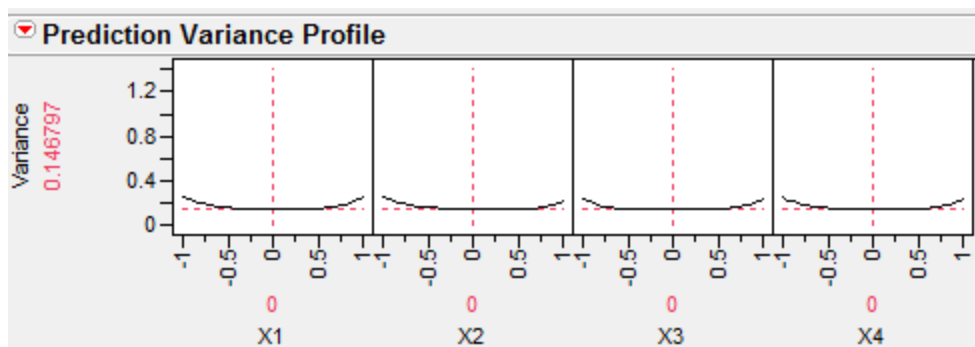
Figure 87, Prediction variance profile for eight factor I-optimal design[16]

The program JMP 7 [16] was used to create these designs. Using the design of experiments (DOE) functions, a custom design was created. Eight continuous factors were used in the model. The model was specified as a response surface model (RSM), which by default includes the main effects, two level interactions, and quadratic effects. The number of runs was selected to be 64, which is the default number of runs. Since the order of the runs does not influence the responses, randomization was not required.

Table 28, Coded eight factor I-optimal design

Run No.	x_1	x_2	x_3	x_4	x_5	x_6	x_7	x_8
1	-1	-1	-1	-1	0	1	-1	1
2	-1	-1	-1	0	-1	0	0	1
3	-1	-1	-1	1	1	-1	1	1
4	-1	-1	-1	1	1	1	-1	-1
5	-1	-1	0	-1	-1	-1	1	1
6	-1	-1	1	-1	1	-1	-1	-1
7	-1	-1	1	0	0	0	1	0
8	-1	-1	1	1	-1	-1	0	-1
9	-1	0	-1	-1	1	1	1	-1
10	-1	0	-1	1	0	-1	-1	-1

Run No.	x_1	x_2	x_3	x_4	x_5	x_6	x_7	x_8
11	-1	0	0	-1	-1	0	-1	0
12	-1	0	0	1	1	0	0	1
13	-1	0	1	0	1	1	0	1
14	-1	1	-1	-1	1	-1	-1	1
15	-1	1	-1	0	-1	-1	1	-1
16	-1	1	-1	1	0	1	1	1
17	-1	1	0	0	1	0	0	0
18	-1	1	0	1	-1	1	0	-1
19	-1	1	1	-1	-1	1	1	1
20	-1	1	1	-1	0	0	-1	-1
21	-1	1	1	-1	1	-1	1	1
22	-1	1	1	1	0	-1	-1	1
23	0	-1	-1	-1	1	0	0	0
24	0	-1	0	-1	-1	1	1	-1
25	0	-1	0	0	0	-1	-1	0
26	0	-1	1	1	-1	1	-1	1
27	0	-1	1	1	1	1	1	-1
28	0	0	-1	0	0	0	1	1
29	0	0	0	0	0	0	0	-1
30	0	0	0	0	0	0	0	0
31	0	0	0	0	0	0	0	0
32	0	0	0	0	0	0	0	0
33	0	0	1	-1	0	-1	0	1
34	0	0	1	1	-1	0	1	0
35	0	1	-1	-1	-1	1	-1	-1
36	0	1	-1	1	-1	-1	-1	0
37	0	1	0	-1	0	-1	0	0
38	0	1	0	0	1	1	-1	0

Run No.	x_1	x_2	x_3	x_4	x_5	x_6	x_7	x_8
39	0	1	1	1	1	-1	0	-1
40	1	-1	-1	-1	-1	-1	-1	1
41	1	-1	-1	0	1	1	0	-1
42	1	-1	-1	1	-1	-1	1	-1
43	1	-1	-1	1	-1	1	1	0
44	1	-1	0	-1	1	1	1	1
45	1	-1	0	1	0	0	-1	-1
46	1	-1	1	-1	-1	1	0	0
47	1	-1	1	-1	1	-1	1	-1
48	1	-1	1	0	-1	0	1	1
49	1	-1	1	1	1	-1	-1	1
50	1	0	-1	1	1	1	-1	1
51	1	0	0	0	1	-1	1	0
52	1	0	0	1	0	1	0	0
53	1	0	1	0	1	1	-1	-1
54	1	1	-1	-1	-1	0	1	0
55	1	1	-1	-1	1	-1	-1	-1
56	1	1	-1	0	0	-1	0	1
57	1	1	-1	1	1	0	1	-1
58	1	1	0	0	-1	1	-1	1
59	1	1	0	1	-1	-1	1	1
60	1	1	1	-1	0	1	1	-1
61	1	1	1	-1	1	0	-1	1
62	1	1	1	0	-1	-1	-1	-1
63	1	1	1	1	0	1	-1	0
64	1	1	1	1	1	1	1	1

An example of a design like this is shown in Table 28[39]. The design in Table 28 is coded using -1, 0, and 1. These coded values must be changed to the dimensionless values required for the design, and then converted to the actual dimensional values.

5. Mapping the hypercube

An example of how the coded values are mapped to physical dimensions follows. In Table 28, the value of x_1 (the stator aspect ratio, R_{SDL}) is coded as -1, 0, and 1. It was stated in Table 2 (p. 37) that the range of x_1 for the design space is between 0.5 and 4.0. This range is too large to be mapped using a single response surface model. For this reason a smaller hypercube would be used. For our example we will assume that this hypercube maps x_1 from 1.41-2.00. The value of x_1 in Table 28 coded as -1 would map to 1.41. The value coded as 0 would map to 1.68. The value coded as 1 would map to 2.00. The first column of Table 28 becomes:

Table 29, First column (x_1) of the I-optimal design for the example

Run No.	x_1 coded value	x1		Run No.	x_1 coded value	x1		Run No.	x_1 coded value	x1
1	0	1.68		23	0	1.68		44	1	2.00
2	-1	1.41		24	0	1.68		45	1	2.00
3	-1	1.41		25	0	1.68		46	1	2.00
4	-1	1.41		26	0	1.68		47	1	2.00
5	-1	1.41		27	0	1.68		48	1	2.00
6	-1	1.41		28	0	1.68		49	1	2.00
7	-1	1.41		29	0	1.68		50	1	2.00

---

[39] File "8 Factor 64 Runs A"

Run No.	x_1 coded value	x1		Run No.	x_1 coded value	x1		Run No.	x_1 coded value	x1
8	-1	1.41		30	0	1.68		51	1	2.00
9	-1	1.41		31	0	1.68		52	1	2.00
10	-1	1.41		32	0	1.68		53	1	2.00
11	-1	1.41		33	0	1.68		54	1	2.00
12	-1	1.41		34	0	1.68		55	1	2.00
13	-1	1.41		34b	0	1.68		56	1	2.00
14	-1	1.41		35	0	1.68		57	1	2.00
15	-1	1.41		36	0	1.68		58	1	2.00
16	-1	1.41		37	0	1.68		59	1	2.00
17	-1	1.41		38	0	1.68		60	1	2.00
18	-1	1.41		39	0	1.68		61	1	2.00
19	-1	1.41		40	0	1.68		62	1	2.00
20	-1	1.41		41	0	1.68		63	1	2.00
21	-1	1.41		42	1	2.00		64	1	2.00
22	-1	1.41		43	1	2.00				

If the region of the design space with x_1 larger than 2.00 was to be modeled, a new hypercube would be created. This hypercube would model x_1 from 2.00-2.83. The machine designs which were not shared would be analyzed and a new response surface model would be created for that hypercube. 23 data points were analyzed in the previous hypercube which had an x_1 value of 2.00, and are common to both design spaces. Therefore, the response of approximately one third of the data points would have already been determined.

6. Extending a fractional factorial model

Extending the design space can be done for a number of reasons, including:

- To create designs which are more optimal than those already found

- To evaluate the effect limiting constraints (such as diameter) have on performance

- To learn what performance can be obtained in other regions of the design space

- To learn about interactions between various dimensions

Figure 88 represents data points taken for a Box-Behnken design, where there are three variables in the design, and each variable has three levels in the design space. In this figure, 13 designs (spheres) are shown.
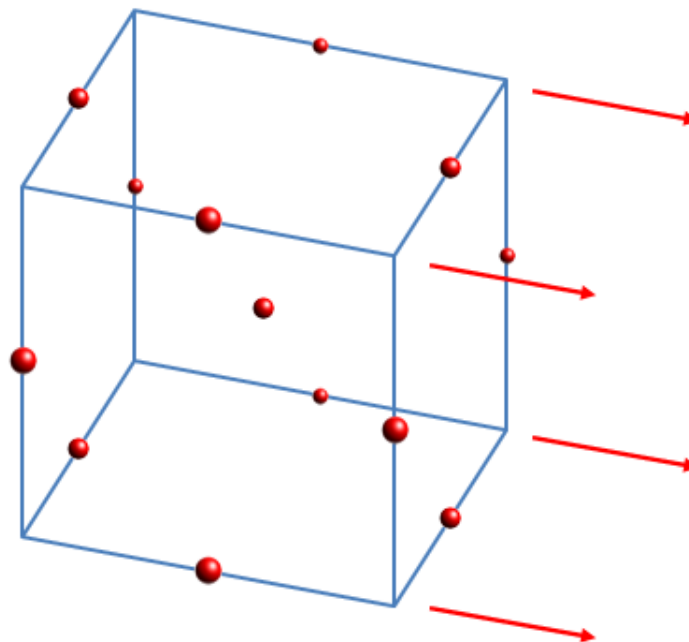
Figure 88, Extending a hypercube with 3 variables, at 3 levels

The goal is to find the optimum design in the design space. However, when the mathematical model of the response to these points is created, the optimum may fall on

the right boundary of the design space. For this case, the design space would be extended to the right, in the direction of the red arrows.
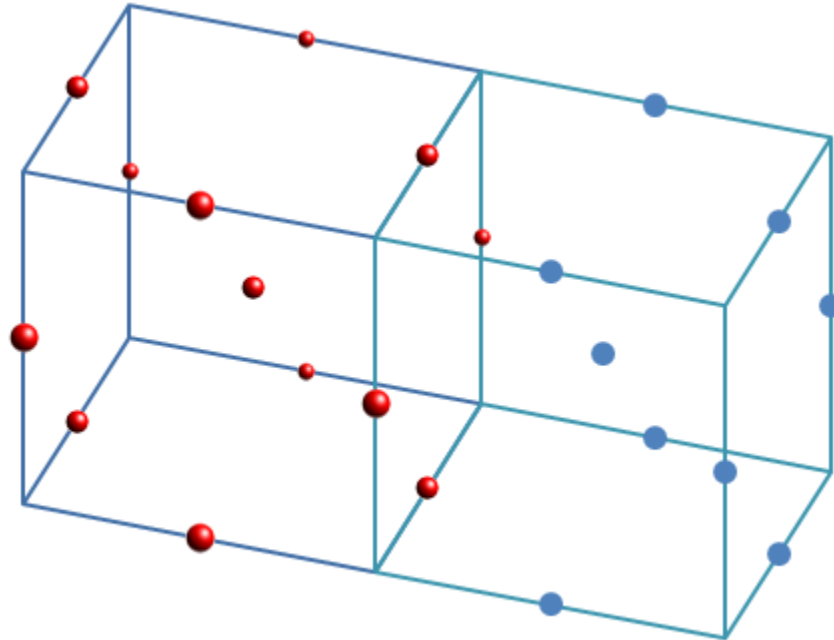
Figure 89, Hypercube with design space extended to right

To extend the design space to the right, a layer could be added to the right, with levels which are spaced the same distance apart as the previous layer. This is shown in Figure 89. With the three factor Box-Behnken design, this works well, as the four points on the right hand face of the old designs are re-used in the new design. As additional factors are added to the Box-Behnken design, the faces will not always be identical on opposing sides. This is shown in Figure 90, which uses color and shape to model a four factor design.
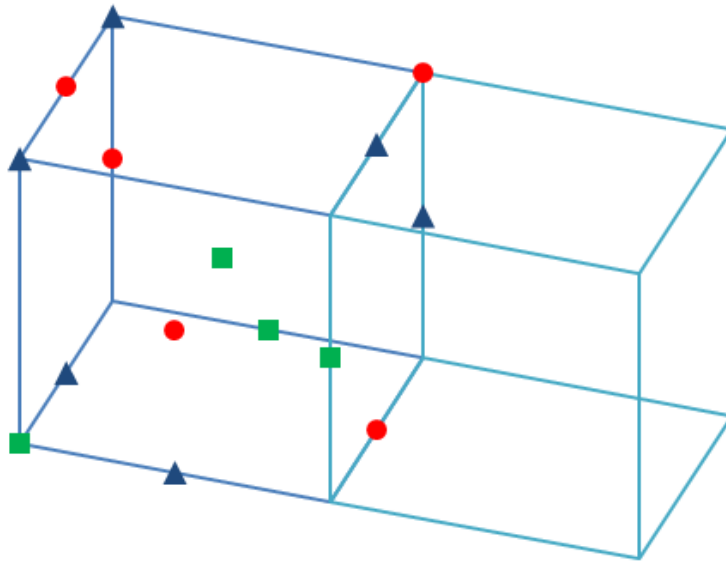
Figure 90, Hypercube with additional parameter shown by colors

The three initial parameters are represented by their location in space. The fourth parameter is represented by using red circles, green squares and blue triangles. If the new design space is achieved by translating the first hypercube design, the new design is shown in Figure 91. On the earlier hypercube, the left hand and right hand points were simply offset from each other, by changing one parameter. For this figure, the points on the right side of the left hand hypercube are not simply offset from the values on the left side of the hypercube.

Therefore, if the new design space is created by offsetting the points from the previous model, all 15 data points in the adjacent hypercube are new designs, and must be analyzed. These points are shown in Figure 91 (the new points on the shared plane are slightly offset from the lines, for visibility).
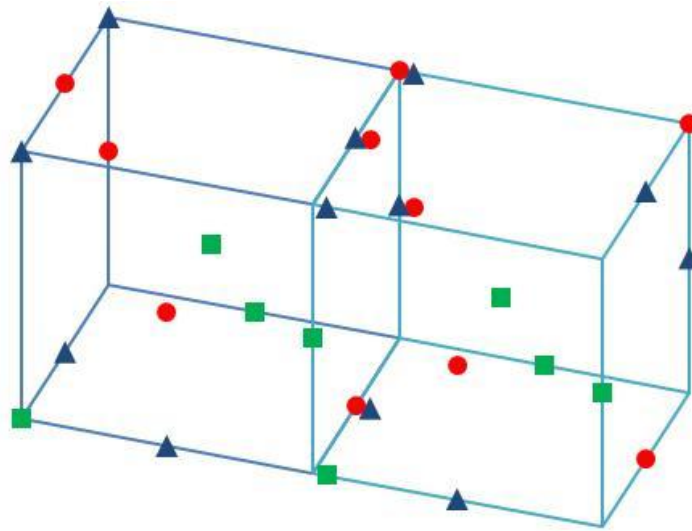
Figure 91, Hypercube with unnecessary points duplicated

Extending the design space in this manner is valid, but requires analyzing more designs than are desired. Instead, the left most points of the initial cube could have been reflected, using the central (gray) plane as the mirror surface.

This is shown in Figure 92.
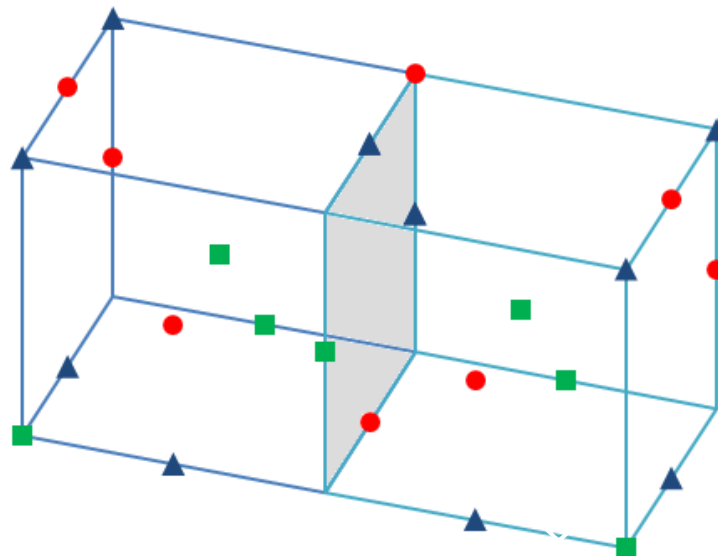
Figure 92, Design hypercube extended by reflecting the design

For a case with only four variables, ten points would be added, rather than fifteen. When the same concept is used with an I-optimal design, each hypercube consists of 64 designs. When the design space is extended, as shown here, typically one third of the points can be re-used. The next portion of the design space can be analyzed much more rapidly using this reflective technique.

7. Extending the designs, when exploring the design space

As the optimum is moved away from, the machine's performance degrades. It is not necessary to always extend the design space using the previous parameter ranges. In the optimum region of the design space, the range for a variable might be 0.1. To improve the variance of the model, as the design spaces are further from the optimum, it will be advantageous to reduce the size of the ranges. For the next interval, the range might be reduced to 0.06 or 0.08. If all other variables maintain their same values, one third of the data from the previous hypercube design are still available for the new RSM.

G.   Analysis of the machine designs

When efficiency is part of the objective function, the optimum efficiency for each of the designs must be determined. This requires that the optimum settings for current and phase angle be found for each speed which is a part of the objective function.

1. Determining the optimum phase angle for peak efficiency

The literature related to machine optimization rarely mentions the phase angle; the optimization of current and phase angle were not considered part of the machine optimization problem. This was true for literature related to analytical methods, and to

methods which employed FEA. It is assumed that determining the efficiency at rated power was done at a single phase angle for all machines. Since the optimum phase angle for a machine varies depending on its geometry, materials, and operating speeds, this simplification may lead to sub-optimal designs. Inclusion of the search for the optimal current and phase angle incurs significant time penalties.[40]

As explained in CHAPTER II.I.1 (p. 57), the golden section search was used to determine the optimum phase angle. This was done because the efficiencies of the machines tend to be unimodal. Minimizing the current rather than the efficiencies can be done in the same way. The results for minimizing current or maximizing efficiency are similar, but for many evaluations, the results not identical.

Modifying the golden section search method

Two modifications were made to the golden section search. The first of these was to eliminate the march to find the initial range. This is a typical modification made to the golden section search method when the initial range can be assumed. The second modification was to eliminate determining the performance at the first and last point of the initial four points.

This was a significant improvement, as typically the first or fourth golden section point are points where the software has difficulty converging. This is often due to the fact that rated power cannot be achieved at one of those two phase angles. After evaluating the second and third (middle) points of the golden section, the first or fourth point of the golden section is immediately eliminated. Therefore, there is no benefit in evaluating this point, and no information is lost.

---

[40] Penalties on the order of 5 to 10 times more function evaluations, for this method.

In most cases, the other unevaluated end point is also thrown away, and no significant information is lost. For the case where an endpoint would not be thrown away, the point closest to it is used. The spacing of the initial endpoints can be located so that the last possible used endpoints are on the boundaries of the phase angle range. This was implemented in the validation algorithms.

Other options to modify the method

It is possible that more rapid optimization would occur if a specific phase angle setting were initially assumed (probably a setting that is speed dependent) and perform optimizations on design spaces using that assumption, until the optimal local design space has been found. This would be followed by including the effects of current and phase on the local design space. This technique was not used, but is a possible rapid search technique. This method will have more variance for the initial search.

The use of the Fibonacci search method was considered in place of the golden section method, as it converges slightly faster than the golden section method. This search method is based on the Fibonacci sequence – 1, 1, 2, 3, 5, 8, 13, 21 … where each number in the sequence is the sum of the previous two numbers. Like the golden section search, it is also a region elimination method.

2. Determining the required current

From the literature and experience, it was seen that efficiency is a convex function of current. This is shown in Figure 93. This figure shows not only the fact that the function is unimodal, but also that a fairly good curve fit can sometimes be obtained. This is not always the case, but this observation led to improvements in the convergence algorithm.

Current Requirement vs Phase Angle

$$y = 0.00015x^3 + 0.02815x^2 - 2.23062x + 166.63458$$
$$R^2 = 0.99624$$

$$y = 0.000315x^3 + 0.007169x^2 - 1.419922x + 157.321087$$
$$R^2 = 0.997378$$

Legend:
- 0 to 65
- 15 to 65
- Poly. (0 to 65)
- Poly. (15 to 65)

X-axis: Phase Angle, gamma, degrees
Y-axis: Current, I, Amps
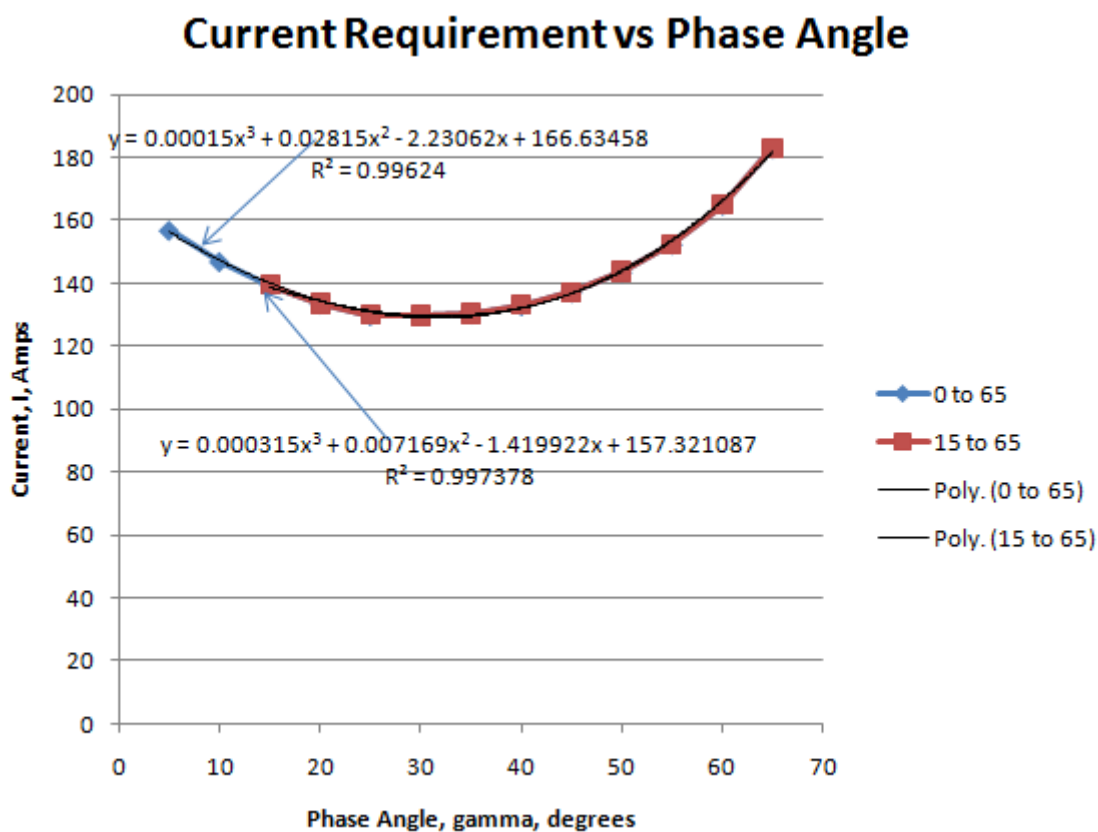
Figure 93, Current requirement vs. phase angle, showing curve fit

For a given phase angle, a method was used to set the current, and later improved. Initially, the algorithm predicted the current setting to obtain the specified power. The machine was evaluated at this current and phase angle. If the power achieved was within the desired error level (0.5%) the current search loop was terminated. Otherwise, Newton's method was used to determine subsequent current settings, until convergence was achieved. Convergence for one point is shown in Table 30. Setting the convergence limits to 0.5% was satisfactory for the method. Tightening the convergence yielded slight improvements to the variance of the model.

Table 30, Convergence for a single point using Newton's method

Iteration	Current, A	Power, kW
1	470.5	45.422
2	518.0	47.615
3	546.2	48.801

A second method was prompted by the following power equation for IPM machines:

$$P = m\left(EI_q + I_d I_q \left(X_d - X_q\right)\right) \tag{4.21}$$

where the number of phases is *m*, the back EMF is *E*, and the d- and q-axes

reactances are X_d and X_q. The d- and q-axes current (I_d and I_q) are defined as:

$$I_d = -I \sin \gamma$$
$$I_q = I \cos \gamma \tag{4.22}$$

The first component of equation (4.21) [mEI_q] is the magnetic torque, and the second

term [$m\, I_d\, I_q\, (X_d - X_q)$] is the reluctance torque. The theory was that if the back EMF and

d- and q-axis reactances from the initial current setting are known, a better approximation

for the subsequent data point could be made, compared to using Newton's method. This

would speed convergence. However, X_d and X_q are not constants, nor are they

calculable functions of current. As an example, for a machine that was fairly efficient,

the following data points were given by the algorithm (the same machine and initial data

point as in Table 30):

Table 31, Convergence using reactances

Iteration	Current, A	X_d, ohms	X_q, ohms	Back EMF, V	Power, kW
1	470.5	0.1492	0.2491	36.0297	45.422

Iteration	Current, A	X_d, ohms	X_q, ohms	Back EMF, V	Power, kW
2	506.5	0.1451	0.2357	35.0407	47.615
3	526.5	0.1427	0.2288	34.5127	48.801
4	536.5	0.1414	0.2256	34.2544	49.390
5	541.5	0.1408	0.2240	34.1269	49.676
6	544.5	0.1405	0.2230	34.0508	49.863

The reactances and back EMF vary with current. While the current for this data point increased by 15.7%, X_d decreased by 5.8%, and X_q decreased by 10.5%. This is due to the non-linearity in the steel. Figure 94 is a plot of the normalized reactances of one specific machine vs. current. Because of this variation of reactances, a simple calculation using X_d and X_q to calculate the required current was not effective. Research into this approach may be pursued in the future.
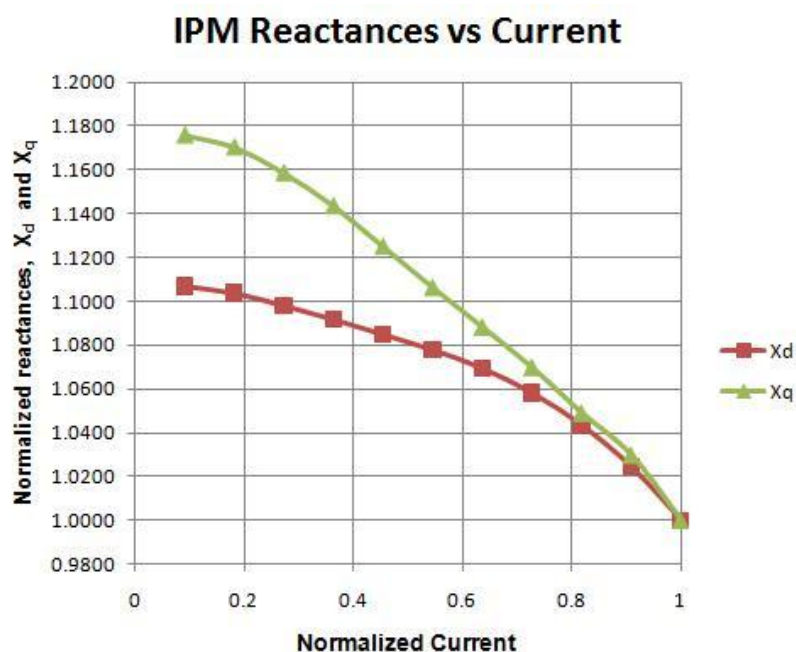
Figure 94, Normalized reactances vs. normalized current

In Figure 95, the phase angle was changed, while the current was held constant. This figure shows the reactances and normalized reactances, which are the reactances divided by their peak values. Again, X_d and X_q were not constant values. For this method to be effective it must converge more rapidly than Newton's method converged, which typically happened within three points.
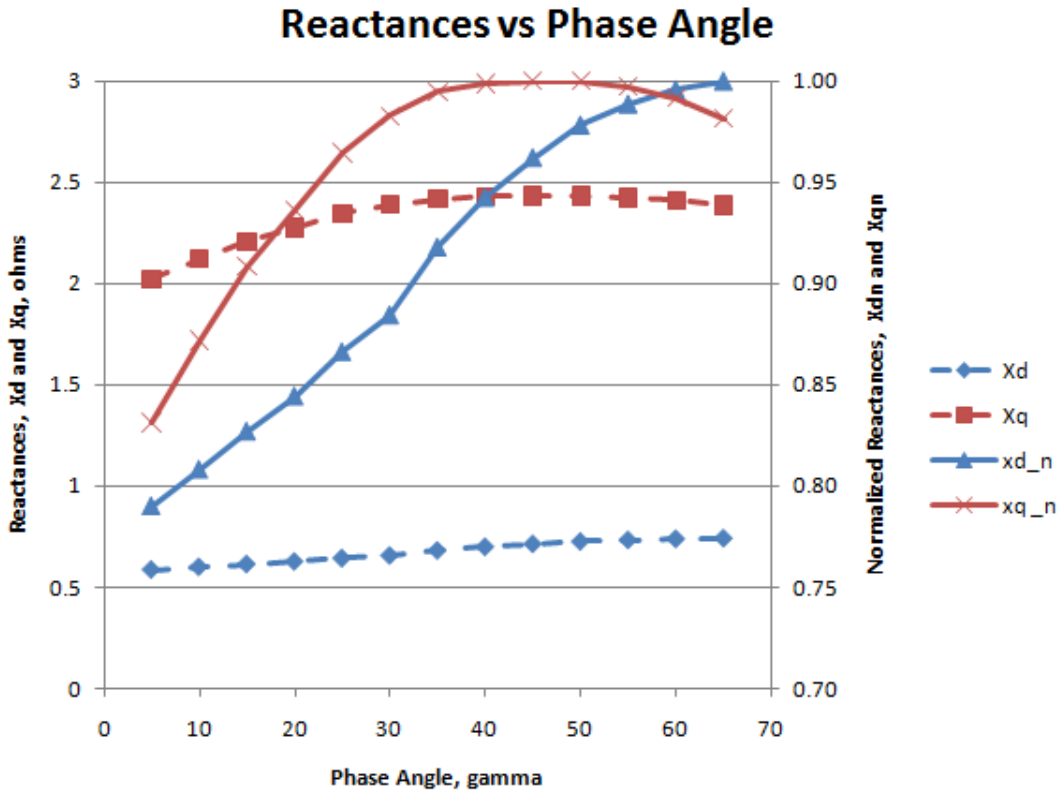
Figure 95, Xd and Xq reactances varying with current and phase angle

For one set of 64 machine designs, the use of Newton's method required 2320 evaluations of current and phase angle to find the optimum current and phase angle settings for two speeds. This was an average of 36.25 iterations per point. For the same set of machine designs, using the reactances to estimate successive points yielded 2363

evaluations, or an average of 36.9 evaluations per design. Therefore, a simple use of the reactances in determining the succeeding current value was not pursued.

While the direct use of the back EMF and reactances did not lead to faster convergence, it led to another option. (4.21) can be simplified to:

$$P = k_1 I_q + k_2 I_d I_q \tag{4.23}$$

where k_1 and k_2 are derived from (4.21). As mentioned earlier, the variables I_q and I_d are the q and d-axis current.   (4.23) can be rewritten as:

$$P = k_1 I \cos(\gamma) + k_3 I^2 \cos(\gamma)\sin(\gamma) \tag{4.24}$$

where I is the rms current per phase, and k_3 is a constant derived from the above equations. For a given phase angle γ, (4.24) can be rewritten:

$$P = k_4 I + k_5 I^2 \tag{4.25}$$

where k_4 and k_5 are constants derived from the above equations. This equation infers that power is proportional to one constant multiplied by the current (I), and a second constant multiplied by the current squared (I²). This equation indicates that if the current is increased linearly, with the use of Newton's method, too much power will be achieved with the second current setting. Similarly, if the power is initially too high, and current is reduced linearly, the power achieved will be too low.

A trial was set up were the second current setting was based on whether the current needed to increase or decrease. If the current needed to increase, the increase in current was multiplied by a specific factor. This factor was initially set at 0.7. A set of 64 machines were analyzed using this setting. The factor was then adjusted until the minimum number of function evaluations was achieved. It was determined that using a

factor of 0.75 resulted in the most rapid convergence. This number may not be optimal for all machines, but did increase the speed of convergence for the design space that was evaluated.

A similar method was used when the initial current setting was too high. For this case, the optimal factor was 1.30. In other words, when Newton's method would reduce the current setting by 10 amps, the current was instead be reduced by 13 amps. If Newton's method would increase the current setting by 10 amps, it was instead increased by 7.5 amps.

3. Changing the number of turns per coil

When the desired current could not be achieved, the current waveform was typically distorted, as seen in Figure 96. For this specific control method, the current is controlled to stay within the two smooth sinusoidal bands.
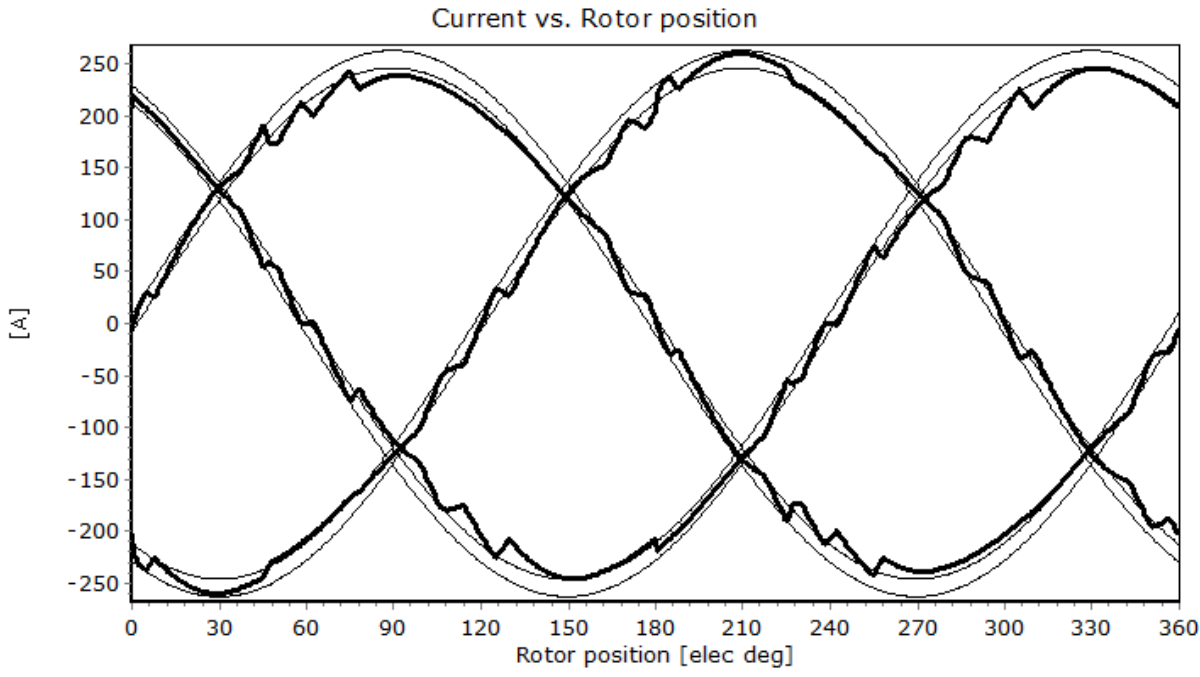
Figure 96, Current waveform with the original number of turns per coil

When the current could not stay within these bands, the algorithm reduced the number of turns per coil. When this was done, as can be seen in Figure 97, the waveform improved. The need to reduce this current was determined by comparing the commanded rms current with the achieved rms current, as explained in 'Qualifying the mesh, and determining the number of turns per coil' on page 56.

When the number of turns was reduced, the current was increased so that the desired power could be achieved. There were cases when the turns had to be reduced more than once, or where the machine was not able to achieve rated power, regardless of the number of turns.
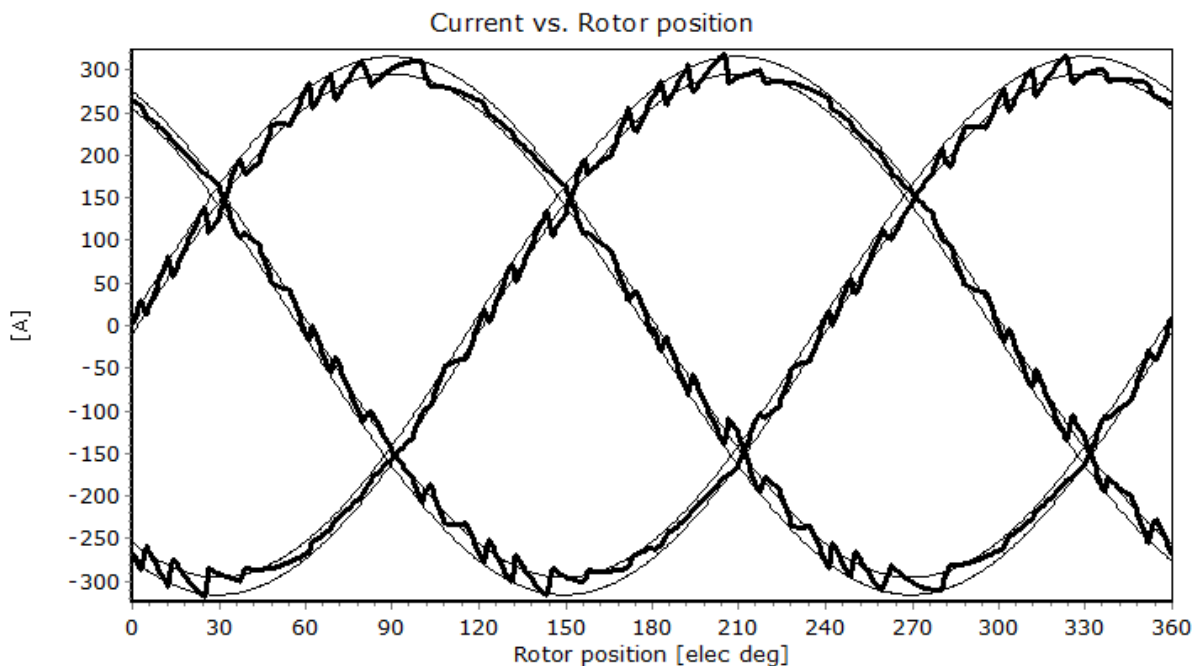
Figure 97, Current waveform with turns reduced

When this change was made to the algorithm, the number of objective function evaluations for the 64 designs reduced from 2320 to 2100.

Each of the 64 designs requires the correct current and phase angle at seven phase angles and two speeds, so that 14 points are being determined per design. For the first two or three phase angles, convergence typically happened within two or three evaluations. As the phase angles became closer and closer to each other (using the golden section method), convergence typically happened in either one or two function evaluations, in efficient regions of the design space.

4. Using a curve fit to predict the current to achieve rated power

The following method was also adopted: after the current for the first three phase angles was determined, a quadratic curve was fit through those points. The resulting equation was used to predict the current at the next phase angle. This method was based on constant power curves seen in the literature, showing that current vs. phase angle tends to be a smooth function. Therefore, a quadratic curve through the closest three known points should yield an accurate estimate. This modification increased the rate of convergence.

5. Summary of the convergence effects of modifications to the algorithm

Table 32 lists some of the modifications made to the algorithm to increase the speed of convergence, in the order they were attempted. The methods are cumulative, assuming the previous methods were successful.

Table 32, Method changes to increase the speed of convergence

Method	Object Function Evaluations
For all phase angles after the origin phase angle, begin with the optimal current from previous design.[41]	2320
If the current waveform was distorted, reduce the number of turns, and increase the current to the equivalent number of amp turns	2100
To predict current at a new phase angle, use the reactances and back EMF of previous points to estimate the next current value	2425
If the phase angle evaluations for three points exist, curve fit the 3 previous points to estimate the current at the next phase angle.	2047
If at least one previous design exists, use the current from the previous phase angle evaluated to estimate the first two phase angle points of the new design	2029
If power was too low on the first trial (for a given phase angle), increase the current by by 0.75 of recommended increase for the second trial (calculated from Newton's method).[42]	1737
If the power is too high on the first current setting (for a given phase angle) increase the recommended current adjustment by 1.3.	1702

6. Options that could speed up convergence

While the method developed requires fewer function evaluations than other methods described in the literature, and is quicker than can be done using trial and error methods, further improvements can be made. At the lowest machine speed, a curve similar to Figure 98 was often achieved. When trends such as this are observed, the algorithm could modify its search parameters, so that it begins more near the assumed optimal phase angle (e.g. at a higher phase angle for this case). This should decrease the convergence time.

---

[41] In other words, the same current setting was used for all phase angles initially.

[42] Had tried other numbers, such as 0.8, but 0.75 was optimal. This number might be varied, depending on how much reluctance and magnetic torque are in the machine.
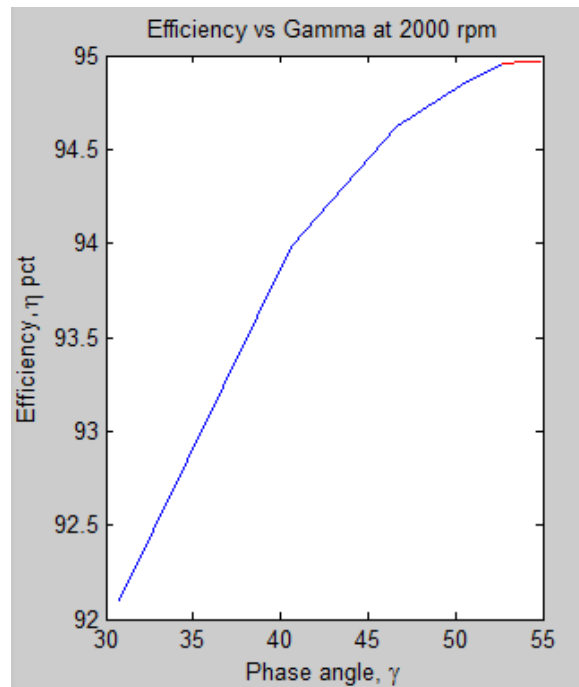
Figure 98, Example of results using golden section method at 2000 rpm

The use of other search methods prior to creating a response surface was mentioned earlier. One of these was to begin with a conjugate direction method, and then create the response surface when the region of the optimal design was determined. A method found in the literature would be to begin with fractional factorial models with only 2 levels, and require fewer evaluations, until the optimal design space has been identified.

H.   The use of multiple response surfaces

For RSM, a single response surface is typically created from the data. However, multiple response surfaces have been used. For the validation examples, the objective function was the minimum efficiency obtained at two operating conditions. Initially, a single response surface was created based on this objective function. This response surface had a very poor fit.

A second approach was to create separate response surfaces at each specified test point (the speed and power requirement). These models had a much lower variance, indicating that this method more accurately predicted the efficiency of the machines. After the response surfaces had been modeled, the optimization algorithm used the models to determine the value of the objective function, and then optimize it. This method could be extended to a larger number of performance points. It also can be extended to include other factors, such as current requirements, cogging torque, etc.

Response surfaces can be created to determine the masses or volumes. For the most part, the masses and volumes can be determined from the dimensionless parameters and the stator volume, but stresses which affect the bridge and posts will change the magnet volume. If magnet cost is part of the objective function, response surfaces for magnet mass may be needed.

To add response surfaces at additional operating conditions requires analyzing the machine at those speeds and power levels, the additional data points will slow down the algorithm approximately linearly.

An attempt was made to include a penalty function (when not achieving rated power), when creating the response surface. This distorted the response surface.

I.   Creating families of machines

In machine design, it is common that a single lamination design may be used for machines which have multiple power settings. This is typically done by lengthening the stator, and sometimes by increasing the speed of the machine. For these cases, multiple response surfaces could be created for the family of machines, or for specific machines in

the family. The objective function would include calculations which yield a combination of designs which are optimized for each power level, with the same lamination. These machines might have differing torque densities, in order to achieve their required specifications.

J.   Rapidity of the algorithms

In order to find the solution rapidly, a number of techniques were used.

- By using dimensionless parameters, and setting up realistic boundaries, only physically realizable geometries were created

- The golden section method (or Fibonacci), allowed for the number of phase angle points (7), and the rate of phase angle convergence, to be known ahead of time.

- The application of Newton's method for determining the correct current to achieve rated power resulted in convergence typically in 3 or fewer function evaluations.

- Having some dimensions (such as slot opening) dependent on other dimensions made modification of designs quicker, as those dimensions were modified automatically.

- Modifying Newton's method, by multiplying the adjustment current of the second point by a constant (based on whether the first point was higher or lower than desired) decreased the number of objective function evaluations by approximately 15%.

- Using a curve fit of the first three points of the phase angle vs. current allowed for convergence typically on the first or second attempt of successive points.

- Having the algorithm create the 64 machine designs, based only on the center point of the I-optimal design and the parameter ranges, made creating the design spaces instantaneous.

- Using I-optimal designs, a design method was created which required only 64 data points for the initial response surface, rather than 81 points for a CCD, or 113 for a BB design.

- Mirroring the hypercube design reduced the analysis of additional data points, when the design space needed to be extended

- The algorithm indicates which direction subsequent hypercubes should analyze, if the optimum is not achieved. This reduces the time required to make these decisions. This could have been automated, so that the process would add and analyze design spaces without operator intervention.

- Because the hypercube designs have all dimensions defined simultaneously, it is possible to verify that all of the designs can be meshed in a short period of time[43]

- Because the algorithm verifies that all designs can mesh, before detailed analysis, the program does not halt due to meshing errors. Once designs were verified, the algorithm could run unattended.

Increasing the rapidity based on special objective functions

For the objective function used in the validation examples, an additional reduction in the number of objective functions is possible (though it was not implemented). This consists of evaluating the first few designs at both performance points. Because the objective function for validation was based on the lowest efficiency of the machine at two speeds, the other designs in the hypercube could be evaluated only for the performance point (speed) which had yielded the lowest efficiency.

---

[43] The location of successive design point in PSO and other stochastic methods, is based on the analysis of present points, and therefore, subsequent designs cannot be meshed early on in the evaluation process.

A response surface for this performance point could then be created. The optimum value (design) for this response surface would be found. This 'optimal' design would then be analyzed at the other performance point. Since this objective function is based on the lowest efficiency, if the efficiency at the second performance point was higher than at the first performance point, the optimum design had been found. If efficiency at the second performance point was lower, then all designs in the design set would have to be evaluated. For this case, the number of analyses of the machine would be the same as if this method had not been implemented. For the case where this method succeeded, analyses would have been cut approximately in half. It is helpful to recognize objective functions of this type.

CHAPTER V.   CONCLUSIONS

This chapter describes the conclusions and contributions of this research, and future work which this research leads to.

A.   Conclusions

Accurate response surface models of IPM machines can be created using eight dimensionless parameters. These models can be created from the analysis of 64 machines, for each portion of the design space which is analyzed. Additional design spaces typically require 42-64 machines to be analyzed.

These models can be used to determine the optimum machine design for IPM machines. This method was validated for machines ranging in power from 25 kW to 200 kW, and it is likely that the method works for machines of larger and smaller power levels.

A method for rapid optimization was accomplished by:

- Defining dimensionless parameters for IPM machines

- Creating methods to quickly set up the problem

- Creating methods to speed up the performance analysis of the machine

- Using experimental (I-optimal) designs which require a minimum number of data points

- Using multiple response surfaces for the same design set.

Problem set up was simplified by having the global design space predefined, with smaller design regions easily selected, using eight parameters. As the parameters were dimensionless, initial estimates could be made about where the optimum was located.

Designs were created automatically using I-optimal designs, which excel at creating predictive response surfaces. Structural FEA was incorporated in the program so that the geometry defined was structurally sound, while efficiently using the magnet mass.

Performance analysis was sped up by developing methods to rapidly determine the optimum settings of current and phase angle for each performance point. This consisted of modifying Newton's method to determine the correct current at each phase angle, and modifying the golden section search method to determine the correct phase angle. Other features described in the text were also included to speed up analysis.

Only 64 data points for eight factors were required, based on using I-optimal designs, from design of experiments methodology. These were used to create response surfaces. An addition to this technique was mirror imaging of the I-optimal design when extending the design space, so that data could be reused, rather than recreated.

During the development of this method, it was found that it was useful to set up separate response surfaces for each operating condition specified. Each of these response surfaces predicts the performance of the machine at a specific speed and power level. The objective functions were based on these multiple response surfaces, rather than having a single response surface, based on a complex objective function. This allowed multiple objective functions to be used on the acquired data, and allowed for objective functions to be redefined after analysis was complete.

B.   Contributions of this research

The primary contributions of this research lie in the following areas:

- Development of a practical method for rapid IPM machine design

- Extensive use of dimensionless optimization, including defining eight parameters which are effective for achieving optimization in IPM machines

- The use of dimensionless optimization in a way that minimizes physically non-realizable geometry

- The use of multiple response surfaces to define the objective function

- The inclusion of structural FEA as part of the design process

- The use of the structural FEA and performance data to modify the geometry during the optimization

C.   Future research

The following are areas for future research:

- The use of dimensionless parameters for other machine types, including induction machines, surface permanent magnet machines, switched reluctance machines, synchronous machines, and axial flux machines

- A study of the impact of various specifications on the parameters for optimal designs

- A study of the most effective range sizes for the parameters which were defined

- A study of the interactions between the dimensionless parameters

- Characterizing the design space, so that the opportunities to achieve high efficiency with variations in the stator aspect ratio can be understood

- Development of a means to incorporate demagnetization into the method defined by this research

APPENDIX 1.   I-OPTIMAL DESIGN

The I-optimal design in Table 33 was created using JMP® 7.0.2, © 2007 SAS

Institute, Inc. This I-optimal design was used in the creation of the design hyperspaces

used for validating the method developed by this research. The designs were not

randomized, as the results of the simulations are not affected by the order in which they

are run. Run number 1 is the center point of the design.

Table 33, Coded I-optimal design

Run no.	x_1	x_2	x_3	x_4	x_5	x_6	x_7	x_8
1	0	0	0	0	0	0	0	0
2	-1	-1	-1	-1	-1	-1	1	1
3	-1	-1	-1	-1	1	1	-1	-1
4	-1	-1	-1	1	1	-1	0	0
5	-1	-1	0	-1	1	1	1	1
6	-1	-1	0	1	-1	1	0	0
7	-1	-1	1	-1	0	-1	-1	-1
8	-1	-1	1	1	0	0	1	-1
9	-1	0	-1	-1	-1	0	0	-1
10	-1	0	-1	0	0	1	1	1
11	-1	0	0	0	-1	-1	1	-1
12	-1	0	0	0	0	0	-1	0
13	-1	0	1	1	-1	-1	0	1
14	-1	0	1	1	1	1	-1	1
15	-1	1	-1	-1	-1	-1	-1	1
16	-1	1	-1	0	0	0	0	-1
17	-1	1	-1	1	1	0	1	1
18	-1	1	1	-1	-1	0	1	1

Run no.	x_1	x_2	x_3	x_4	x_5	x_6	x_7	x_8
19	-1	1	1	-1	1	-1	0	0
20	-1	1	1	-1	1	1	1	-1
21	-1	1	1	1	-1	1	0	-1
22	-1	1	1	1	1	-1	-1	-1
23	0	-1	-1	-1	1	-1	1	-1
24	0	-1	-1	0	1	0	-1	1
25	0	-1	-1	1	-1	-1	-1	-1
26	0	-1	-1	1	-1	0	1	1
27	0	-1	0	0	1	0	0	-1
28	0	-1	1	-1	-1	1	1	-1
29	0	-1	1	0	-1	1	-1	1
30	0	-1	1	0	1	-1	1	1
31	0	0	-1	-1	0	1	0	1
32	0	0	-1	1	1	1	1	-1
33	0	0	0	-1	0	0	0	0
34	0	0	0	-1	1	-1	-1	1
35	0	0	0	0	0	0	1	0
36	0	0	1	0	0	0	0	0
37	0	1	-1	0	-1	-1	1	0
38	0	1	-1	1	1	1	-1	0
39	0	1	0	-1	-1	1	-1	0
40	0	1	0	0	1	0	0	1
41	0	1	1	1	0	-1	1	0
42	1	-1	-1	-1	-1	0	-1	0
43	1	-1	-1	0	-1	1	1	-1
44	1	-1	-1	0	0	-1	0	0
45	1	-1	0	1	0	1	-1	-1
46	1	-1	0	1	1	1	0	1
47	1	-1	1	-1	1	0	1	0
48	1	-1	1	1	-1	-1	1	-1

Run no.	x_1	x_2	x_3	x_4	x_5	x_6	x_7	x_8
49	1	-1	1	1	1	-1	-1	0
50	1	0	-1	1	-1	1	-1	1
51	1	0	-1	1	1	-1	1	1
52	1	0	0	-1	-1	-1	0	1
53	1	0	1	0	1	1	0	-1
54	1	0	1	1	-1	0	-1	0
55	1	1	-1	-1	1	-1	-1	-1
56	1	1	-1	-1	1	-1	1	1
57	1	1	-1	0	1	1	1	0
58	1	1	-1	1	-1	0	0	-1
59	1	1	0	-1	0	1	1	-1
60	1	1	0	1	0	-1	-1	1
61	1	1	1	-1	-1	-1	-1	-1
62	1	1	1	-1	1	1	-1	1
63	1	1	1	1	-1	1	1	1
64	1	1	1	1	1	-1	1	-1

APPENDIX 2. STRUCTURAL FEA USING MATLAB

Some details of setting up the MATLAB PDE toolbox are explained in this appendix. The creation of the geometry is explained in CHAPTER II.H (page 48). The body forces were set to:

$$F_r = \rho\omega^2 r \tag{5.1}$$

In MATLAB, this requires setting the x and y body forces separately, which are:

$$F_x = \rho\omega^2 x \tag{5.2}$$

$$F_y = \rho\omega^2 y \tag{5.3}$$

where F_x is the body force in the x direction (N/m³), F_y is the body force in the y direction (N/m³), ρ is the density of electrical steel $\left(7650\,kg\,/\,m^3\right)$, ω is the overspeed condition in the specifications (rad/sec), and x and y are the locations of each point in the rotor (m).

MATLAB specifies the Dirichlet boundary condition as:

$$\begin{pmatrix} h_{11} & h_{12} \\ h_{21} & h_{22} \end{pmatrix}\begin{pmatrix} u_1 \\ u_2 \end{pmatrix} = \begin{pmatrix} r_1 \\ r_2 \end{pmatrix} \tag{5.4}$$

To obtain the boundary condition on the lower (horizontal) line, if $h_{21} = 0$, $h_{22} = 1$, and $r_2 = 0$, then u_2 (the y motion) must be 0.

The equation for the upper line boundary condition depends on the number of poles. If the number of poles is four, then the upper line will be at 45°. For this equation, u_1 is

the horizontal (x) direction, u_2 is the vertical (y) direction. To obtain the boundary condition on the upper line (45° line):

If $h_{11} = 0.707$, $h_{12} = -0.707$ and $r_2 = 0$; then $u_1 = u_2$, which describes a 45° line.

If the number of poles is greater than four, the angle of the upper line will be:

$$\alpha = 180 / P \tag{5.5}$$

where α is the angle of the upper line and P is the number of poles.

For this case, $h_{11} = \sin(\alpha)$, $h_{12} = -\cos(\alpha)$, and $r_2 = 0$. This will force u_2 to be $\tan(\alpha)$, which is the equation for that line. These equations were entered in the MATLAB code. The body force was:

$$k_{r11200} = 1.052\,E\,1\,r_{mm}\left(N/mm^2\right)$$
$$= 1.052\,E-2\,r_m\left(kPa\right) \tag{5.6}$$

where k_{r11200} is the force at 11200 rpm (N), r_{mm} is the radius (mm), and r_m is the radius (m). MATLAB requires setting body forces in terms of the x and y directions. Therefore, the body forces at 11,200 were set as:

$$kx = ky = 1.052E4\,r\;\left(N/mm^2 = Pa\right) \tag{5.7}$$

$$= 1.052\,E\,1\,r_{mm}\left(N/mm^2\right)$$
$$= 1.052\,E-2\,r_m\left(kPa\right) \tag{5.8}$$

Therefore, *Kx* was set to 1.052e-2*x (N/cu m), *Ky* was set to 1.052e-2*y, and rho was set equal to 7650 (kg/cu m).[44] Forces for other speeds can be scaled from the above.

---

[44] Kx, Ky, nu and rho are MATLAB variables.

APPENDIX 3.   CONTRACTED AND OPTIMIZED DESIGNS

Contracted and optimized designs for the following laminations were done to the same specifications, 50 kW, 30 Nm/liter @ 4913 RPM. Max operating speed was 6937 RPM. Contracted and DO designs also used the same materials and material files.

Lamination comparison
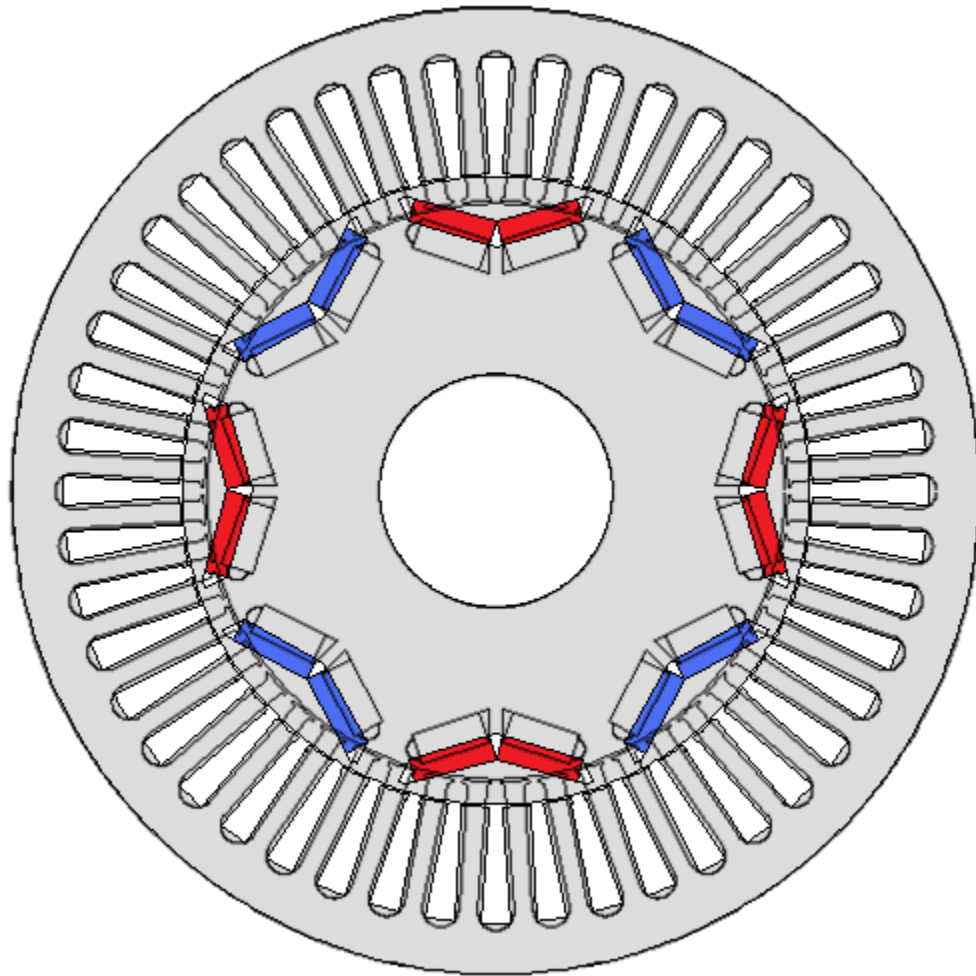
Figure 99, Overlay of contracted generator design (in gray, red and blue), and design optimized using this method

The gray laminations in Figure 99 are the contracted designs. The black lines which have gray on one side, and white on the other are the optimized design. FEA results for these laminations are shown in Figure 100 though Figure 103.

FEA Comparison
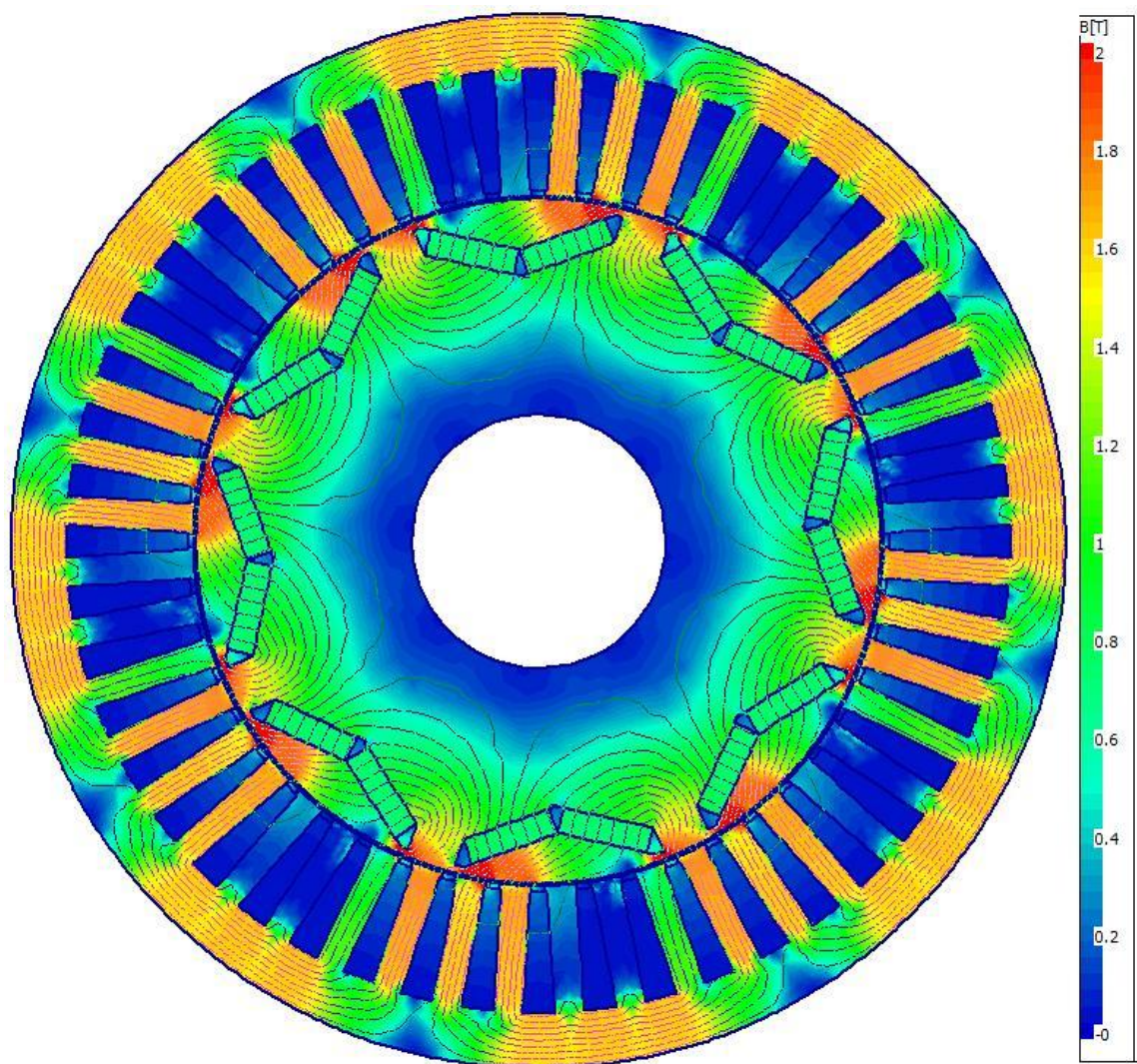
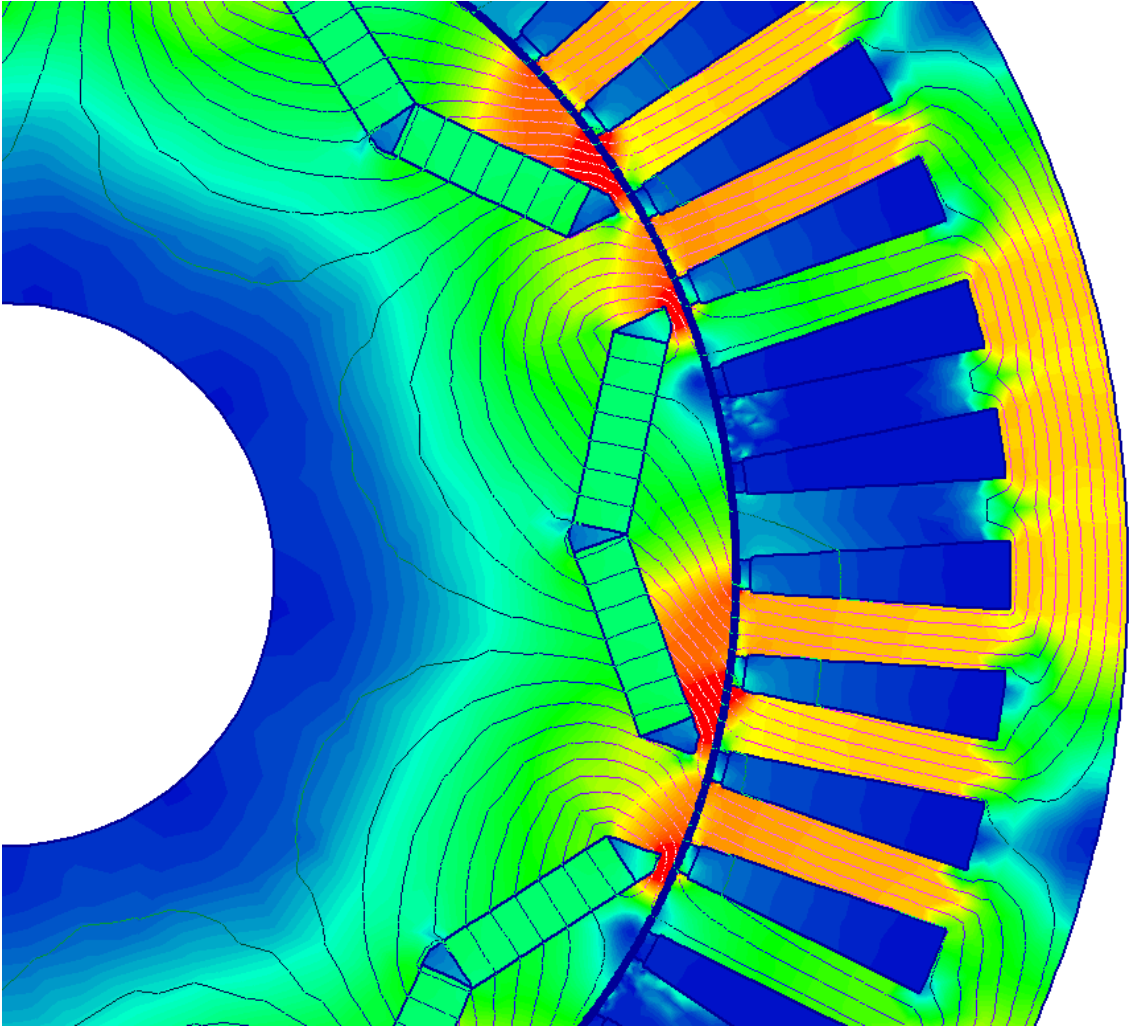**Figure 100, FEA of contracted design at rated power, 4913 RPM, approx. ¾ scale**

Figure 101, Magnified view of FEA of contracted design

The contracted design had a larger rotor, thinner magnets, and a smaller air gap.
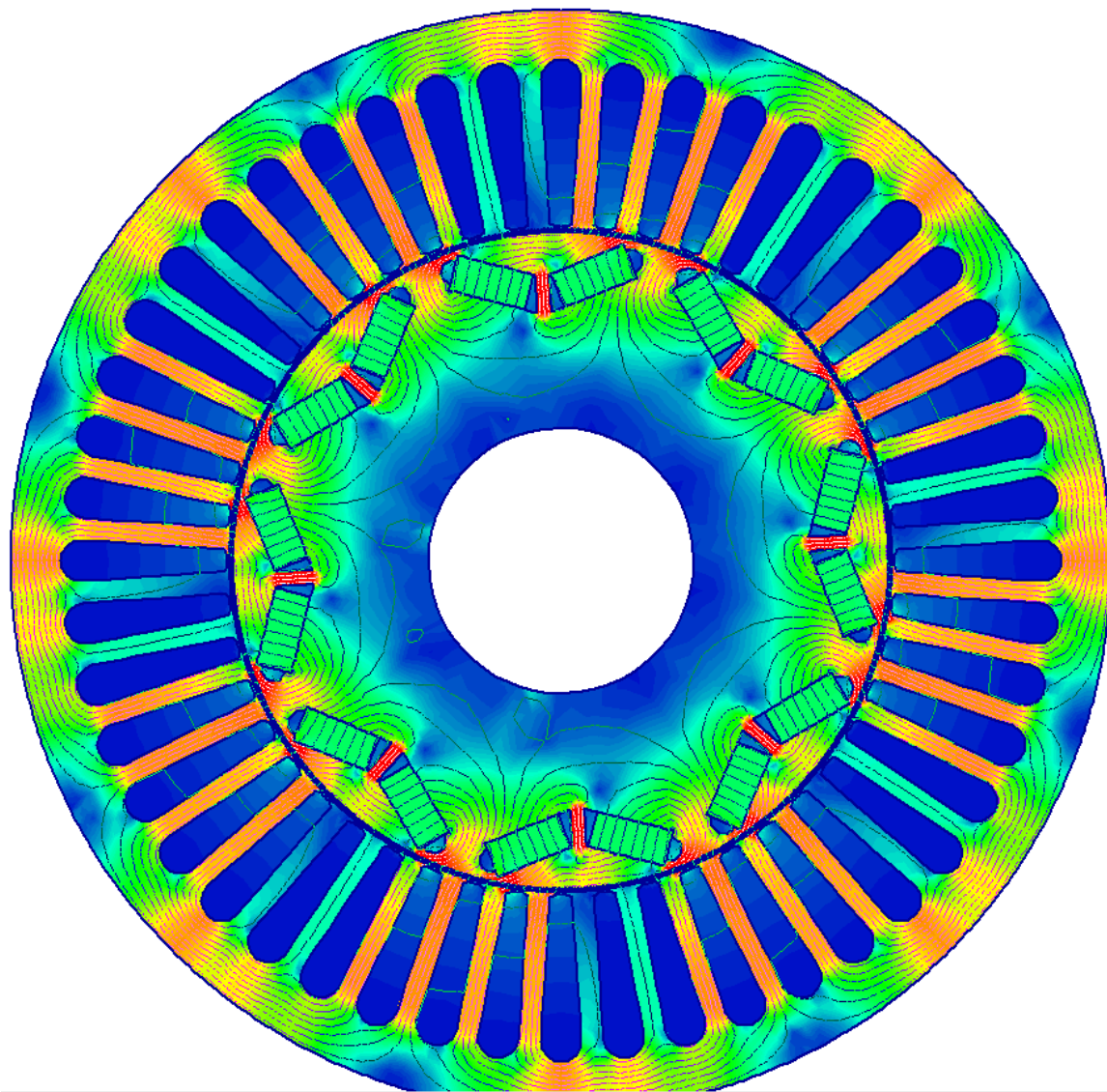
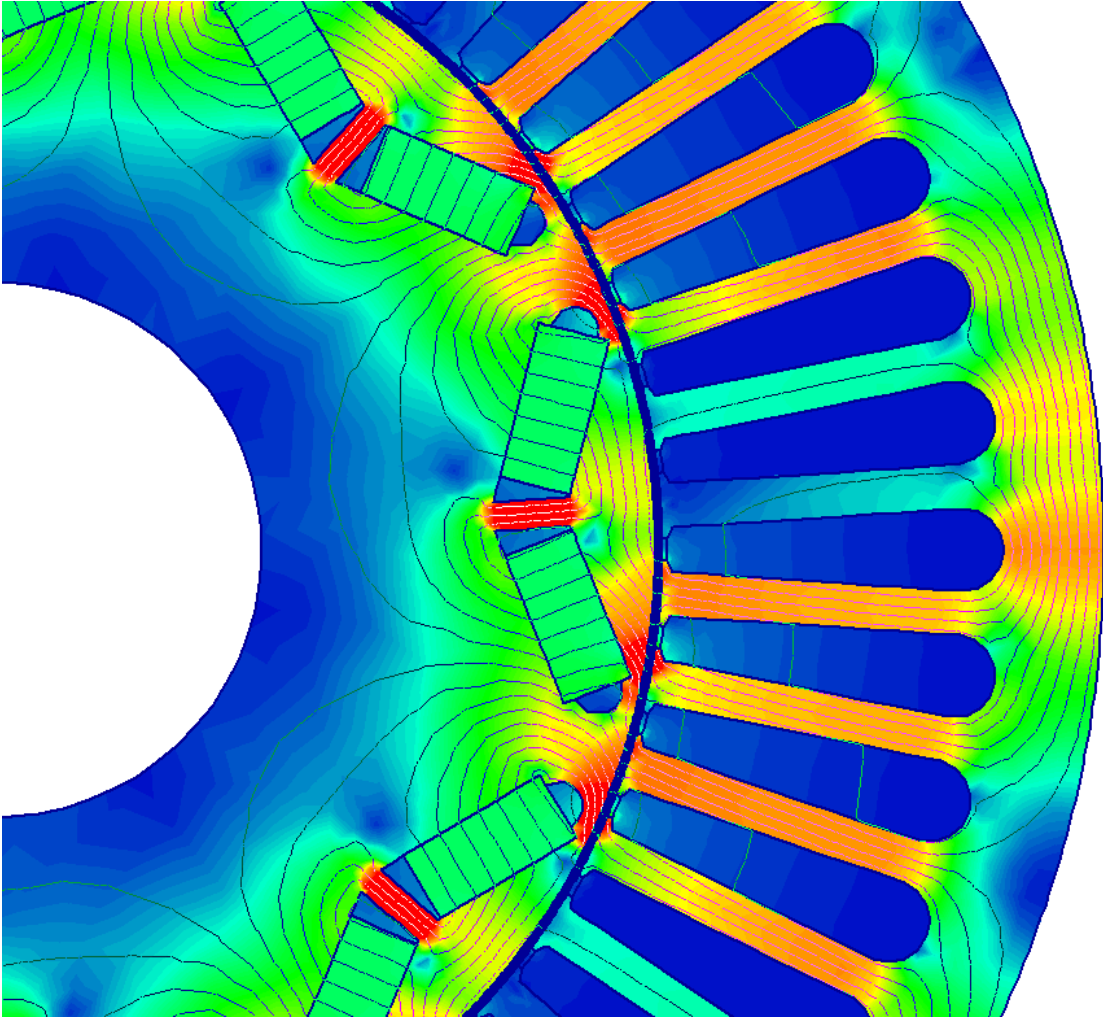**Figure 102, FEA of optimized design at rated power, 4913 RPM**

Figure 103, Magnified view of optimized design at rated power, 4913 RPM

Figure 103 uses the same color scale for flux density as Figure 100

APPENDIX 4.   REVIEW OF METHODS USED FOR ELECTRIC MACHINE OPTIMIZATION

Table 34 lists the methods used in the literature for machine optimization. It lists the methods, number of parameters varied, and the goals of the optimization, if described in the respective literature.

Table 34, Summary of the methods used for machine optimization

Reference	Methods used	Number of parameters varied, units	Goal
[1]	RSM, FFD and CCD	3	Minimize torque ripple
[2]	Stochastic and deterministic		Study global optimization of PM machines
[3]	GA and FEA		Optimize pole shape of a magnet
[4]	Global evolution strategy (GA, simulated annealing, and Monte Carlo)		
[5]	2D and 3D FEA, evolutionary algorithms	9	Design of DC torque motor
[6]	GA with 2D FEA, constant permeability	4, mm	Design of motor pole face with sinusoidal flux density
[7]	GA initially, followed by gradient method	6, mm	Design of motor pole face with sinusoidal flux density
[8]	GA followed by direct search, with FEA	3, mm	Minimizing the ripple torque of a DC motor
[9]	3 different GA, 2 particle based, one ant stigmergy, all with FEA. Saturation	10, mm, step size was 0.1mm Both rotor and stator	Universal motor

Reference	Methods used	Number of parameters varied, units	Goal
	included.		
[10]	SPSA and CGA	5	Induction machine
[14]	Gradient search and golden section		Find optimum current vector for real time control system
[17]		7, dimensionless	Switched reluctance motors
[18]	Stator OD was fixed	4, dimensionless	Switched reluctance motors
[19]	FEA and analytical calculations	1 dimensionless, the split ratio. Step size was 0.5 mm from 5.3 to 8.8 mm	DC brushless motor
[20]		Split ratio	
[21]		Split ratio	Derive formula for optimum split ratio
[22]		Split ratio	Optimized split ratio for a fractional slot IPM machine
[23]	Analytical equations, iron losses neglected	Split ratio	Find optimal split ratio of brushless DC motor
[24]		3 dimensionless, mention saliency ratio (L_d/L_q), CPSR	Design of axially laminated IPM
[25]		Split ratio (called diameter ratio), copper fill factor	High speed PM motor, includes study of torque vs. split ratio, split ratio c. frequency
[26]		3 dimensionless; aspect ratio (L/D of stator), split ratio, tooth length ratio	Optimized design of surface PM machine
[27]		2 dimensionless, the split ratios	Analyze torque of double stator PM machine
[28]		1 dimensionless, slot	Induction AC traction

Reference	Methods used	Number of parameters varied, units	Goal
		width/slot pitch	motors
[29]		3 dimensionless	PM stepping motors
[30]		8 dimensionless	Optimization of IPM machines using dimensionless parameters
[31]			Determine dimensionless parameters for IPM machines
[33]		3 dimensionless	Optimal design of 50 kW IPM machine
[34]		2 dimensionless	Study of optimal tooth geometry for hybrid stator motors
[35]		1 dimensionless	PM synchronous machine design and cogging torque

BIBLIOGRAPHY

[1] Sung-Il Kim, Ji-Young Lee, Jung-Pyo Hong, and Young-Kyoun Kim, "Application of response surface methodology combined with experimental design for improving torque performance of interior permanent magnet synchronous motor," in *2005 IEEE International Conference on Electric Machines and Drives, May 15, 2005 - May 15, 2005*, San Antonio, TX, United states, 2005, pp. 1665-1668.

[2] A. Muetze, "A contribution to identification of convex structures for global optimization of permanent magnet machines," in *Industry Applications Conference, 2005. Fourtieth IAS Annual Meeting. Conference Record of the 2005*, Hong Kong, China, 2005, pp. 266-273.

[3] K. Preis, C. Magele, and O. Biro, "FEM and evolution strategies in the optimal design of electromagnetic devices," *IEEE Transactions on Magnetics*, vol. 26, no. 5, pp. 2181-2183, Sep 1990.

[4] A. Gottvald, K. Preis, C. Magele, O. Biro, and A. Savini, "Global optimization methods for computational electromagnetics," *IEEE Transactions on Magnetics*, vol. 28, no. 2, pp. 1537-1540, March 1992.

[5] F. Arpino, P. DiBarba, P. Navarra, and A. Savini, "3D global optimum of an electromechanical device," *IEEE Transactions on Magnetics*, vol. 30, no. 5 pt 2, pp. 3427-3430, September 1994.

[6] G.F. Uler, O.A. Mohammed, and Chang-Seop Koh, "Utilizing genetic algorithms for the optimal design of electromagnetic devices," *IEEE Transactions on Magnetics*, vol. 30, no. 6, pp. 4296-4298, Nov 1994.

[7] O. A. Mohammed and G. F. Uler, "A hybrid technique for the optimal design of electromagnetic devices using direct search and genetic algorithms," *IEEE Transactions on Magnetics*, vol. 33, no. 2, pp. 1931-1934, March 1997.

[8] Yong-Hwan Oh, Tae-Kyung Chung, Min-Kyu Kim, and Hyun-Kyo Jung, "Optimal design of electric machine using genetic algorithms coupled with direct method," *IEEE Transactions on Magnetics*, vol. 35, no. 3, pp. 1742-1745, May 1999.

[9] Tea Tusar, Peter Krosec, Gregor Papa, Bogdan Filipic, and Jurij Silc, "A comparative study of stochastic optimization methods in electric motor design," *Applied Intelligence*, vol. 27, no. 2, pp. 101-111, October 2007.

[10] F Cupertino, E Mininno, D Naso, and L Salvatore, "A comparison of SPSA method and compact genetic algorithm for the optimization of induction motor position control," in *2007 European Conference on Power Electronics and Applications, EPE*, Aalborg, Denmark, 2007.

[11] J. C. Spall, *Introduction to stochastic search and optimization: estimation, simulation, and control*. Hoboken, New Jersey, United States of America: John Wiley and Sons, 2003.

[12] C. W. Ahn and R. S. Ramakrishna, "Elitism based Compact Genetic Algorithms," *IEEE Transactions Evolutionary Computation*, vol. 7, no. 4, August 2003.

[13] John W Bandler, "Optimization methods for computer-aided design," *Transactions on Microwave Theory and Techniques*, vol. 17, no. 8, pp. 533-552, August 1969.

[14] Xianqing Cao and Liping Fan, "A Quick Efficiency-Optimized Scheme for Vector Controlled Permanent Magnet Synchronous Motor Drive," in *Control, Automation and Systems Engineering, 2009. CASE 2009. IITA International Conference on*, Bangalore, India, 2009, pp. 283-286.

[15] D. P. Mays, "Optimal Central Composite Designs in the Presence of Dispersion Effects," *Journal of Quality Technology*, vol. 31, no. 4, pp. 398-407, October 1999.

[16] SAS Institute Inc., Cary, NC, JMP, Version 7. , 1989-2007.

[17] Z. Q. Zhu, Y. Pang, J. T. Chen, Z. P. Xia, and D. Howe, "Influence of design parameters on output torque of flux-switching permanent magnet machines," in *Vehicle power and propulsion conference (VPPC)*, Harbin, China, 2008.

[18] J. Faiz and J. W. Finch, "Aspects of design optimization for switched reluctance motors," *IEEE Transactions on Energy Conversion*, vol. 8, no. 4, pp. 704-713, Dec 1993.

[19] Tang Yu, Xu Yongxiang, Hu JianHui, Zou Jibin, and Li Shuai, "Optimization of split ratio to design the PM brushless DC motor," in *International Conference on Electrical Machines and Systems, 2009. ICEMS 2009*, Tokyo, Japan, 2009, pp. 1-5.

[20] Y. Pang et al., "Comparative study of flux-switching and interior permanent magnet machines," in *International Conference on Electrical Machines and Systems, ICEMS 2007*, Seoul, Korea, 2007, pp. 757-762.

[21] F. B. Chaaban, "Determination of the optimum rotor/stator diameter ratio of permanent magnet machines," *Electric Machines and Power Systems*, vol. 22, no. 4, pp. 521-531, Jul-Aug 1994.

[22] L.J. Wu, Z.Q. Zhu, J.T. Chen, Z.P. Xia, and G.W. Jewell, "Optimal split ratio in fractional-slot interior permanent magnet machines with non-overlapping windings," in *IEEE International Electric Machines and Drives Conference (IEMDC)*, 2009, pp. 1721-1728.

[23] Y. Pang, Z. Q. Zhu, and D. Howe, "Analytical determination of optimal split ratio for permanent magnet brushless motors," *IEE Proceedings: Electric Power Applications*, vol. 153, no. 1, pp. 7-13, January 2006.

[24] Wen L. Soong, David A Staton, and Timothy J. E. Miller, "Design of a new axially-laminated interior permanent magnet motor," *IEEE Transactions on Industry Applications*, vol. 31, no. 2, pp. 358-367, Mar-Apr 1995.

[25] Nicola Bianchi, Silverio Bolognani, and Fabio Luise, "Potentials and limits of high-speed PM motors," *IEEE Transactions on Industry Applications*, vol. 40, no. 6, pp. 1570-1578, Nov/Dec 2004.

[26] Nicola Bianchi, Silverio Bolognani, and Paolo Frare, "Design criteria for high-efficiency SPM synchronous motors," *IEEE Transactions on Energy Conversion*, vol. 21, no. 2, pp. 396-404, Jun 2006.

[27] Chai Feng, Xia Jing, Gong Hailong, Guo Bin, and Cheng Shukang, "Torque analysis of double-stator permanent magnet synchronous for hybrid electric vehicle," in *IEEE Vehicle Power And Propulsion Conference (VPPC)*, Harbin, China, 2008, p. 5.

[28] R. N. Paul, L. D. Arva, and H. K. Verma, "Studies in design of high torque three-phase squirrel-cage AC traction motor with aluminium alloy rotor bars and parameter optimization using artificial neural networks," in *2008 Joint International Conference on Power System Technology POWERCON and IEEE Power India Conference*, New Delhi, India, 2008.

[29] C. P. Liu, Y. C. Li, K. H. Liu, K. T. Wu, and Y. D. Yao, "Analysis of the performance of permanent magnetic stepping motor with trapezoid stator tooth," *Journal of Applied Physics*, vol. 99, no. 8, p. 3, 2006.

[30] R. D. Bremner, "Dimensionless optimization of a 60 kW IPM machine," in *Power Electronics Machines and Drives (PEMD) 4th IET Conference on*, York, England, 2008, pp. 291-295.

[31] Xu Longya, Fan Tao, and Wen Xuhui, "Synthesis of dimensionless indexes for IPM machine in variable speed operations," in *Electrical Machines and Systems (ICEMS), International Conference on*, Wuhan, China, 2008, pp. 2814-2819.

[32] Anton Antonov. (2001) Making Dimensionless Models. Mathematica notebook, download from Wolfram Research.

[33] Thomas M. Jahns et al., "Design and experimental verification of a 50 kW interior permanent magnet synchronous machine," in *Conference Record - IAS Annual Meeting (IEEE Industry Applications Society)*, Tampa, FL, United States, 2006, pp. 1941-1948.

[34] K. R. Rajagopal, B. Singh, and B. P. Singh, "Optimal Tooth-Geometry for Specific Performance Requirements of a Hybrid Stepper Motor," *IEEE Transactions on Magnetics*, vol. 39, no. 51, pp. 3010-3012, Sep 2003.

[35] Kamel Boughrara, Brahim Ladqem Chikouche, Rachid Ibtiouen, Damir Zarko, and Omar Touhami, "Analytical model of slotted air-gap surface mounted permanent-magnet synchronous motor with magnet bars magnetized in the shifting direction," *IEEE Transactions on Magnetics*, vol. 45, no. 2, pp. 747-758, Feb 2009.

[36] SAS Institute Inc., Cary, NC,. (1989-2007) JMP, Version 7. Software.

[37] Juha Pyrhonen, Tapani Jokinen, and Valeria Hrabovcova, *Design of Rotating Electrical Machines*.: Wiley, 2009.

[38] TJE Miller and Malcolm McGilp, SPEED PC-BDC 9.0 Version 9.0.2.4, SPEED Laboratory, Glasgow, Scotland, 2009.

[39] Priuschat.com. (2010, April) PRIUSchat. [Online]. http://priuschat.com/forums/attachments/gen-iii-2010-prius-main-forum/13377d1236020025-picture-2010-prius-transaxle-compared-others-2010-prius-transaxle.jpg

[40] Peter Campbell. (2010, February) Magnetic Circuit Design: definition of the load line. [Online]. http://www.magnetweb.com/Sect4A.htm

[41] Jacob V Williford Jr., "Electric Motor," 2,939,025, May 31, 1960.

[42] V. B. Honsinger, "Permanent Magnet Motor," 3,126,493, March 24, 1964.

[43] Charles R Steen, "Direct axis aiding permanent magnets for a laminated synchronous motor rotor," 4,139,790, February 13, 1979.

[44] Donald W. Jones, "Permanent magnet rotor ," 4,472,651, September 18, 1984.

[45] "Microcomputer-based control and simulation of an advanced IPM synchronous machine drive system for electric vehicle propulsion," *IEEE Transactions on Industrial Electronics*, vol. 35, no. 4, pp. 547-558, November 1988.

[46] T. M. Jahns, G. B. Kliman, and T. W. Neumann, "Interior permanent magnet synchronous motors for adjustable-speed drives," in *Conference Record - IAS Annual Meeting*, Toronto, Ontario, Canada, 1985, pp. 814-823.

[47] B. J. Chalmers, S. A. Hamed, and G. D. Baines, "Parameters and performance of a high-field permanent-magnet synchronous motor for variable-frequency operation," *IEEE Proceedings, Part B: Electric Power Applications*, vol. 132, no. 3, pp. 117-124, May 1985.

[48] D. R. Cox and N Reid, *The theory of the design of experiments (Monographs on statistics and applied probability; 86)*. Boca Raton, Florida, USA: Chapman & Hall/CRC, 2000.

[49] D. G. Bharadwaj, K. Venkatesan, and R. B. Saxena, "Induction motor design optimization using constrained Rosenbrock method (Hill algorithm)," *Computers & Electrical Engineering*, vol. 6, no. 1, pp. 41-46, Mar 1979.

[50] V. B. Honsinger, "Fields and parameters of interior type ac permanent magnet machines," *IEEE transactions on power apparatus and systems*, vol. PAS-101, no. 4, pp. 867-876, Apr 1982.

[51] Chai Feng, Jing Xia, Hailong Gong, Bin Guo, and Shukang Cheng, "Torque analysis of Double-Stator Permanent Magnet Synchronous for Hybrid Electric Vehicle," in *IEEE Vehicle Power and Propulsion Conference*, Harbin, China, 2008.

[52] A. Ishizaki, T. Tabako, and K. Saitoh, "Prediction and improvement on synchronous performance of ac permanent magnet motor," in *IAS Annual Meeting*, Toronto, Ontario, Canada, 1985, pp. 824-831.

[53] Munehiro Kamiya, Yoshihiro Kawase, Takashi Kosaka, and Nobuyuki Matsui, "Temperature distribution analysis of permanent magnet in interior Permanent Magnet Synchronous Motor considering PWM carrier harmonics," in *International Conference on Electrical Machines and Systems, ICEMS 2007, October 8, 2007 - October 11, 2007*, Seoul, Republic of Korea, 2007, pp. 2023-2027.

[54] J. S. Hsu et al., "Effect of side permanent magnets for reluctance interior permanent magnet machines," in *PESC 07 - IEEE 38th Annual Power Electronics Specialists Conference, June 17, 2007 - June 21, 2007*, Orlando, FL, United states, 2007, pp. 2267-2272.

[55] Alfredo R. Munoz, Feng Liang, and Michael W. Degner, "Evaluation of Interior PM and Surface PM Synchronous machines with distributed and concentrated windings," in *34th Annual Conference of the IEEE Industrial Electronics Society, IECON 2008, November 10, 2008 - November 13, 2008*, Orlando, FL, United states,

2008, pp. 1189-1193.

[56] Izumi Ozawa, Takashi Kosaka, and Nobuyuki Matsui, "Less rare-earth magnet-high power density hybrid excitation motor designed for hybrid electric vehicle drives," in *2009 13th European Conference on Power Electronics and Applications, EPE '09, September 8, 2009 - September 10, 2009*, Barcelona, Spain, 2009, p. NA.